The role of Stress Inducible Protein 1 (STI1) in the regulation of actin dynamics

A thesis submitted in the fulfilment of the requirements for the degree of

Master of Science in Biochemistry

of

Rhodes University

by

Samantha Joy Beckley

January 2015

Abstract

Stress-inducible protein 1 (STI1) otherwise known as Hop (Hsp70/Hsp90 organising protein) is a highly conserved abundant co-chaperone of the Hsp70 and Hsp90 chaperones. STI1 acts as an adapter protein, where it regulates the transfer of protein substrates from Hsp70 to Hsp90 during the assembly of a number of chaperone-client protein complexes. The role of STI1 associating independently with non-chaperone proteins has become increasingly prominent. Recent data from colocalisation and co-sedimentation analyses in our laboratory suggested a direct interaction between STI1 and the cytoskeletal protein, actin. However, there was a lack of information on the motifs which mediated this interaction, as well as the exact role of STI1 in the regulation of cytoskeletal dynamics. Two putative actin binding motifs, DAYKKK (within the TPR2A domain) and a polyproline region (after the DP1 domain), were identified in mammalian STI1. Our data from *in vitro* interaction studies including surface plasmon resonance and high speed co-sedimentation assays suggested that both TPR1 and TPR2AB were required for the STI1-actin interaction, and peptides corresponding to either the DAYKKK or the polyproline motif, alone or in combination, could not block the STI1-actin interaction. Full length mSTI1 was shown to have ATPase activity and when combined with actin an increase in ATPase activity was seen. *Ex vivo* studies using STI1 knockdown shRNA HEK293T cells and non-targeting control shRNA HEK293T cells showed a change of F-actin morphology as well as reduction in levels of actin-binding proteins profilin, cofilin and tubulin in the STI1 knockdown cells. These data extend our understanding of the role of STI1 in regulating actin dynamics and may have implications for cell migration.

Declaration

I declare that this thesis is my own, unaided work. It is being submitted for the degree of Master of Science or Rhodes University. It has not been submitted before for any degree or examination at any other university

……..

Samantha Beckley, January 2015

Table of Contents

List of Figures

List of Tables

List of Abbreviations

Abbreviation	Full name
ABP	Actin binding protein
ADF	Actin depolymerisation factor
ADP	Adenosine diphosphate
ADP.P_i	Inorganic phosphate bound to ADP at the γ-position
ATP	Adenosine triphosphate
BSA	Bovine serum albumin
CCT	Chaperonin containing TCP-1 complex
DMEM	Dulbecco's Modified Eagle Medium
DNA	Deoxyribonucleic acid
E. coli	*Escherichia coli*
ECL	Enhanced chemiluminescence
EDTA	Ethylene diamine tetra-acetic acid
EGF	Epidermal growth factor
FBS	Fetal bovine serum
FPLC	Fast protein liquid chromatography
GDP	Guanosine diphosphate
GSH	Glutathione
GST	Glutathione s-transferase
GTP	Guanosine triphosphate
HEK cells	Human embryonic kidney cells
HEPES	4-(2-Hydroxyethyl)piperazine-1-ethanesulphonic acid
Hop	Hsp70/Hsp90 organising protein
HPLC	High performance liquid chromatography
Hsp	Heat shock protein
Hsp70	Heat shock protein 70 kilodaltons
Hsp90	Heat shock protein 90 kilodaltons

hSTI1	Human stress-inducible protein 1
HUVECs	Human umbilical vein endothelial cells
Ig	Immunoglobulin
IPTG	Isopropyl β-D-1-thiogalactopyranoside
k_{cat}	Turnover number
K_m	Michaelis constant
LIMK	LIM-kinase
MAP	Microtubule associated protein
MARKs	Microtubule-affinity-regulating kinases
MESG	2-Amino-6-mercapto-7-methyl- purine riboside
MOPS	3-Morpholinopropane-1-sulphonic acid
MRM	Multiple selected reaction monitoring
mSTI1	Murine stress-inducible protein 1
NLS	Nuclear localisation signal
NT	Non-targeting
N-WASP	Neuronal Wiskott-Alrich-syndrome protein
PBS	Phosphate buffered saline
PDB ID	Protein Data Bank identification code
P_i	Inorganic phosphate
PIP	Phosphatidylinositol 4-phosphate
PIP_2	Phosphatidylinositol 4,5-biphosphate
PIP5K1	Phosphatidylinositol-4-phosphate 5-kinase type 1
PMSF	Phenylmethanesulphonyl fluoride
PNP	Purine nucleoside phosphorylase
PrP^C	Cellular prion protein
RNA	Ribonucleic acid
SDS	Sodium dodecyl sulphate
SDS-PAGE	Sodium dodecyl sulphate polyacrylamide gel electrophoresis
shRNA	Short hairpin ribonucleic acid

TAE	Tris-Acetate-Ethylene diamine tetra-acetic acid
TBS	Tris buffered saline
TBS-T	Tris buffered saline with Tween-20
TPR	Tetratricopeptide repeat
SPR	Surface plasmon resonance
SRM	Selected reaction monitoring
SSH1-L	Cofilin phosphatase slingshot-1L
STI1	Stress-inducible protein 1
UV	Ultraviolet
V_{max}	Maximum theoretical velocity
WASP	Wiskott-Alrich-syndrome protein
WAVE	WASP-fmaily verprolin-homologous protein
ySTI1	Yeast stress-inducible protein 1
17-AAG	17-Allylamino-17-demethoxygeldanamycin

List of Symbols

Symbol	Explanation
bp	Base pairs
°C	Degrees Celsius
Da	Daltons
g	Gram(s)
g/mol	Gram(s) per mole
kDa	Kilodalton(s)
L	Litre(s)
M	Molar
mA	Milliamp(s)
mg	Milligram(s)
min	Minute(s)
mg/L	Milligram(s) per litre
mg/ml	Milligram(s) per millilitre
ml	Millilitre(s)
mM	Millimolar
mol	Mole
ng	Nanogram(s)
nm	Nanometre(s)
nM	Nanomolar
nM/min	Nanomolar per minute
OD_{600}	Optical density at 600 nm
RU	Response unit(s)
U	Unit(s)
U/ml	Unit(s) per millilitre
V	Voltage
v/v	Volume per volume

w/v	Weight per volume
x *g*	Relative centrifugal force to gravity
%	Percent
α	Alpha
β	Beta
µg	Microgram(s)
µg/ml	Microgram(s) per millilitre
µl	Microliter(s)
µl/min	Microliter(s) per minute
µM	Micromolar
γ	Gamma

Acknowledgements

I would like to thank my supervisor, Dr. Adrienne Edkins, for her help, guidance, and encouragement throughout this research project. Her incredible knowledge and passion for the subject has been invaluable and has kept me motivated. I would also like to express my gratitude to my co-supervisor, Professor Gregory Blatch. His insight and enthusiasm has greatly contributed toward this project.

I would also like to thank the members, our research unit, BioBRU. Their knowledge, friendliness and support created a special atmosphere to work in, which made the last three years of my studies enjoyable. I would also like to give a special thank you to Dr. Jo-Anne de la Mare and Tamarin Perks, their friendship, help and support has meant so much to me.

I would like thank my family especially, Andy, Cyndy and Jem for their support throughout my studies. There would be no dissertation without their help, and in particular their computer skills. A special mention must also be given to Lee, who was kind enough to proofread my thesis.

Lastly, I would like to thank the National Research Foundation (NRF) for funding.

Chapter 1: Literature Review

1.1 Cell Migration and Metastasis

Cell migration is an important process in all organisms. It is vital in numerous aspects of human life, including embryonic morphogenesis, tissue repair and regeneration and the immune response (Yamaguchi and Condeelis, 2007). Cell migration typically occurs in a succession of steps called the motility cycle (Figure 1.1), which includes the formation of cell membrane protrusions (Mitchison and Cramer, 1996; Rottner and Stradal, 2011). Prior to the formation of the protrusion, the cell must first become polarised in a front to back manner. This is done by the reorganisation of the microfilament and microtubule cytoskeleton, which are comprised of actin and tubulin, respectively (Woodham and Machesky, 2014). The protrusive force generated by the actin fibres pushes the membrane forward in the direction of migration and allows the formation of these protrusions. These protrusions then adhere to the extracellular matrix, generating force and allowing translocation of the cell body. Finally, retraction of the trailing edge occurs. The process is controlled by signalling pathways cascading from the Rho family GTPases(Abraham et al., 1999; Rottner and Stradal, 2011; Yamazaki et al., 2005). Cells have the ability to form a number of different membrane protrusions which are named according to their shape. These include filopodia, which are needle-shaped protrusions, pseudopodia which are rounded in shape and lamellipodia, which are two dimensional structures that are flat and veil shaped (Ridley, 2011; Taylor and Condeelis, 1979).

Cell migration is also an important process in metastasis. Metastasis is the spread of cancerous cells from the primary tumour site and the relocation and growth of these cells in a secondary site (Bravo-Cordero et al., 2012). In order for this to occur the cells must invade the basement membrane and the surrounding tissue, after which cells must enter the bloodstream by intravasation and, after survival in the bloodstream, must undergo extravasation and grow at the newly formed secondary tumour site (Bravo-Cordero et al., 2012). Cell migration is an imperative component in many of these steps. Metastasis is responsible for the majority of

deaths due to cancer (WHO, 2014). Therefore, control of the cell migration processes is theoretically beneficial when treating tumours (Yamazaki et al., 2005).

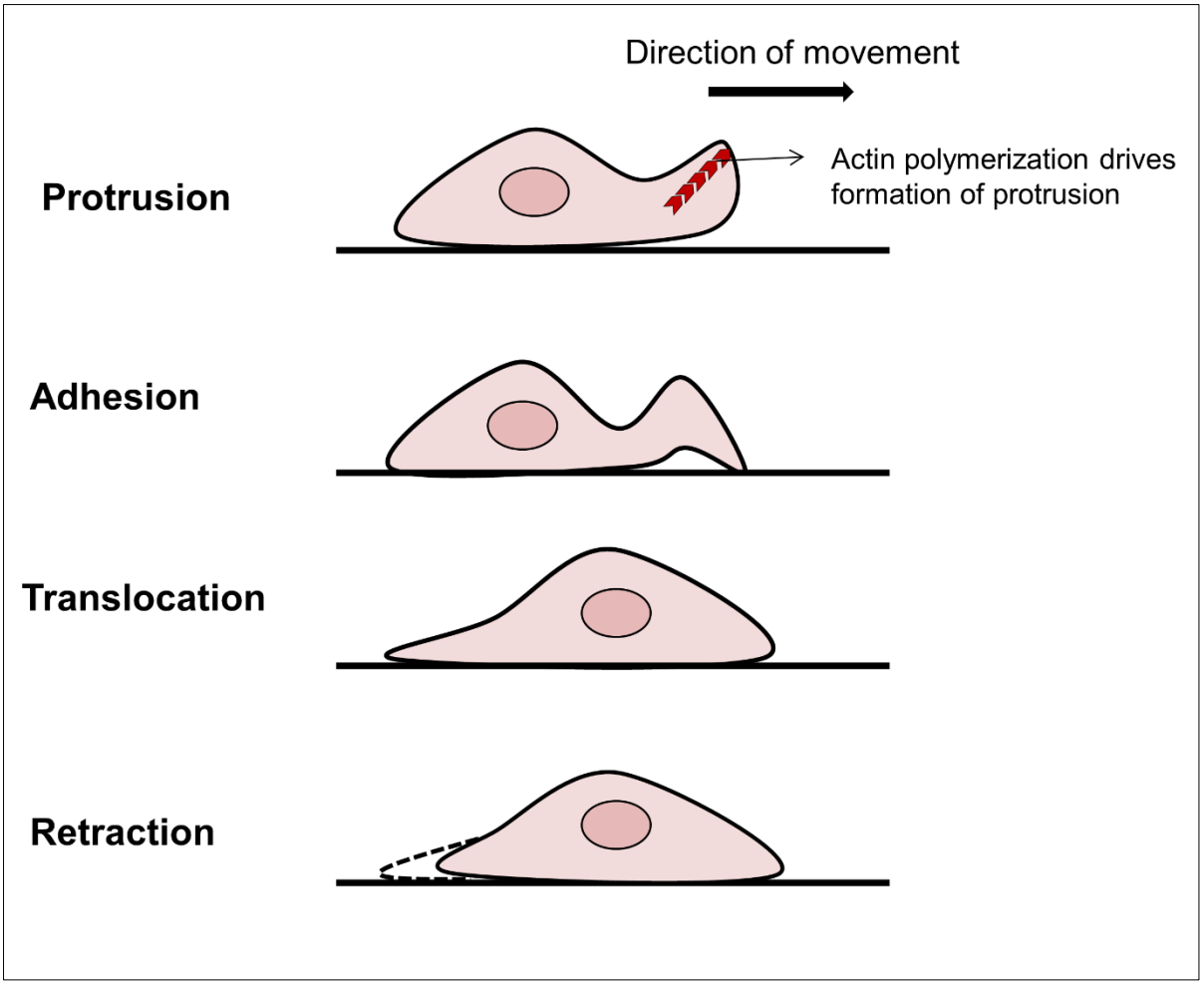

Figure 1.1 - Schematic diagram showing the process of cell migration.

Protrusions are formed at the leading edge of a cell due to actin polymerisation, which pushes the cell membrane forward. The protrusion then adheres to the extracellular matrix via focal adhesion points. This is followed by the translocation of the cell body and the retraction of the trailing edge (Adapted from Yamazaki et al., 2005)

1.2 The Cytoskeleton

The cytoskeleton consists of three components; intermediate filaments, microtubules and microfilaments (Liang and MacRae, 1997). The microtubules have a hollow cylindrical structure and are made up of various isoforms of tubulin. The intermediate filaments are made up of fibrous proteins that are super-coiled into rope-like cables. A number of different classes of intermediate filament proteins exist (Franke et al., 1978; Liang and MacRae, 1997). Lastly, microfilaments mostly consist of the protein actin, and are the thinnest and most flexible component of the cytoskeleton (Ishikawa et al., 1968; Wen and Janmey, 2011). As the microtubules and microfilaments are mostly involved in cell migration (Woodham and Machesky, 2014), these cytoskeletal components will be focused on for the remainder of this section.

1.2.1 Microtubules and tubulin

Microtubules are made of protofilaments consisting of α- and β- tubulin heterodimers which are organised in a head to tail manner. Thirteen of these protofilaments allow the formation of a hollow tubule (Mandelkow et al., 1995). The one end of the filament is referred to as the plus or dynamic end; and at this end β-tubulin is exposed and is undergoing shrinking (catastrophe) or growing (Kirschner and Mitchison, 1986). The presence of a guanosine triphosphate (GTP) cap regulates whether the microtubule is growing or shrinking (Howard and Hyman, 2009; Mitchison and Kirschner, 1984). Growth of microtubules occur when GTP bound tubulin binds to the end of the microtubule and it forms a stabilising GTP cap. When the GTP becomes hydrolysed and forms guanosine diphosphate (GDP), the bound tubulin changes conformation and becomes bent outward resulting in the promotion of depolymerisation of the microtubule (Howard and Hyman, 2009; Mitchison and Kirschner, 1984).

The minus end of the microtubule is typically embedded in the main microtubule organising centre and does not undergo any growth (Kaverina and Straube, 2011). In cells, microtubules do not spontaneously grow or shrink. Instead, this seems to be spatially and temporally regulated, whereby microtubules in the cytoplasm are consistently growing but those at the edge of the cell are undergoing more stochastic transitions between growth and shrinkage (Komarova et al., 2002). These dynamics are controlled by a number of microtubule regulatory factors otherwise known as microtubule associated proteins (MAPs) (Kaverina and Straube, 2011).

Microtubules function in cell polarisation during cell migration. This is achieved by the asymmetrical distribution and dynamics of the microtubules. In the front of the cell, there is a greater amount of microtubules in comparison to the rear end of the cell (Fukata et al., 2002; Kaverina and Straube, 2011). There is also an increased amount of stabilisation of the microtubules as well as the inhibition of regulatory factors which promote catastrophe of the microtubules (Mimori-Kiyosue et al., 2005; Niethammer et al., 2004). At the rear end of the cell, there is a surplus of catastrophe promoting factors, particularly at the adhesion sites located at the trailing edge of the cell (Niethammer et al., 2004). These tubulin binding proteins are subsequently regulated by microtubule-affinity-regulating kinases (MARKs) by phosphorylating MAPs at their tubulin binding domain, resulting in their detachment from tubulin (Drewes et al., 1998).

1.2.2 Microfilaments and actin

The actin cytoskeleton is largely responsible for the formation of the protrusive structures at the leading edge of a motile cell. There are two forms of actin present in the cell, the monomeric globular form otherwise known as G-actin, which has a molecular mass of 42 kDa and is soluble; and the polymerised, filamentous form, F-actin, which makes up the helical

microfilaments of the cytoskeleton (Dominguez and Holmes, 2011). Each of the subunits of F-actin is arranged in a head to tail fashion which results in the filament having two opposing molecular polarities at each end (Dominguez and Holmes, 2011). In order for a filament to form it is necessary for actin nucleation to take place, whereby an actin dimer or trimer must be produced (Sept and McCammon, 2001; Tobacman and Korn, 1983). The one end of the formed filament is known as the minus end or the pointed end, whereas the other end is known as the plus end, fast growing end or the barbed end (Dominguez and Holmes, 2011). Typically it is the barbed end which is positioned towards the leading edge of the cell (Atilgan et al., 2005; Small et al., 1978). The barbed end is favoured for actin assembly and therefore growth. This end grows approximately 5-10 times faster than the pointed end during polymerisation, whereas, during the steady state of actin polymerisation, the assembly rate at the plus end occurs at the same rate as disassembly at the minus end (Lorenz et al., 1993; Steinmetz et al., 1997). This process is known as actin treadmilling and forms the basis for protrusion formation (Figure 1.2).

In the monomeric form, actin hydrolyses adenosine triphosphate (ATP) at a very slow rate. Upon polymerisation, there is a conformational change of the subunits, which results in the more rapid hydrolysis of ATP. At this point, an intermediate phase exists, where ADP.P_i (inorganic phosphate bound to ADP at the γ-position) is bound to actin. The γ-phosphate slowly dissociates from actin. At the pointed end, the older adenosine diphosphate (ADP)-bound actin can be dissembled more rapidly from the filament. Following this event, actin monomers are recycled as nucleotide exchange occurs and the actin monomer can once again bind to the actin filament (Pollard and Borisy, 2003; Watanabe and Mitchison, 2002). Together this results in slow treadmilling. A number of proteins which bind to actin, otherwise known as actin binding proteins, increase this rate to promote actin treadmilling and allow cell motility (Fujiwara et al., 2007; Pollard and Borisy, 2003). For example, ADF/cofilin (actin depolymerisation factor)

increases the rate of treadmilling by binding ADP-actin and promoting the dissociation of actin monomers from the pointed end of the filament (Paavilainen et al., 2004; Ressad et al., 1998). Another actin binding protein, profilin, is also able to increase the rate of actin treadmilling by promoting nucleotide exchange as well as encouraging the binding of new actin monomers at the barbed end of the filament (Ampe et al., 1988; Baek et al., 2008; Didry et al., 1998).

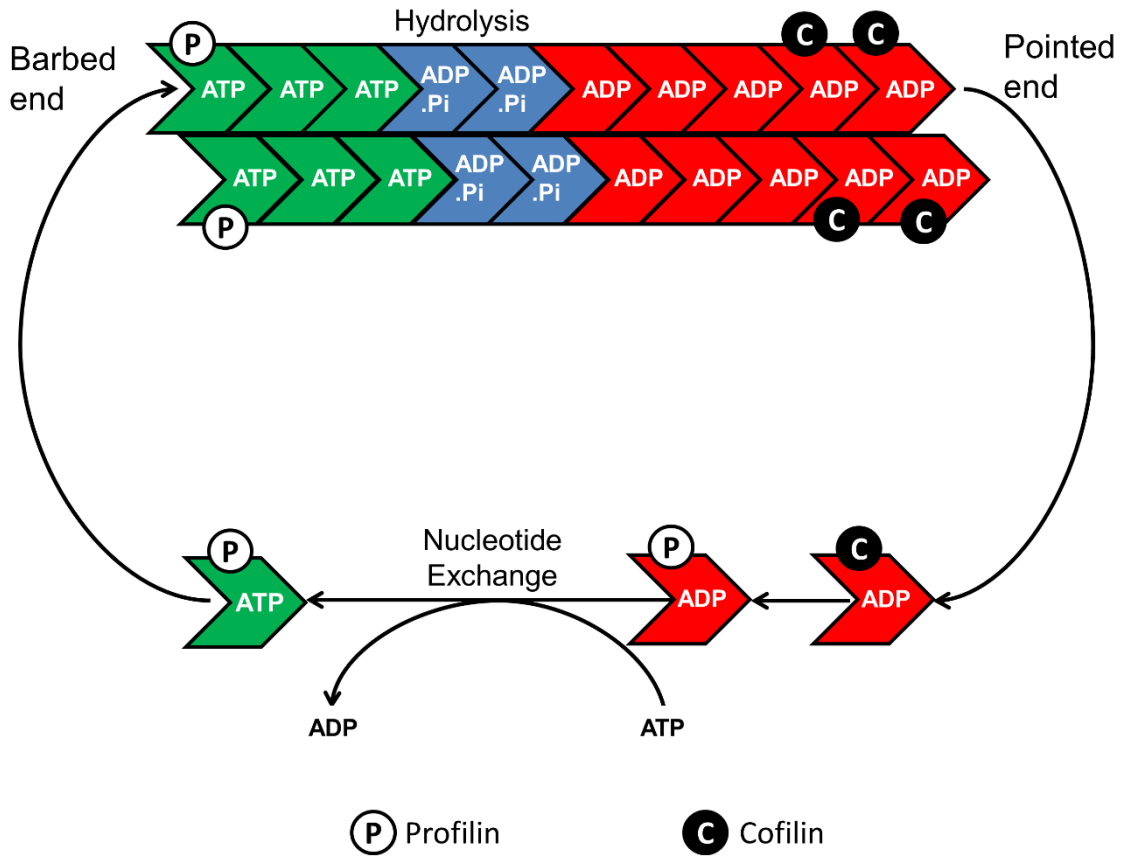

Figure 1.2 – The treadmilling process in F-actin.

Schematic diagram showing the mechanism of actin treadmilling, where the addition of ATP-bound actin at the barbed end occurs with assistance from profilin. ATP is hydrolysed as the filament matures which eventually results in the release of P_i. ADP-bound actin is depolymerised from the pointed end by cofilin, after which the actin monomer is bound by profilin to promote nucleotide exchange, allowing the monomer to be recycled (Adapted from Holt and Koffer, 2001)

1.3 Signalling pathways in actin dynamics

Signalling pathways in actin dynamics differ between various types of migration, such as amoeboid, mesenchymal or collective cell migration as well as in the formation of different membrane protrusions (Insall and Machesky, 2009; Lammermann et al., 2008; Mitchison and Cramer, 1996). For the purpose of this thesis, the signalling pathways for lamellipodia in mesenchymal migration will be focused on.

The Rho family of small GTPases is very important, as they are some of the earlier proteins to be stimulated by growth factors in the cascade of cell signalling which results in actin polymerisation and cell migration (Nobes and Hall, 1995; Ridley and Hall, 1992). This is done as they cycle between the inactive GDP-bound state and the active GTP-bound state. When in the GTP-bound state, the Rho proteins are able to stimulate downstream effectors. Within this family of proteins, RhoA, Rac1 and Cdc42 are most commonly involved in actin polymerisation, usually in the stimulation of the WASP (Wiskott-Alrich-syndrome protein) family proteins which include WASP, neuronal WASP (N-WASP) and WASP-fmaily verprolin-homologous protein (WAVE) (Miki and Takenawa, 1998; Miki et al., 1998; Symons et al., 1996). WASP/WAVE proteins induce actin polymerisation via the Arp2/3 complex. In the lamellipodium, the Rho family proteins, Cdc42 and Rac1, stimulate WASP and WAVE isoforms respectively, which in turn lead to the activation of the actin nucleating activity of the Arp2/3 complex (Machesky and Insall, 1998; Suetsugu et al., 1999a).

The Arp2/3 complex is important in assisting in the nucleation of the actin filament. In order for conditions to be energetically favourable for polymerisation, a nucleus of three actin monomers must be available (Havrylenko et al., 2014; Mullins et al., 1998). The Arp2/3 complex allows nucleation to occur from the side of existing filaments; this results in

branching, an important feature for cell motility (Mullins et al., 1998; Winder and Ayscough, 2005).

1.4 Actin Binding Proteins

Downstream of the signalling proteins which control actin dynamics exist a number of proteins which directly interact with actin. There are several different types of actin binding proteins (ABPs) which are generally classified by the form of actin to which they bind. This includes monomeric actin (G-actin), filamentous actin (F-actin) and bundled actin (Winder and Ayscough, 2005).

G-actin binding proteins have a number of functions which regulate the dynamics of the actin cytoskeleton. In order for cell migration to occur it is necessary to ensure the amount of G-actin available is regulated. One of the functions of G-actin binding proteins is to sequester the monomeric pool of actin. This group of ABPs also bind ADP bound monomeric actin that has been severed from filaments, while other ABPs assist in the nucleotide exchange of ADP to ATP. Thereafter, monomeric ABPs deliver the ATP bound actin to the barbed end of the filament. Furthermore, some are involved with the nucleation process itself, assisting in the formation of new filaments (Kinley et al., 2003). There are a number of monomer actin binding proteins present in the cell, each of these can be grouped in six major classes; profilin, ADF/cofilin, twinfilin, Srv2/cyclase-associated protein (CAP), WASP/WAVE and verprolin/WASP-interacting protein (WIP) (Paavilainen et al., 2004).

Many F-actin binding proteins are responsible for the regulation of actin filament growth, as well as its stability and disassembly (Casella et al., 1987; Mullins et al., 1998; Ressad et al., 1998). Capping proteins control the length of the filament by binding either the barbed or pointed end of actin (Casella et al., 1987; Weber et al., 1994). By capping the barded end of a

filament the ABP (like gelsolin and tensin) prevents the addition of more actin monomers and therefore stops filament growth. Binding the pointed end of actin, however, results in a decrease in the loss of actin monomers leading to enhanced depolymerisation of the filament. F-actin binding proteins are often involved in the alteration of the geometry of the filament (McGough et al., 1997). An example of ABP with such a function is cofilin. Although this protein has been previously classified as a G-actin binding protein, it is also a well-studied and essential F-actin binding protein (Bravo-Cordero et al., 2013). Cofilin is largely responsible for the depolymerisation of actin filaments (Carlier et al., 1997). Tropomyosins belong to another significant family of F-actin ABPs as they stabilise the filament and protect it from severing proteins such as cofilin (Ujfalusi et al., 2012; Weigt et al., 1990).

Actin bundling proteins assist in the arrangement of the newly formed actin filaments into parallel or anti parallel alignments on formation of linear arrays. These proteins typically have two actin binding domains or a single binding site, in which case, the protein would occur as a dimer (Winder and Ayscough, 2005). The topography of these proteins has an effect on whether the bundles formed are tight or loose. ABPs which have two actin binding sites result in tight bundles, whereas ABPs with one binding site per subunit result in more loose bundles (Courson and Rock, 2010; Stevenson et al., 2012).

Another group of proteins exists, known as side-binders and signallers (Winder and Ayscough, 2005). These bind F-actin and function within the signalling networks in order to recruit other proteins which assist in the remodelling of the actin filaments. These include proteins such as vasodilator-stimulated phosphoprotein (VASP) and vinculin, whose polyproline regions are typically associated with the recruitment of profilin (Holt and Koffer, 2001).

Of these ABPs, some are essential for actin turnover in migrating cells. Two of these essential proteins include cofilin and profilin (Bisi et al., 2013; Le Clainche and Carlier, 2008).

1.4.1 Cofilin

Cofilin is a small protein of 18 kDa and has two isoforms, cofilin 1 and cofilin 2. Cofilin 1 is found in the majority of adult and embryonic cells, whereas cofilin 2 is only found in muscle cells (Vartiainen et al., 2002). Cofilin binds to the ADP-bound F-actin at the pointed end of the filament and promotes dissociation of the monomer (Paavilainen et al., 2004). In doing so, it results in a thirty fold increase in the rate at which monomers are dissembled, therefore increasing the rate of treadmilling (Ressad et al., 1998). After the disassembly of actin monomers from the filament, cofilin inhibits ADP exchange (Carlier et al., 1997). The affinity of cofilin for G-actin is regulated by cofilin phosphorylation at the residue Ser_3. Therefore, when cofilin becomes phosphorylated, ADP-G-actin is released and nucleotide exchange can occur (Agnew et al., 1995; Morgan et al., 1993). This phosphorylation is regulated by LIM-kinase proteins 1 and 2 (LIMK-1 and LIMK-2), where LIMK-1 is mostly found in neuronal cells and LIMK-2 is found in the majority of cell types (Arber et al., 1998; Bernard et al., 1994; Yang et al., 1998). The LIMK proteins are in turn controlled by members of the small GTPase family (Yang et al., 1998). Cofilin activity is also controlled by the membrane lipids phosphatidylinositol 4-phosphate (PIP) and phosphatidylinositol 4,5-biphosphate (PIP_2). These membrane lipids bind to the actin binding site of cofilin at residues 104-115 and by doing so inhibit this domain (Yonezawa et al., 1990; Yonezawa et al., 1991a). Cofilin is also found in the nucleus under conditions of cellular stress. A nuclear localisation signal (NLS) exists on cofilin, and during heat shock the NLS becomes exposed and available to bind a nuclear transport factor allowing passage of cofilin through nuclear pores via active transportation (Iida et al., 1992).

1.4.2 Profilin

Profilin is solely an actin monomer binding protein with a molecular mass of 19 kDa. It is highly expressed and distributed throughout the cytoplasm (Ampe et al., 1988; Buss et al.,

1992). It functions in the promotion of nucleotide exchange in actin monomers which have been released from the actin filament. This is achieved by controlling the opening of the nucleotide cleft by binding subdomains 1 and 3 of actin near the hinge, which in turn results in a 10 000 fold increase in the rate of nucleotide exchange (Baek et al., 2008; Goldschmidt-Clermont et al., 1992). In the presence of cofilin, profilin is able to promote filament turnover. While cofilin promotes disassembly of actin monomers at the pointed end, profilin promotes the association of actin monomers at the growing end. This is done by inhibition of the hydrolysis of the ATP bound to actin, therefore maintaining the high affinity of the actin monomer for the growing end of the filament (Ampe et al., 1988; Didry et al., 1998). Similarly to cofilin, PIP and PIP_2 have the ability to inhibit the binding of profilin to actin, and therefore play a role in the regulation of profilin activities (Goldschmidt-Clermont et al., 1990).

1.5 The interaction between ABPs and actin

Each of these ABPs requires a specific motif to interact with actin. A number of different motifs exist, with some ABPs containing more than one (Table 1.1). Only a handful of these interactions have been studied in detail with the complex structure determined (Dominguez, 2004).

Cofilin has more than one actin binding site. The hexapeptide sequence (DAIKKK) was studied as it is identical to the evolutionary conserved N-terminal portion of tropomyosin, another well described ABP (Hitchcock-DeGregori and Heald, 1987). The DAIKKK region of tropomyosin is thought to possibly play a regulatory role in the tropomyosin-actin interaction (Yonezawa et al., 1989). Cofilin and tropomyosin compete with one another for the binding of F-actin. Yonezawa et al. (1989) suggested that the lysine and alanine residues of this motif may play an important role in the cofilin-actin interaction. It was proposed that the interaction between cofilin and actin may occur at the N-terminal portion of actin, which is rich in acidic residues,

which would suggest an electrostatic interaction with the basic residues of the DAIKKK motif. This was supported by the finding that the binding of cofilin to actin was inhibited at high ionic strengths, and the three consecutive basic lysine residues present in the sequence were ideal for this type of interaction (Yonezawa et al., 1989). Although this motif was shown to bind to actin, the heptapeptide sequence alone was unable to depolymerise F-actin and did not show pH-dependent activity. Consequently, it was later determined that cofilin has another actin binding motif which is necessary for the cofilin-actin interaction (Yonezawa et al., 1991b). This second region found to interact with actin was between the Trp_{104} – Met_{115} residues of cofilin. A dodecapeptide designed around this region was found to inhibit the cofilin-actin interaction as well as inhibit the depolymerisation action of cofilin (Yonezawa et al., 1991b).

In the case of profilin, the sequence of residues, GTAANVVEKLADYLIGQGF are responsible for actin binding. Furthermore, single amino acids have been identified which are responsible for the interaction (Schlüter et al., 1998; Wittenmayer et al., 2004). The structure of profilin bound to actin has also been determined, describing the regions of profilin which make contact with actin (Kaiser and Pollard, 1996; Schutt et al., 1993). In the human profilin-actin interaction, the Tyr_{59} residue has been shown to be important in the actin interaction. Point mutations of this residue (Y59A) result in a dramatic reduction in the ability of profilin to bind actin, but do not have an effect on the interaction with profilin and polyproline regions (Wittenmayer et al., 2004).

Amongst the known interactions, there seems to be a common hydrophobic cleft with which ABPs associate (Dominguez, 2004). The cleft is located between subdomains 1 and 3 of actin. The C-terminal portion of actin may also be involved as it typically lines the cleft. The cleft is thought to be highly adaptable as it binds a variety of proteins and is long enough to simultaneously bind more than one protein whose binding sites do not overlap (Dominguez, 2004). Proteins that would be able to interact with this cleft require an α helix with few exposed

and conserved hydrophobic amino acids (Dominguez, 2004). Both cofilin and profilin are examples of proteins known to interact with this cleft (Baek et al., 2008; McGough et al., 1997). A hydrophobic pocket also exists at the front of the hydrophobic cleft that is conserved and is thought to play an important role in mediating protein-protein interactions (Dominguez, 2004). More recently, areas of charged residues have been shown to interact with a hydrophilic cleft of the actin monomer, located between subdomains 3 and 4. Little is known about the role of this hydrophilic cleft in the interaction on actin and actin binding proteins (Chen et al., 2013).

Table 1.1 - Examples of known actin binding proteins with their functions and actin binding motifs

Actin binding Protein	Sequence	Function	Reference
Cofilin	DAIKKK, WAPECAPLKSKM	Binds ADP-bound F-actin and promotes dissociation of the monomer.	(Yonezawa et al., 1989; Yonezawa et al., 1991)
Caldesmon	NLKGAANAEAGSEKLEKQQEAAVE	Actin, myosin, tropomyosin, Ca^{2+} and calmodulin regulator.	(Wang et al., 1991)
MARKs	KRFSFKKSKLSGFSFKKN	Involved in actin crosslinking; weak bundling activity.	(Hartwig et al., 1992)
Myosin II head	IRICRKG, YRGKKQ, EGGGGKKGGKKKGSSF	ATP hydrolysis; movement of cell body; generation of cell polarity.	(Vandekerckhove and Vancompernolle, 1992)
Profilin	GTAANVVEKLADYLIGQGF	Sequesters G-actin	(Vandekerckhove et al., 1989)
Villin	PAAFSALPRWKQQNLKKEKGLF	Mediates polymerisation of actin through the severing, capping and nucleation of actin filaments	(Finidori et al., 1992; Friederich et al., 1992)

1.6 Molecular Chaperones and the cytoskeleton

Molecular chaperones are a conserved group of proteins which primarily function to assist in protein folding, prevent protein aggregation and assist in protein transportation under stressed conditions. Under normal cellular conditions, molecular chaperones are responsible for the maintenance of protein stability and protein translocation (Hartl and Hayer-Hartl, 2002; Sreedhar et al., 2004). The term "molecular chaperone" was first used for the protein nucleoplasmin, which was able to assist in the formation of nucleosomes but was not a component of the nucleosome (Laskey et al., 1978). Certain members of the heat shock protein (Hsps) family function as molecular chaperones. The mammalian Hsp are divided into multiple families according to their molecular weights (i.e. Hsp100, Hsp90, Hsp70, Hsp60, Hsp40 and small Hsps) (Liang and MacRae, 1997). Two of the most important Hsps in regulating protein homeostasis are the Hsp70 and Hsp90 molecular chaperones.

1.6.1 Heat Shock Protein 70

There are 13 different isoforms of heat shock protein 70 (Hsp70) in humans and they are present in a variety of cellular compartments. Under unstressed and stressed conditions, Hsp70 assists in the folding of newly formed proteins, the transport of proteins and vesicles, the assembly and disassembly of multi-protein complexes, as well as the degradation of denatured proteins (Bercovich et al., 1997; Frydman, 2001; Pratt and Toft, 2003). In cancer cells, Hsp70 is overexpressed and this is commonly associated with a poor prognosis (Murphy, 2013).

Though Hsp70 is not known to bind to actin, it has been found to play a role in actin dynamics in cells exposed to hyperthermia. Under these conditions, cofilin phosphatase slingshot-1L (SSH1-L) becomes insoluble, therefore leaving cofilin phosphorylated and inhibited. When Hsp70 is overexpressed, SSH1-L becomes soluble once again, resulting in the

dephosphorylation of cofilin and allowing the ABP to carry out its function (Simard et al., 2011). Hsp70 has also been shown to bind tubulin *in vitro* in the same region in which MAPs bind tubulin. Additionally, the putative tubulin binding site on Hsp70 is related to the motif with which MAP1B binds tubulin (Sanchez et al., 1994). Interestingly, Flaherty et al. (1991) reported a similarity between the atomic structures of the rabbit skeletal actin ATPase domain and the Hsp70 N-terminal ATPase domain. Between the two ATPase domains only 39 residue pairs are identical and 56 pairs are conservative substitutions out of a total of 241 residues. This information suggests that the two proteins may share a common ancestral molecule (Flaherty et al., 1991).

1.6.2 Heat Shock Protein 90

Heat shock protein 90 (Hsp90) is one of the most abundant molecular chaperones in eukaryotic cells. There are five different isoforms of Hsp90 that have been identified. Two are present in the cytoplasm, namely Hsp90α and Hsp90β, while glucose regulated protein 94 (Grp94) is found in the endoplasmic reticulum. Other forms include mitochondrial tumour necrosis factor receptor-associated protein 1 (TRAP1) and membrane-Hsp90N, which is still disputed by some as a bona fide isoform. All five of these isoforms have a similar structure and function, which is achieved via a general mechanism involving a cyclic conformational change dependent on ATP hydrolysis (Johnson, 2012). Hsp90 exists in the cell as a homodimer where each subunit is composed of three domains, the N-terminal ATPase domain, the middle domain which is involved in client protein binding and the C-terminal which contains protein-protein interaction and dimerization motifs (Prodromou and Pearl, 2003). Hsp90 works together with a number of co-chaperones and its client proteins in a multichaperone complex. This is done via a cyclic conformational change in Hsp90 whereby the binding of ATP results in a mature complex. This state allows the correct folding and stabilisation of the client protein. As a result of hydrolysis of ATP to ADP the client protein can be released (Li et al., 2012). Hsp90 has also

been found to be over-expressed in carcinoma cells, this over-expression may be vital for growth as well as survival of carcinoma cells (Mosser and Morimoto, 2004; Tsutsumi and Neckers, 2007).

It is known that Hsp90 binds to actin *in vitro* (Koyasu et al., 1986). This has been further explored to find that Hsp90 plays a role in the bundling of actin filaments which have been formed via N-WASP and Arp2/3 complex (Park et al., 2007). Hsp90 has been shown to play a role in the stabilisation of F-actin fibres in tumour cells, whereby the inhibition of Hsp90 using the ATP competitive inhibitor 17-allylamino-17-demethoxygeldanamycin (17-AAG) resulted in decreased F-actin bundling at the plasma membrane and a loss of cellular integrity in neuroblastoma cells (Chaturvedi and Sreedhar, 2010). Conversely, a study by Amiri et al. (2007) using HeLa cells suggested that inhibition of Hsp90 by geldanamycin or 17-AAG results in the activation of Rho and this increases the amount of actin stress fibres via the Rho/ROCK signalling pathway. More recently, Taiyab & Rao (2011) have suggested that, upon inhibition of Hsp90 using 17-AAG, the levels of Hsp90 rise and decrease cell motility. It was also put forward that the increased levels of RhoA were associated with Hsp90 inhibition (Taiyab and Rao, 2011).

Hsp90 also has the ability to affect actin dynamics via cofilin through the LIMK-1 protein, one of the downstream effectors of Rho/ROCK. Hsp90 plays a role in the stabilisation of LIMK-1 by increasing its half-life. Furthermore, Hsp90 is involved in the promotion of the formation of the LIMK-1 homodimer (Li et al., 2006). This in turn promoted the inactivation of cofilin by phosphorylation through LIMK-1 (Li et al., 2006).

Not only does Hsp90 have a major impact on the actin cytoskeleton, Hsp90 has also been shown to bind tubulin *in vitro* and, upon binding, was seen to inhibit tubulin polymerisation (Garnier et al., 1998). In a different study, Hsp90 was confirmed to bind tubulin but was also

shown to protect tubulin against thermal denaturation. This was prevented by the addition of the Hsp90 inhibitor, geldanamycin (Weis et al., 2010).

1.7 Stress-Inducible Protein 1

Some of these molecular chaperones have co-chaperones which act as non-client binding proteins and assist in the functioning of the chaperones. Hsp70 and Hsp90 share a co-chaperone termed stress-inducible protein 1 (STI1) which is a well conserved and abundant protein (Nicolet and Craig, 1989; Schmid et al., 2012). Due to its ability to bind the Hsp70 and Hsp90 simultaneously, STI1 is also often referred to as Hsp70/Hsp90 organising protein (Hop). The homologues of the protein are found in a large variety of organisms; this includes the human (hSTI1), mouse (mSTI1), yeast (ySTI1) and plants amongst others (Blatch et al., 1997; Honore et al., 1992; Nicolet and Craig, 1989; Zhang et al., 2003). STI1 functions as an adapter protein, where it binds with and coordinates Hsp70 and Hsp90 during the assembly of a number of client protein complexes. It does so by directing Hsp90 to the Hsp70-client protein complexes (Chen and Smith, 1998). STI1 has both intra- and extracellular functions and has also been shown to be essential in embryonic development in the mouse (Beraldo et al., 2013).

STI1 is approximately 60 kDa in size, and its structure consists of three tetratricopeptide repeat (TPR) domains, each domain consisting of three TPR motifs. Each motif consists of conserved degenerate 34-amino acid sequences which makes up two anti-parallel α-helices, each of which are amphiphilic (Blatch and Lässle, 1999). The TPR domain consists of 3 pairs of these anti-parallel α-helices arranged in a parallel manner, which allows the formation of a groove. It is the groove of the TPR domains which is involved in the binding of ligands (Blatch and Lässle, 1999; Russell et al., 1999). Two other smaller domains are also present in STI1, these domains contain an aspartic acid-proline (DP) repeat motif. Altogether the domains are arranged as TPR1, DP1, TPR2A, TPR2B DP2 (Carrigan et al., 2005). TPR1 occurs at the N-terminal of

the protein and is known to interact with Hsp70. The C-terminal domain, TPR2B, is also believed to interact with Hsp70, yet the functions of the two domains seem to be redundant. TPR2A and TPR2B on the other hand interact with Hsp90 (Flom et al., 2007; Lee et al., 2012). Currently, there are no confirmed proteins that interact with the final C-terminal TPR2B domain alone, but it has been speculated that tubulin interacts with the C-terminal TPR domain (Flom et al., 2006; Lee et al., 2013). Domain:domain binding may also have an effect on the interaction of STI1 with Hsp70, as mutation of a carboxylate clamp point in the domains TPR2A or TPR2B decreases the Hsp70-STI1 interaction (Carrigan et al., 2006). There has been much debate as to whether STI1 functions as a dimer or as a monomer or both *in vivo*. Studies have suggested the TPR2A domain is essential for dimerisation (Flom et al., 2007). On the other hand, more recent studies by Yi et al., (2010) provided evidence of STI1 only existing as a monomer. Of the three TPR domains, only two of the crystal structures have been determined in mammals. The crystal structures of TPR1 and TPR2A along with their ligands, Hsp70 and Hsp90 respectively, have been determined (Scheufler et al., 2000). Although, the structure of both DP1 and DP2, as well as the TPR2AB domains have been determined in yeast (Schmid et al., 2012).

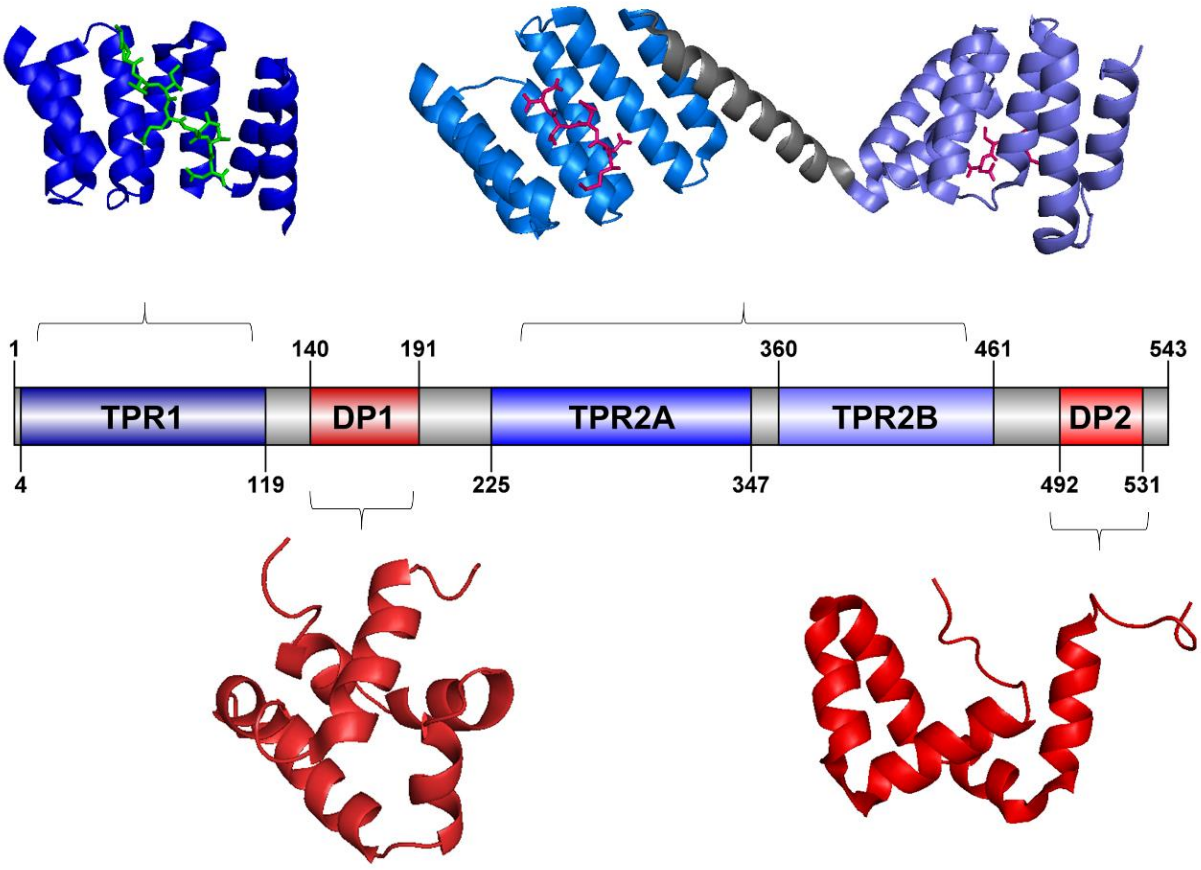

Figure 1.3 – The three dimensional structure of the STI1 domains

The diagram represents the three tetratricopeptide repeat (TPR) domains displayed in blue with their corresponding chaperone derived peptides to which they bind. Hsp70 (green) binds TPR1 via the GPTIEEVD motif and Hsp90 (pink) binds TPR2A with the MEEVD motif and the TPR2B domains with the EVD residues (Scheufler et al., 2000; Schmid et al., 2012). The residues comprising the two DP structures are displayed in red (Carrigan et al., 2005). The schematic diagram was generated using DOG 9 and PyMOL was used for the visualisation of all PDB text files. PDB IDs: 1ELR, 3UQ3, 2LLV, 2LLW.

This year, hSTI1 was shown to have the ability to bind and hydrolyse ATP, and upon doing so, undergo conformational changes (Yamamoto et al., 2014). The STI1 binding capabilities of ATP were comparable to those of Hsp70 and Hsp90, but STI1 was found to hydrolyse ATP more slowly than either Hsp70 or Hsp90. Furthermore, Hsp70 and Hsp90 change conformation upon nucleotide binding, whereas it appeared STI1 only changed conformation during ATP hydrolysis (Hessling et al., 2009; Lee et al., 2012; Yamamoto et al., 2014). The exact motif responsible for the ATPase activity could not be identified, but using a number of STI1 truncations it was determined that the TPR1-DP1-TPR2A portion of the protein had the greatest levels of ATPase activity (Yamamoto et al., 2014).

In addition to its interactions with the Hsp70 and Hsp90 chaperones, STI1 plays a prominent role as the extracellular receptor for the cell surface glycoprotein, namely cellular prion protein (PrP^C). The STI1 residues essential for this interaction have been established as Glu_{230}-Leu_{245}, and deletion of this region as well as the use of a peptide against this region results in loss of STI1- PrP^C binding (Zanata et al., 2002). Initially, this interaction was shown to have neuroprotective and neuritogenic properties in rat and mouse retinal explants and hippocampal cells (Lopes et al., 2005; Zanata et al., 2002). The PrP^C interaction with STI1 has also been shown to play a role in development, as it was shown to assist in the development of astrocytes and play a role in the protection of astrocyte death (Hartmann et al., 2013). In rats, the PrP^C-STI1 interaction was shown to modulate both long term and short term memory. The loss of this interaction has been found to result in the inhibition of these forms of memory (Coitinho et al., 2007). Through the STI1- PrP^C interaction, STI1 has also been shown to play a role in assisting in recovery from ischemic conditions. STI1 has been found to be up regulated in human and rodent brains following ischemia and promoted the proliferation of bone marrow derived cells (BMDCs) to the ischemic brain (Beraldo et al., 2013; Lee et al., 2013).

1.7.1 The role of STI1 in cell migration

There have been a number of recent reports on the role of STI1 in cell migration and its interaction with the cytoskeleton in a variety of cell types. In human glioblastoma cells, STI1 secreted from microglia cells increased cell proliferation (Fonseca et al., 2012). Furthermore, it was shown that recombinant STI1, as well as microglial secreted STI1, could promote cell migration of glioblastoma cells. It was speculated that this increase in cell migration occurs via the modulation of matrix metallopeptidase 9 (MMP-9), as MMP-9 activity decreased in the presence of an anti-STI1 antibody (Fonseca et al., 2012).

STI1 has been found to directly interact with chaperonin containing TCP-1 complex (CCT). CCT functions to assist in the correct folding of cytoskeletal proteins, including actin and tubulins. Studies have found that STI1 promotes nucleotide exchange on CCT, namely the disassociation of ADP which is then replaced by ATP. Similar to the interaction of STI1 with Hsp90, STI1 preferentially binds the ATP bound form of CCT which has a lower affinity for substrate binding (Gebauer et al., 1998).

Li et al. (2012) have recently provided evidence of STI1 playing a role in regulating angiogenesis; the process of development of new blood vessels from pre-existing ones, in which endothelial cell migration has a major contribution. Angiogenesis also plays a vital role in tumour growth, progression and metastasis in cancer (Cavallaro and Christofori, 2000). This particular study found that STI1 had a significant influence on cell polarisation as well as membrane ruffling at the leading edge of the endothelial cells, two important processes of cell migration. STI1 was also shown to interact directly with tubulin, which makes up the microtubules of the cytoskeleton (Li et al., 2012; Liang and MacRae, 1997). It was also determined that STI1 interacted with the tubulin either via the TPR1 or TPR2B domains, but not via the TPR2A domain. Truncation of this region resulted in the strongest binding affinity to tubulin/microtubules (Li et al., 2012).

STI1 has also recently been shown to directly bind a member of the small GTP-binding proteins, Rnd1 (de Souza et al., 2014). This Rnd protein is mostly found in humans in the liver and brain tissues, where is it associated with lipid rafts (Chardin, 2006; Oinuma et al., 2012). The STI1-Rnd1 interaction was shown to have an effect on the actin cytoskeletal dynamics by preventing cell collapse induced by Rnd1 and plexin-A1 in Cos-7 cells, and enhancing the establishment of longer neurites in PC-12 cells (de Souza et al., 2014).

In our laboratory, Willmer et al. (2013) showed colocalisation between STI1 and the actin pathway signalling protein, RhoC. Knockdown of STI1 resulted in decreased levels of RhoC. Additionally, Willmer et al. (2013) provided evidence of the colocalisation of STI1 and actin at the leading edges of pseudopodia in breast cancer cells using confocal microscopy. Further evidence was given of the STI1-actin interaction *in vitro* using an actin co-sedimentation assay. It was also found that STI1 knockdown resulted in the reduced formation of pseudopodia and consequently suggested that STI1 may play a role in the mediation of migration by interacting with actin during the reorganisation of the actin cytoskeleton in the formation of pseudopodia (Willmer et al., 2013). However, the motif by which STI1 binds actin was not defined in this study.

1.8 Research Motivation

Earlier work completed in our laboratory has suggested an interaction between STI1 and actin *in vitro*. Knockdown of STI1 using ribonucleic acid (RNA) interference lead to defects in pseudopodia formation by breast cancer cells. These data, together with the findings that demonstrate that STI1 can bind to the cytoskeletal protein, tubulin, have suggested that STI1 may regulate cytoskeletal dynamics by multiple mechanisms. However, there is a lack of information on the precise interaction between STI1 and actin and its role in cell migration. There is no data regarding the domains or motifs that mediate the interaction between STI1 and actin. It is therefore necessary to study the interaction to gain a better understanding of how these two proteins interact if we are to understand the role of STI1 in cytoskeletal reorganisation and in turn cell migration.

1.9 Hypothesis

One or more motifs exist within the STI1 sequence which binds actin resulting in the promotion of actin polymerisation. This is done by affecting the ATPase function of actin and possibly via the recruitment of other actin binding proteins.

1.10 Objectives

- Investigate the localisation of hSTI1 with cytoskeletal proteins and actin binding proteins in breast cancer cells
- Identification of putative actin binding motifs in STI1
- *In vitro* study of the interaction between STI1 and actin;
- Assessment of endogenous ATPase activity of murine STI1;
- Investigate the effect of STI1 on the ATPase function of actin;
- Investigate the effect of knockdown on levels and localisation of cytoskeletal protein and actin binding proteins

Chapter 2: Methods

2.1 Scanning for actin related motifs in the human STI1 amino acid sequence

To investigate whether actin or actin binding protein related motifs were present in the human STI1 (hSTI1) amino acid sequence, the sequence (AAH02987.1) was run through two online programmes, Scansite Motif Finder (http://scansite.mit.edu/motifscan_seq.phtml) and Motif Scan (http://myhits.isb-sib.ch/cgi-bin/motif_scan) which searched for various motifs present in proteins. Using the Scansite Motif Finder, the criteria were set to scan for all motifs using a high stringency level. Motif Scan was used with all the default settings. Once the scan was completed all selected identified motifs were further investigated.

2.2 Comparison of the cofilin canonical binding actin site to the hSTI1 putative actin binding site

The cofilin structure (PDB: 1Q8X) and hSTI1 TPR2A domain structure (PDB: 1ELR) were acquired from the RCSB Protein Data Bank. These structures were viewed and edited in a molecular visualisation programme, PyMOL (The PyMOL Molecular Graphics System, Version 1.5.0.4 Schrödinger, LLC). The relevant residues of the proteins were highlighted using various features of the programme. The structures, the positioning and orientation of the putative actin binding site of the hSTI1 domain as well as the canonical actin binding motif were focused on, after which the information was compared.

2.3 Pairwise alignment of hSTI1 and mSTI1 amino acid sequences

In order to determine the similarity between human (hSTI1) and murine STI1 (mSTI1) a pairwise alignment was performed of the two sequences. The STI1 amino acid sequences were obtained from NCBI for *Homo sapiens* (human: CAG38750.1) and *Mus musculus* (mouse: AAH03794.1). The multiple sequence alignment tool MAFFT was used with default

parameters to complete a pairwise alignment between the two sequences (McWilliam et al., 2013). The alignment files were viewed and the similarity and identity percentages were calculated using the BioEdit software (Hall, 1999).

2.4 Competent cell production

The two competent bacterial *Escherichia coli* (*E. coli*) cell strains, JM109 and XL1 Blue, were produced by the $CaCl_2$ method (Hanahan et al., 1991). The stocks of both strains were readily available in the laboratory. The cells were inoculated in 2 x YT broth (1.6% w/v tryptone, 1% w/v yeast extract, 0.5% w/v NaCl) overnight with shaking at 37°C. A volume of 25 ml of overnight culture was transferred into a volume of 200 ml of 2 x YT broth and grown with shaking at 37°C until an OD_{600} of 0.6 – 0.8 was reached. The cells were collected by centrifugation in a JA-14 rotor at 3800 x *g* for 10 minutes at 4°C. The supernatant was removed and pellets were resuspended in 8 ml RF1 buffer (100 mM KCl, 50 mM $MnCl_2$, 30 mM Potassium acetate, 10 mM $CaCl_2$, 15% v/v glycerol) and stored on ice for 20 minutes. Cells were centrifuged at 3800 x *g* for 10 minutes at 4°C and resuspended in 2 ml RF2 buffer (10 mM MOPS, 10 mM KCl, 75 mM $CaCl_2$, 15% v/v glycerol). Cells were aliquoted and stored at -80°C until use.

2.5 Transformation of pGEX4T-1 and pGEX3X plasmids into bacterial cells

The bacterial expression vectors (Table 2.1) were transformed into the cloning strain of *E. coli* competent cells, JM109. An amount of 100 ng DNA (deoxyribonucleic acid) per 50 µl competent cells were used for transformations. The competent cells mixed with DNA were kept on ice for 30 minutes and heat shocked at 42°C for 45 seconds. The competent cell and DNA mixture was put back on ice for 5 minutes. A volume of 250 µl 2 x YT broth was added to the competent cell mixture. The competent cells were incubated and grown without

antibiotics at 37°C for 1 hour. The competent cells were plated on an agar plate (1.6% w/v tryptone, 1% w/v yeast extract, 0.5% w/v NaCl, 1.5% w/v bacteriological agar) with ampicillin (100 µg/ml) and incubated and grown overnight at 37°C. The plasmids were isolated using the GeneJET™ Plasmid Miniprep kit (Cat #: K0503, Thermo Scientific) according to the manufacturer's instructions.

In order to confirm the correct plasmids were isolated, restriction endonuclease digestions were carried out. All plasmids (500 ng) were digested using the *Pst*I restriction endonuclease enzyme (5 units) (Table 2.1) with the complementary buffer. The digestions were incubated for 1 hour at 37°C. The total reaction volume was loaded onto a 1% (w/v) agarose gel in Tris-Acetate-EDTA (TAE; 40 mM Tris, 20 mM acetic acid, 1 mM EDTA, pH 7.6). Samples were loaded with DNA loading buffer (0.25% w/v bromophenol blue, 25% v/v glycerol). The agarose gel electrophoresis ran at 100 V for 1 hour 45 minutes, after which the bands produced were visualised under ultraviolet light using the UVIpro Chemi system (UVItec).

Table 2.1 - pGEX4T-1 and pGEX3X plasmids encoding GST and mSTI1 protein and truncations

Plasmid name	Protein encoded#	STI1 Residues	STI1 Domains	Diagnostic restriction enzyme endonuclease
pGEX3X4T-1	GST	N/A	N/A	*Pst*I
pGEX3X700	GST-N217 (C-terminal truncated mSTI1)	1-217	TPR1 and DP1	*Pst*I
pGEX3X1400	GST-C334 (N-terminal truncated mSTI1)	208-543	TPR2AB and DP2	*Pst*I
pGEX3X2000	GST-FL543 (full length mSTI1)	1-543	TPR1, DP1, TPR2AB and DP2	*Pst*I

#Refer to Figure 3.6 for schematic representations of the various mSTI1 truncations

2.6 Generation of plasmid maps

The DNA sequence for the pGEX4T-1 plasmid was obtained from the Addgene vector database. The pGEX3X700, pGEX3X1400 and pGEX3X2000 plasmids were sequenced (Inqaba Biotec). The sequences were entered in BioEdit software and a plasmid map was generated for each vector which depicted the glutathione s-transferase (GST) tag and the mSTI1 coding region as well as the positions of the *PstI* restriction sites recognised by the restriction endonuclease digestion enzymes.

2.7 Protein induction study

The pGEX4T-1 and pGEX3X vectors encoding glutathione-S-transferase (GST) and the full length and truncated mSTI1 proteins as GST fusions, respectively, were transformed using XL1 Blue *E. coli* competent cells. A single colony of each plasmid was inoculated into 5 ml of 2 x YT broth with ampicillin (100 µg/ml) and incubated with shaking at 37°C overnight. The culture was used to inoculate 50 ml of 2 x YT with ampicillin broth and incubated at 37°C until an OD_{600} reading of 0.6 to 0.8 was reached. Protein expression was induced with isopropyl β-D-1-thiogalactopyranoside (IPTG; 1 mM) and the culture continued to shake at 37°C, during which 2 ml samples were taken at hourly intervals from the culture (up to 6 hours as well as an overnight sample). From the samples, 1 ml was used to obtain an OD_{600} reading and the other 1 ml was centrifuged for 1 minute at 13 000 x *g*. The supernatant was removed and the pellet was resuspended in Tris-Buffered Saline (TBS; 50 mM Tris-HCl, pH 7.6, 150 mM NaCl). The volume of TBS used was dependent on the OD_{600} reading and was calculated using formula (OD_{600}/0.5 x 150 = x ml TBS). From each of the resuspended samples, 80 µl was mixed with 20 µl of 5 x sodium dodecyl sulphate (SDS) sample buffer (250 mM Tris-HCl, pH 6.8, 10% w/v SDS, 30% v/v glycerol, 5% v/v β-mercaptoethanol, 0.02% w/v bromophenol blue) and

boiled for 5 minutes in a water bath. Samples were stored at -20°C until analysis by sodium dodecyl sulphate polyacrylamide gel electrophoresis (SDS-PAGE).

2.8 SDS-PAGE and Coomassie Staining

Samples were analysed using discontinuous sodium dodecyl sulphate polyacrylamide gel electrophoresis (SDS-PAGE) according to Laemmli, (1970). The proteins were separated using a 12% (v/v) or 14% (v/v) resolving gel (1.5 M Tris-HCl, pH 8.8), depending on the sizes of the proteins to be resolved, and a 4% (v/v) stacking gel (0.5 M Tris-HCl, pH 6.8). The gels underwent electrophoresis for 1 hour and 30 minutes at 100 V in 1 x SDS running buffer (0.25 mM Tris, 192 mM glycine, 1% w/v SDS). Gels were stained by Coomassie staining (0.25% w/v Coomassie Blue R250, 40% v/v methanol, 7% v/v glacial acetic acid) for 1 hour, followed by a destain solution (40% v/v methanol, 7% v/v glacial acetic acid) which required a number of changes. This was repeated until the background became clear and the blue protein bands were visible.

2.9 GST and GST-mSTI1 protein expression and purification using glutathione (GSH) affinity chromatography

The pGEX4T-1 and pGEX3X plasmids were transformed into XLI Blue competent cells as described previously. After a single colony was selected, it was inoculated in 25 ml of 2 x YT broth with ampicillin and incubated at 37°C overnight with shaking. The culture was added to 225 ml 2 x YT broth with ampicillin and was kept at 37°C while shaking until an OD_{600} value of 0.6-0.8 was reached. IPTG (1 mM) was added to the culture and protein expression was induced for 3 hours with shaking at 37°C. The GST-tagged proteins were purified using an adapted batch purification protocol in the Pierce® Glutathione (GSH) Agarose User Manual. In order to prepare the *E. coli* lysate, cells were collected by centrifugation at 6000 x *g* at 4°C

for 15 minutes. The supernatant was removed and discarded. The pellet was resuspended in 5 ml cold TBS and lysozyme (1 mg/ml) and phenylmethanesulphonyl fluoride (PMSF; 1 mM) was added. The resuspended cells were sonicated at 4°C over a period of 6 minutes with 30 seconds on and 30 seconds off, and thereafter centrifuged at 4300 x *g* (Megafuge 1.0R, Heraeus) at 4°C for 45 minutes and the supernatant was collected.

A final bed volume of 0.2 ml GSH agarose (Cat #: 16100, Thermo Scientific) per 1 ml lysate was used to isolate GST-tagged proteins. The beads were incubated with the *E. coli* lysate for 30 minutes at room temperature with mixing. The beads were collected by centrifugation at 500 x *g* for 5 minutes. The supernatant was decanted and discarded. The beads were washed three times using 1.5 ml TBS, whereby the beads were collected by centrifugation at 500 x *g* for 5 minutes between each wash step. The beads were transferred to a 1.5 ml microfuge tube and elutions (GSH elution buffer; 10 mM glutathione, 50mM Tris-HCl, pH 8.0) were carried out as described in the manual and repeated three times. At each step of the purification, 80 µl samples were taken and mixed with 20 µl of 5 x SDS sample buffer. The samples were run on an SDS-PAGE gel and analysed using Coomassie staining and/or western blot analysis. Protein concentration was determined using the Nanodrop2000 spectrophotometer (Thermo Scientific).

2.10 GST tag cleavage of the purified mSTI1 protein and its truncations at the Factor Xa site

For some studies, the GST tag was cleaved from the mSTI1 proteins using the Factor Xa Cleavage Capture kit (Millipore, United States of America). To determine the optimal incubation period and Factor Xa concentration, purified GST-N217 was used for small scale optimisation. GST-N217 (10 µg) bound to GSH agarose beads was incubated at 25°C in a 50 µl reaction with Factor Xa at various concentrations (0, 4, 10 and 20 µg/ml). Samples were

taken at increasing incubation times (2, 4, 8 and 16 hours), mixed with 5 x SDS sample buffer and boiled for 5 minutes. Samples were analysed using SDS-PAGE followed by Coomassie staining.

Following the optimisation process, GST-tagged mSTI1 proteins were purified from the respective induced *E.coli* lysates as described in section 2.9, with the exception that the proteins were not eluted from the GSH-resin. Instead, the GST-mSTI1 proteins bound to the GSH agarose beads were incubated with the Factor Xa enzyme (10 μg/ml) overnight at 25°C. This cleaved the GST tag and released the mSTI1 proteins into solution. The mixture was subsequently incubated with prepared 2 x settled bed volume of Xarrest agarose beads for 10 minutes which bound the Factor Xa enzyme. The Xarrest and GSH agarose beads were removed by placing the total volume into a spin filter column which was centrifuged at 1000 × *g* for 5 min. The cleaved GST-tag bound to the GSH resin and the Xarrest agarose beads were retained by the spin filter column. The mSTI1 proteins were eluted and a sample of each protein taken for SDS-PAGE and western blot analysis. Following the cleavage of the GST tag of the proteins GST-N217, GST-C334 and GST-FL543, the proteins were henceforth referred to as N217, C334 and FL543 respectively.

2.11 Western blot analysis

Proteins were transferred from a SDS-PAGE gel to a nitrocellulose membrane and visualised according to Towbin et al. (1979). After running a SDS-PAGE gel, the gel and a nitrocellulose membrane (Bio-Rad) were soaked in western transfer buffer (25 mM Tris, 190 mM glycine, 20% v/v methanol) buffer for 10 minutes. The resolved proteins were transferred onto the nitrocellulose membrane using a Semi Dry blot apparatus (SD20 Semi Dry Maxi, Lasec) at 400 mA for 50 minutes. Transferred proteins were visualised on the membrane using Ponceau stain (0.5% w/v Ponceau S, 1% v/v glacial acetic acid). The Ponceau stain was washed off

using TBS and the membrane was blocked using a blocking solution (5% w/v milk powder in TBS) for 1 hour at room temperature with shaking. The membranes were incubated with the appropriate primary antibody overnight at 4°C with gentle rocking. The membrane was washed using TBS-T (1% v/v Tween-20 in TBS) for 5 minutes with shaking at room temperature; this was repeated 3 times. The appropriate species specific HRP conjugated secondary antibody (see appendix for details) was incubated in blocking solution with the membrane at room temperature for 2 hours. The wash step was repeated three times. Using Clarity Enhanced Chemiluminescence (ECL) western substrate (Cat #: 170-5067, Bio-Rad) the membrane was visualised using the ChemiDoc™ XRS+ system (Bio-Rad).

2.12 Surface plasmon resonance spectroscopy

The surface plasmon resonance spectroscopy experiment was conducted by Morgan Hunter. All reactions were carried out using a ProteOn™ XPR36 Protein Interaction Array System (Bio-Rad) at 25°C with the running buffer, 40 mM HEPES-NaOH, pH 7.4, 150 mM KCl and 5 mM $MgCl_2$. The ProteOn™ GLM Sensor chip (Cat #: 176-5012, Bio-Rad) was initiated using 50% (v/v) glycerol and preconditioned using 0.05% (w/v) SDS and 100 mM HCl at 30 µl/min with successive 60 µl pulses in the horizontal and vertical directions. After which, a pulse each with a volume of 150 µl comprising a 1:1 mixture of EDAC and Sulfo-NHS at 30 µl/min was used to activate the GLM chip surface. Actin (rabbit muscle, Cat #: P5204, Abnova) at concentrations of 10 and 100 µg/ml in phosphate buffered saline (PBS; 137 mM NaCl, 2.7 mM KCl, 10 mM Na_2HPO_4, 2 mM KH_2PO_4) was immobilised on two ligand channels at levels equivalent to ±800 RU and ±8000 RU, respectively, in 10 mM sodium acetate, pH 4.5 (determined by preconcentration pH scouting). Free amines were blocked on a third ligand channel using 1 M ethanolamine and used as an inline reference. GST, GST-N217, GST-C334 and GST-FL543 sensograms were collected as a 100 µl/min injection for 90 seconds followed

by a 600 seconds delay where dissociation was monitored. The chip was regenerated by an 18 second pulse injection of 10 mM Tris, pH 8.0, 3 M guanidine-HCl. Duplicate injections were performed for each concentration (5 – 1000 nM) where blank buffer injections were used as a double reference subtraction. Data analysis was completed using BIAevaluation 4.1.1 (GE Healthcare) and Prism 4 (Graphpad Software).

2.13 Detection of the binding capabilities of mSTI1 with F-actin

Prior to the co-sedimentation binding assay, polymerised actin was prepared. Actin (rabbit muscle, Cat #: P5204, Abnova) was resuspended in cold buffer G (5 mM Tris-HCl, pH 8.0, 0.2 mM $CaCl_2$) at a concentration of 1 mg/ml. In order to initiate actin polymerisation a volume one tenth of the entire actin volume needed was added of polymerisation buffer (100 mM Tris-HCl, pH 7.5, 500 mM KCl, 20 mM $MgCl_2$, 10 mM ATP). The mixture was incubated for 1 hour at room temperature (25°C), after which the protein was immediately used in various binding assays (sections 2.13-2.15).

This high speed co-sedimentation protocol was adapted from the actin co-sedimentation assay described by Srivastava & Barber (2008). In each reaction requiring actin, 20 µg of the prepared polymerised F-actin was aliquoted into centrifugation tubes. In the test reactions without actin, 20 µl buffer F (90% v/v buffer G, 10% v/v polymerisation buffer) was aliquoted into centrifuge tubes. An equal amount of the test proteins (20 µg), which included GST, GST-N217, GST-C334 and GST-FL543 or bovine serum albumin (BSA), N217, C334 and FL543, with or without mSTI1 derived peptides (20 µg) was added to the reaction. In reactions with no test protein, an equal volume to that of the test protein was added of the appropriate elution buffer instead. In the case of the GST tagged proteins, GST elution buffer was used and, in the case of the untagged protein, 1 x cleavage buffer was used. The reactions were mixed by pipetting and incubated for 30 minutes at 25°C. In order to make up each of the reactions to equal

volumes (50 – 60 µl), depending on protein volumes required) buffer F was slowly pipetted down the side of the tube to ensure the reaction was not disturbed. The tubes were immediately centrifuged at 150 000 x *g* at 25°C for 1 hour 30 minutes with the Optima™ MAX-XP Ultracentrifuge (Beckman Coulter). The supernatants from each reaction were collected and mixed with 5 x SDS-PAGE sample buffer in a 5:1 ratio and stored at -20°C until needed. The pellets were resuspended in distilled water of an equal volume to the supernatant. In order to ensure the pellets were fully resuspended, the solution was pipetted up and down for 30 minutes, kept on ice for 10 minutes and pipetted up and down for another minute and mixed with 5 x SDS sample buffer in a 5:1 ratio. Samples were analysed by SDS-PAGE and Coomassie staining.

In order to estimate the binding affinity of mSTI1 to F-actin, reactions were set up using equal amounts of actin with increasing amounts of FL543. Prepared F-actin was placed in 5 centrifugation tubes (20 µg per tube). Another five tubes each contained 20 µl of buffer F. The tubes containing or lacking actin were combined with increasing amounts of FL543, i.e. 5 µg, 10 µg, 20 µg, 30 µg and 40 µg. After which, the reactions were processed in the same procedures as described above. Samples were analysed by SDS-PAGE and Coomassie staining. The densitometry of the FL543 bands and actin bands was measured using ImageJ software.

2.14 Detection of the ability of mSTI1 to enhance the formation of actin filaments

Actin (rabbit muscle, Cat #: P5204, Abnova) resuspended in buffer G was aliquoted (20 µg per reaction) into the necessary centrifuge tubes to be incubated with or without the control BSA or test protein, FL543. A volume of 20 µl of buffer G was pipetted into reactions that did not include actin. An equal amount of BSA or FL543 (20 µg) was added to the centrifuge tubes.

The elution buffer of FL543, 1 x cleavage buffer, was added as an equal volume to that of FL543 to the actin reaction containing BSA or FL543. The reactions were mixed by pipetting and incubated at 25°C for 30 minutes. A volume of 2.5 µl of polymerisation buffer was added to each tube and incubated for a further 30 minutes at 25°C. All reactions were made up to an equal volume of 50 µl by pipetting buffer F along the side of the tube. The tubes were centrifuged at 150 000 x *g* at 24 °C for 1 hour 30 minutes. The supernatants were removed and stored with 5 x SDS-PAGE sample buffer (in a 5:1 ratio) at -20°C. The pellets were resuspended as described above (Section 2.13) in distilled water in a volume equal to the supernatant and mixed with 5 x SDS-PAGE sample buffer in a 5:1 ratio. All samples were analysed by SDS-PAGE with Coomassie staining.

2.15 Detection for the ability of mSTI1 to promote the formation of actin bundles

The setup of all test tubes for the detection of actin bundling capabilities (low speed co-sedimentation assay) were carried out identically to the detection of F-actin binding capabilities. With the exception that only the GST-cleaved mSTI1 proteins were used (FL543, C334 and N217). The reactions underwent the same incubation periods at the same temperature. On centrifugation, the tubes were spun at a lower speed of 14 000 x *g* at 25°C for 1 hour. The supernatant and pellets were prepared and stored as samples in the same procedure as previously described.

2.16 mSTI1 ATPase activity assay

The mSTI1 truncations, as well as the full length protein, were tested for ATPase activity at increasing concentrations of 1.5 µM, 3 µM and 6 µM using the EnzChek phosphate assay kit according to manufacturer's instructions. In an ultraviolet (UV) compatible 96-well plate (Cat

#: 3635, Corning), each of the proteins was mixed with the recommended volume of distilled water, 20 x reaction buffer, 2-amino-6-mercapto-7-methyl- purine riboside (MESG) and purine nucleoside phosphorylase (PNP). Prior to the addition of the substrate, ATP, the reactions were incubated at 37°C for 10 minutes. ATP (0.5 mM) was added to initiate the reaction. Controls included in the experiment included no test protein, but included the substrate, ATP. The plate was incubated at 37°C for 4 hours, UV absorbance readings were taken every 10 minutes using the Synergy Mx microplate reader (BioTek) and recorded with the Gen5™ Data Analysis Software (BioTek). The absorbance was used in order to determine the rate of inorganic phosphate (P_i) being produced with the use of the phosphate standard curve. The linear rates for each of the reactions to the same time point were calculated and compared using the Prism 4 (Graphpad Software).

For the purpose of acquiring kinetic data, the above reaction was conducted, with the exception that a constant concentration of 2.5 μM FL543 was used with increasing ATP substrate concentrations (0 mM – 1 mM). These data were plotted and fitted to Michaelis-Menten graph which was used to determine the kinetic parameters with the Prism 4 (Graphpad Software).

2.17 Detection of the stimulation of actin ATPase activity by mSTI1

For the purpose of this assay, actin (rabbit muscle, Cat #: A2522, Sigma-Aldrich) was resuspended in cold distilled water at a concentration of 1 mg/ml. A concentration of 5 μM actin (rabbit muscle, Cat #: A2522, Sigma-Aldrich) was incubated with increasing but submolar concentrations (0.5 μM, 1.0 μM, 1.5 μM, 2.0 μM, 2.5 μM and 3.0 μM) of the full length mSTI1 protein, FL543. The various concentrations of FL543 were also incubated alone in order to assess endogenous ATPase activity. The reactions were initiated with $MgCl_2$ (2 mM) and $CaCl_2$ (50 mM) to initiate polymerisation and ATP (0.5 mM) to begin ATP hydrolysis. The P_i production was measured as described previously (Section 2.16).

The above experiment was repeated with the addition of the STI1 derived peptides, where a constant concentration of 2.5 μM FL543 was used together with 5 μM actin. The peptides (PP1, PP1scr, TPR2, and TPR2scr) (Figure 3.3) were incubated separately with the mixture at a concentration of 5 μM and 50 μM. In another experiment, the test peptides (PP1 and TPR2A) were incubated together and the scrambled peptides (PP1scr and TPR2scr) were incubated together in the reaction at 50 μM each. The P_i production was measured as described previously (Section 2.16).

2.18 Maintenance of HEK293T and Hs578T cell lines

The HS578T breast cancer cell line was maintained in Dulbecco's Modified Eagle Medium (DMEM) with 10% (v/v) fetal bovine serum (FBS), 2 mM L-Glutamine, 100 U/mL PSA and 2 mM insulin at 37°C, with 9% CO_2. The non-targeting (NT) and STI1 shRNA HEK293T cell lines were previously developed in our laboratory (Contu, 2014). These two cell lines were used to compare the effects of the depletion of STI1 in cells (STI1 shRNA HEK293T) in comparison to cells with normal levels of STI1 (NT shRNA HEK293T). These stable cell lines were prepared by transfection of cells using a pTRIPZ plasmid expressing a non-targeting short hairpin RNA (shRNA) or shRNA sequence specific for the knockdown of STI1. The NT and STI1 shRNA HEK293T cell lines were maintained in DMEM with 10% (v/v) FBS, 2 mM L-Glutamine, 0.1 mM non-essential amino acids, 1 mM sodium pyruvate, 100 U/ml PSA, 500 μg/mL G418 and 2 μg/ml puromycin at 37°C, with 9% CO_2.

2.19 Actin binding and cytoskeletal protein levels in NT and STI1 shRNA HEK293T cell lines

NT and STI1 shRNA HEK293T whole cell lysates were provided by Ianthe Wingate (Rhodes University, South Africa). Cells were induced to express either the control or Hop specific

shRNA with 1 µg/ml doxycycline 24 hours after seeding. Subsequent to this, the cell culture medium was spiked with 1 µg/ml doxycycline every 24 hours for a period of 72 hours. Normal conditions for cell line maintenance were kept throughout. Following the 72 hour period, the cells were trypsinised and counted. The cells were spun down at 720 x *g* for 2 minutes at 4°C and resuspended in 5 x clear SDS sample buffer (250 mM Tris-HCl, pH 6.8, 10% w/v SDS, 30% v/v glycerol, 5% v/v β-mercaptoethanol) at $5x10^3$ cells/µl. The samples were vortexed and boiled for 5 minutes. Prior to SDS-PAGE and western blot analysis the samples were mixed with 5 x SDS sample buffer. A total of 5 x 10^4 cells were loaded per lane.

2.20 Immunofluorescence and confocal microscopy

Glass coverslips were coated in 0.1% (w/v) gelatin and dried for 30 minutes at 37°C. The NT and STI1 shRNA HEK293T cell lines were seeded at 1 x 10^5 cells/ml on to the gelatin coated coverslips. After the cells were incubated for 24 hours at 37°C at 9% CO_2, the medium was replaced with fresh medium containing 1 µg/ml doxycycline for induction of the shRNA. The cells were incubated under the same conditions for 72 hours. The cells were serum starved by removing the medium and incubating the cells in Opti-MEM® Reduced Serum Medium (Cat #: 31985-062, Life Technologies) for 30 minutes. Actin polymerisation was stimulated in the cells by replacing the reduced serum medium with normal complete medium for 15 minutes. The cells were washed with cold PBS and fixed using ice cold ethanol. The coverslip was allowed to air dry and the cells permeabilised in 0.1% (v/v) Triton-X in PBS for 10 minutes at room temperature. Cells were blocked with 1% (w/v) BSA/TBS-T (1% v/v Tween-20 in TBS) for 45 minutes at room temperature with gentle rocking. Primary antibodies (see appendix) were incubated with the cells in 0.1% (w/v) BSA-TBS-T, using a 1:100 dilution, overnight at 4°C with gentle rocking. Cells were washed twice for 5 minutes with 0.1% (w/v) BSA/TBS-T. The appropriate fluorescently labelled species specific secondary antibodies were incubated

with the cells using a 1:500 dilution in 0.1% (w/v) BSA/TBS-T, for 1 hour at room temperature with gentle rocking. Cells requiring F-actin staining were subsequently incubated for 30 minutes with Actin Green™ 488 Ready Probes® Reagent (2 drops/ml PBS) (Cat #: R37110, Life Technologies). Following the incubation steps, cells were washed twice in 0.1% (w/v) BSA/TBS-T for 5 minutes. After a brief rinse with distilled water containing Hoechst 33342 (1 μg/ml) to stain the nuclei, the coverslips were allowed to air dry before mounting. The dried coverslips were mounted on to microscope slides using DAKO fluorescent mounting medium (Cat #: S3023). The edges of the coverslips were sealed using nail varnish and allowed to dry. Cells were visualised using the Zeiss LSM 780 confocal microscope. Images were processed and analysed using ZEN 2012 software (Zeiss) or ImageJ.

The immunofluorescence staining was repeated with untreated Hs578T cells using the exact protocol except with the following modifications. Cells were seeded at 1 x 10^4 cell/ml and grown until 60% confluent on normal glass coverslips and doxycycline induction was not required.

Chapter 3: Results

3.1 Colocalisation of hSTI1 and Hsp90 with cytoskeletal and actin binding proteins in Hs578T cells

Willmer et al., (2013) previously showed in our laboratory that hSTI1 colocalised with total actin in Hs578T breast cancer cells. In order to investigate whether hSTI1 associated with F-actin, or known actin binding proteins, colocalisation studies were completed in the Hs578T cell line (Figure 3.1). Actin binding proteins probed for included cofilin and profilin as both have been shown to affect actin dynamics (Finkel et al., 1994; Yang et al., 1998). Hsp90, one of the chaperones which interacts with STI1, has also been shown to play a role in actin dynamics (Park et al., 2007; Taiyab and Rao, 2011). In order to investigate whether the hSTI1-actin interaction may be in complex with STI1, or whether hSTI1 and Hsp90 may bind any actin binding proteins in complex, Hsp90 was also probed for. Pixel-on-pixel colocalisation of protein signals was compared using average Pearson's coefficients (Rr) for multiple images and the product of the differences from the mean (PDM) images which were generated using ImageJ software (Li et al., 2004).

The Pearson's coefficient represents the correlation of the intensity distribution between two channels. Values can vary between -1 and 1, where -1 represents complete negative correlation of the channels, 0 indicates no significant correlation and 1 represents perfect correlation (Zinchuk et al., 2007). The PDM image exhibits regions where the pixels are equal to the PDM value which are pseudocoloured yellow, whereas blue represents areas of complete exclusion (Higashi et al., 2010).

Hsp90 and hSTI1 showed strong colocalisation as the high Pearson's coefficient ($Rr = 0.871 \pm 0.085$) demonstrated a high correlation between the intensity of the two channels (Figure 3.1A). This was further validated by the merged and PDM image where hSTI1 and Hsp90 were both localised throughout the majority of the cytoplasm as well as at points at the leading edges of

the lamellipodia (Figure 3.1A). This correlates with literature describing an interaction between hSTI1 and Hsp90 (Johnson et al., 1998). The colocalisation analysis of the hSTI1 and actin channels showed a relatively low correlation of the channel intensities (Rr = 0.590 ± 0.38). Nonetheless, the PDM analysis in Figure 3.1B (hSTI1 + F-actin) revealed that in certain regions and F-actin structures, hSTI1 and F-actin were colocalised. Colocalisation areas included smaller actin fibres in the cytoplasm and along the thicker bundles of F-actin formed by parallel actin filaments in the long extensions of the cell (Figure 3.1B, hSTI1 + F-actin, PDM image, arrows 1 and 2, respectively). The Pearson's coefficient value between Hsp90 and F-actin (Rr = 0.651 ± 0.060) was similar to that of hSTI1 and F-actin. The areas of colocalisation of Hsp90 and F-actin appeared to vary slightly from the areas in which hSTI1 and F-actin colocalised (Figure 3.1B). In certain areas where Hsp90 and F-actin were shown to be excluded from one another in blue (Figure 3.1B, Hsp90 + F-actin, PDM image), hSTI1 and F-actin were shown to colocalise in yellow (Figure 3.1B, hSTI1 + F-actin, PDM image). This suggested a potential for hSTI1 and Hsp90 to interact with F-actin independently from one another.

Hsp90 and hSTI1 were shown to strongly colocalise with cofilin as both had high intensity pixel-on-pixel correlation values with cofilin (Rr = 0.938 ± 0.005 and 0.947 ± 0.015, respectively) (Figure 3.1C). In the case of hSTI1 and cofilin, and Hsp90 and cofilin, the patterns of colocalisation in the cells appeared to be similar. The proteins appeared to colocalise in the cytoplasm of the cells, as well as within the filopodia at the leading edges of the lamellipodia (Figure 3.1C, hSTI1 + cofilin, Hsp90 + cofilin, merged, PDM image, shown by arrow 1). This indicated a possibility of hSTI1 and Hsp90 having a role together in influencing actin dynamics via cofilin. Similar trends were seen with hSTI1 and profilin, and Hsp90 and profilin, whereby high Pearson coefficients (Rr = 0.865 ± 0.048 and 0.877 ± 0.022, respectively) indicated high correlation of the channel intensities between the two sets of proteins. hSTI1 and profilin, and Hsp90 and profilin, were found to colocalise in the cytoplasm as well as at the leading edges

of the lamellipodia (Figure 3.1D, hSTI1 + profilin, Hsp90 + profilin, merged, PDM image, shown by arrow 1). Interestingly, cells with a longer morphology and without lamellipodia seemed to have less colocalisation of hSTI1 and profilin and Hsp90 and profilin (Figure 3.1D, PDM image).

Another cytoskeletal protein which hSTI1 and Hsp90 are known to bind and interact with is tubulin (Garnier et al., 1998; Li et al., 2012). Therefore, it was also determined whether this protein association was inferred via colocalisation analysis in breast cancer cells (Figure 3.1E). The intensity correlation of hSTI1 and tubulin (Rr = 0.661 ± 0.038) suggested partial colocalisation. Hsp90 was found to be highly associated with tubulin as the intensity correlation of the two channels were very close to the value of 1 (Rr = 0.937 ± 0.015).

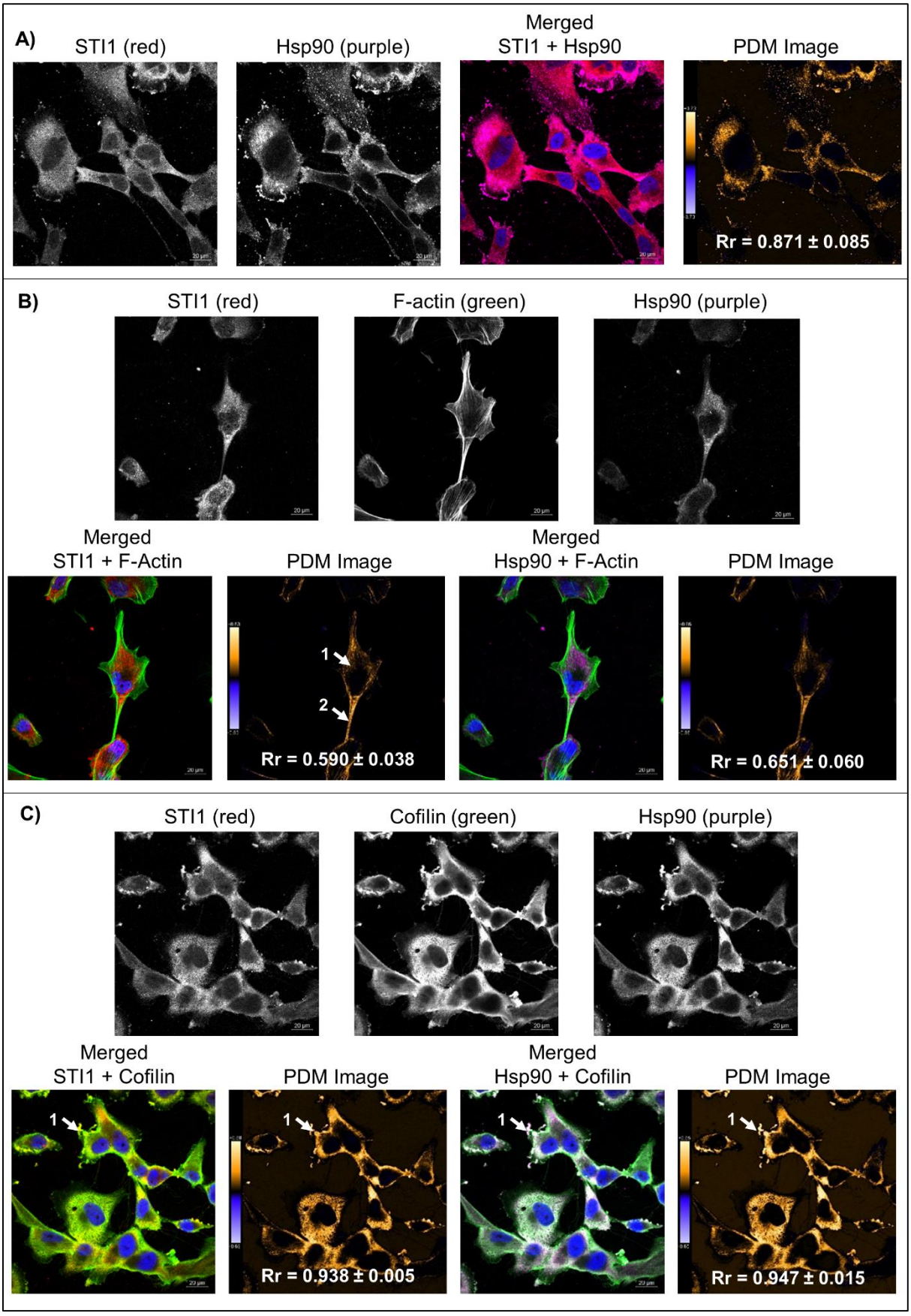

Figure 3.1 - hSTI1 and Hsp90 colocalise with tubulin, F-actin, cofilin and profilin

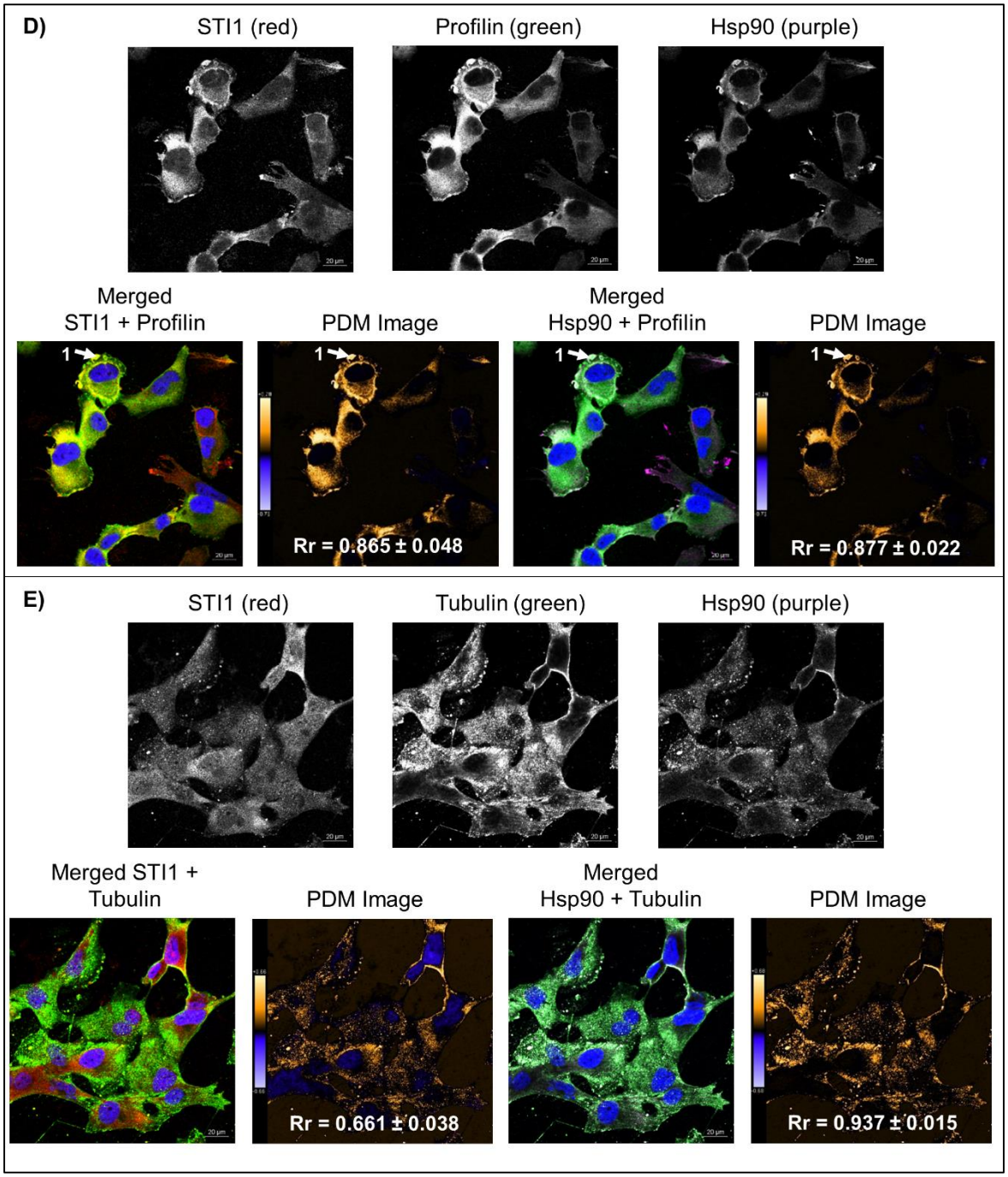

Figure 3.1 - hSTI1 and Hsp90 colocalise with tubulin, F-actin, cofilin and profilin

Hs578T cells were seeded on to glass coverslips and incubated until cells were 60% confluent. Actin polymerisation was induced by serum starvation for 30 minutes followed by serum replenishment. The cells were washed with PBS, fixed with ice cold ethanol and permeabilized with 0.1 % (v/v) Triton-X in PBS. The cells were stained with the appropriate primary and secondary antibodies for STI1, cofilin and profilin (all red) and Hsp90 (purple). F-actin was stained using ActinGreen™ 488 ReadyProbes® and the nucleus was stained blue by washing the cells with Hoechst (1 µg/ml). Coverslips were mounted onto microscopic slides using DAKO mounting medium. Cells were visualised using the Zeiss LSM 780 confocal microscope and all images captured using the equivalent laser settings. Images were processed and analysed using the intensity correlation analysis plugin on the ImageJ software (Li et al., 2004). The first row of images represents staining alone for each of the images. The second row represents the merged images of the two analysed channels and the PDM image with the calculated average Pearson's coefficient (Rr) for A) STI1 and Hsp90, B) STI1/Hsp90 and F-actin, C) STI1/Hsp90 and cofilin, D) STI1/Hsp90 and profilin, E) STI1/Hsp90 and tubulin. Scale bars represent 20 µm. Colours refer to merged images, proteins alone are shown in black and white. Arrows indicate areas of interest. Data are averages or representative of triplicate fields of equivalent cell numbers.

3.2 Identification of putative acting binding motifs in human STI1 (hSTI1)

The previous experiment showed that hSTI1 and F-actin colocalised in breast cancer cells. Moreover, earlier work in our laboratory has shown that hSTI1 co-sedimented with actin *in vitro*, suggesting a direct interaction between hSTI1 and actin (Willmer et al., 2013). Using two online motif prediction tools, a putative actin binding motif was found after the DP1 domain of hSTI1 (Figure 3.2). A proline rich area was highlighted by Motif Scan (http://scansite.mit.edu/motifscan_seq.phtml) as a weak match. Reinforcing this observation, Scansite motif finder (http://myhits.isb-sib.ch/cgi-bin/motif_scan), identified this area as a motif recognised by Src homology-3 (SH3) domains. SH3 domains are characterised by their protein-protein interactions with proline-rich domains (Alexandropoulos et al., 1995). In some cases, the polyproline region is followed by a region of positively charged, basic amino acids (Saksela and Permi, 2012). This characteristic is present in hSTI1, as the polyproline region is followed by a two lysine residues (Figure 3.2B). As well as binding to actin interacting proteins containing SH3 domains, polyproline regions are known to bind actin and play a role in actin polymerisation (He et al., 2009; Holt and Koffer, 2001; Kay et al., 2000; Urbanek et al., 2013). The WASP and tau proteins have demonstrated the ability to bind actin via a polyproline region, but the exact sequence of polyproline residues which bind actin on the amino acid sequences have not yet been determined (He et al., 2009; Urbanek et al., 2013). WASP consists of nine sets of five consecutive proline residues in the polyproline region, some of which have been identified as SH3 binding domains due to the following basic amino acids. The sets of proline residues with no basic amino acids were identified to be more important in the actin interaction, though the presence of all nine polyproline sets resulted in the strongest actin interaction (Urbanek et al., 2013). Furthermore, Urbanek et al. (2013) demonstrated in yeast, that a third of proteins containing five or more consecutive prolines were actin associated or involved in actin regulation. These data suggested the polyproline region of hSTI1 could be

involved in a direct interaction with actin or may indirectly be involved in the regulation of actin.

The hSTI1 amino acid sequence was also manually searched for known actin binding motifs from literature (Table 1.1). The residues DAYKKK present in the TPR2A domain were determined to be similar to the actin binding residues in the protein cofilin, DAIKKK (Yonezawa et al., 1989). The three dimensional structures of the cofilin and hSTI1 motifs are available as PDB files from the RCSB Protein Data Bank with the identification codes 1G8X and 1ELR, respectively. An analysis was done using PyMOL to examine the positioning of the amino acids comprising the DAYKKK motif in STI1 in comparison to the positioning of the cofilin DAIKKK motif amino acids. A similar analysis could not be completed with the polyproline motif as this structure is not available.

It was observed that the DAIKKK motif in human cofilin (Figure 3.2C) was situated at the end of an α-helical structure. The aspartic acid and the three lysine residues were solvent exposed and projected outward from the helix surface. The DAYKKK motif in human STI1 was found in the TPR2A domain of STI1, positioned at the end of an α-helix (Figure 3.2D). The motif was also in close proximity to the binding site of Hsp90. The tyrosine residue is involved in Hsp90 interactions and this specific residue is close to, and orientated towards Hsp90. The tyrosine residue makes important contacts with the methionine residue within the MEEVD sequence of Hsp90 (Odunuga et al., 2003; Scheufler et al., 2000). Similar to the DAIKKK motif in cofilin, the aspartic acid and three lysine residues were all solvent exposed. This similarity in the orientation of lysine and aspartic acid residues, together with the polar, charged nature of the amino acids, would suggest the residues were available for electrostatic protein-protein interactions and might represent a putative actin binding motif.

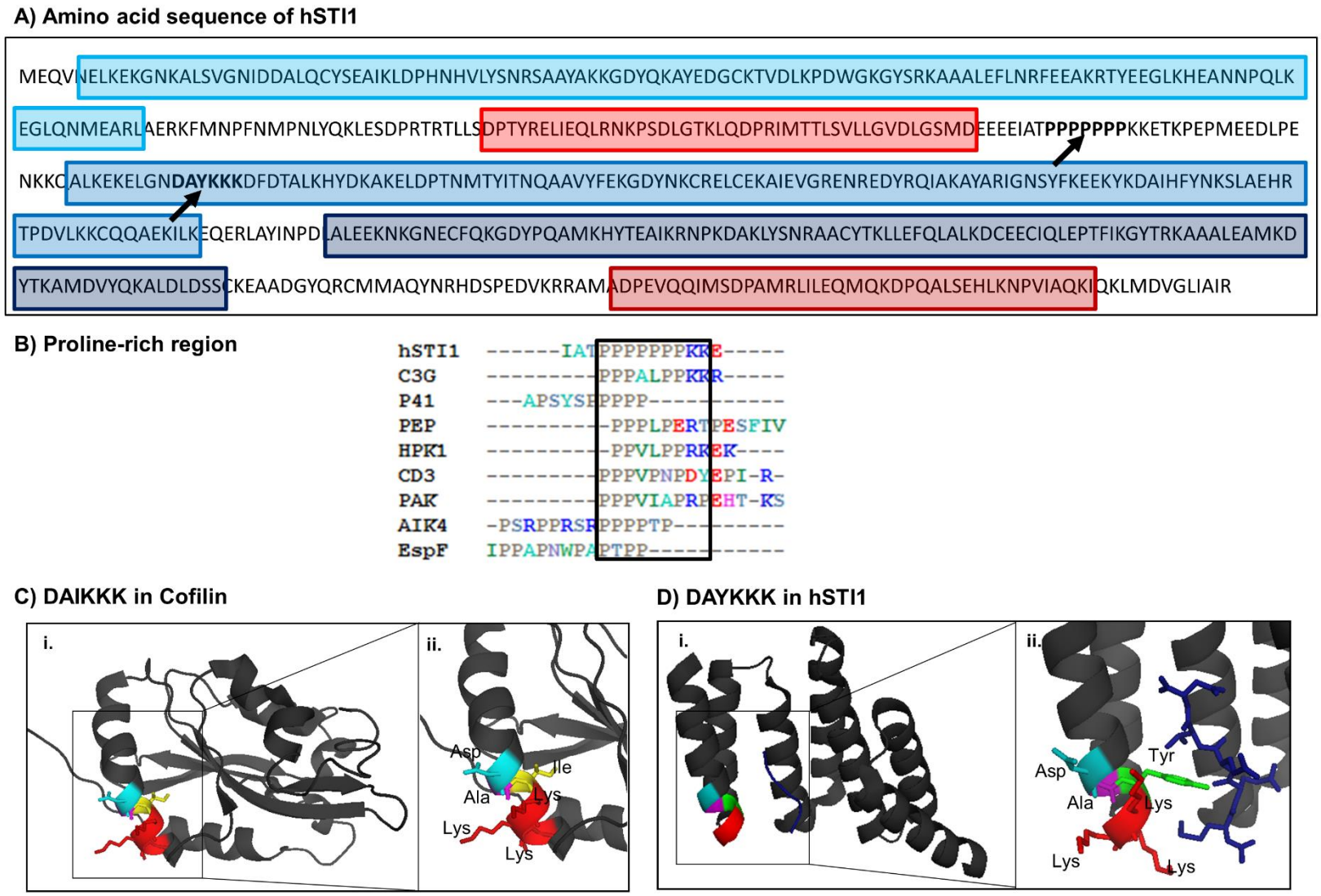

Figure 3.2 - Identification of putative actin binding sites in the hSTI1 sequence

Figure 3.2 - Identification of putative actin binding sites in the hSTI1 sequence

A) Amino acid sequence of hSTI1 (AAH02987.1). The three TPR domains are shown in boxes coloured light blue (TPR1), blue (TPR2A) and dark blue (TPR2B), the two DP domains are shown using red (DP1) and dark red (DP2) boxes and two putative actin binding sites are shown by an arrow and with a bold font. B) Putative SH3 binding motif of hSTI1 aligned with other known peptides or proteins which bind SH3 domains using Clustal Omega software and edited using the BioEdit program, positively charged amino acids are shown in red, negatively charged amino acids are shown in blue and all other amino acids are grouped by the default BioEdit colour table. The conserved polyproline region with the basic amino acids are shown within the black outline C) i. Human cofilin (PDB: 1Q8X) - coloured residues highlight the canonical actin-binding motif DAIKKK. The aspartic acid residue is coloured cyan, lysine residues are coloured red, alanine is coloured magenta and the isoleucine is coloured yellow. ii. Close up of the DAIKKK motif. D) i. TPR2A domain of STI1 (PDB: 1ELR) with coloured residues highlighting the potential actin-binding motif. Lysine residues are coloured red, alanine is coloured magenta and the tyrosine is coloured green. ii. Close up view of the DAYKKK motif. Structural images were viewed and exported in PyMOL.

3.3 Design of peptides targeting putative actin binding regions

Peptides, based on the putative actin binding sites identified, were designed to interrupt the STI1-actin interaction (Figure 3.3). The key residues were selected as those thought to possibly bind actin with additional residues included in the peptide before and after the key residues in order to ensure the peptide was of optimal length and hydrophobicity to allow easy purification. The scrambled versions of the designed peptides were used as a negative control as they contained the same amino acids but in a different order.

The polyproline and polyproline scrambled peptides (PP1 and PP1scr) contained 13 amino acid residues and had a hydrophobicity value of 12.39 and 18.6, respectively. The peptides on average should have a molecular weight of 1368.65 g/mol, and a predicted monoisotopic molecular weight of 1367.78 Da (Krokhin et al., 2004). The monoisotopic weight is the lowest possible molecular weight isotype of the peptide (Fountain, 2001). The peptide's theoretical pI was calculated to be pH 9.9. Together, this resulted in a peptide which was predicted to be easy to synthesise and purify (Figure 3.3A and B). Although it must be taken into consideration that, due to the high content of proline in the peptides, the proline may occur in different configurations, which may affect the binding capacity of the peptide. The synthesised peptides were predicted to be compatible with selected reaction monitoring (SRM) and multiple SRM (MRM), which are non-scanning mass spectrometry techniques (Krokhin et al., 2004, Thermo Fisher Scientific Biopolymer, Ulm, Germany). The TPR2A peptide and the scrambled version (TPR2 and TPR2Ascr) were both predicted to be easily synthesised and purified (Figure 3.3A and B). The peptides were 10 amino acids in length with an average molecular weight of 1243.34 g/mol. The monoisotopic value for these peptides was 1242.59 Da. The unscrambled and scrambled peptides only differ in hydrophobicity, the unscrambled peptide had a value of 10.37, whereas the scrambled peptide increased slightly to 12.46. The peptides had a theoretical

pI value of 6.9. The only foreseeable problem mentioned was the deamidation of asparagine would result in an aspartic acid residue instead. This in turn would result in a mass shift of +1 Da. The presence of the aspartic acid residue which is followed by a small amino acid, in this case alanine, could fragment due to acid catalysed formation of cyclic imide (Oliyai and Borchardt, 1993). The peptides were predicted to be compatible with SRM/MRM. All peptides were synthesised appropriately and confirmed by mass spectrometry (data not shown).

A) PP1 peptide

Input Sequence:	IATPPPPPPPKKE
Analysed Sequence:	I-A-T-P-P-P-P-P-P-P-K-K-E
Sequence length:	13
Hydrophobicity:	12.39
Mw average:	1368.6533 g/mol
Mw monoisotopic:	1367.7814
Theoretical pI:	pH 9.9

Synthesis/Purification:
Difficult — Easy

SRM/MRM compatibility:
Bad — Good

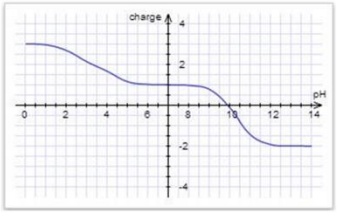

B) PP1 peptide scrambled

Input Sequence:	PIPKPTPEPAPKP
Analysed Sequence:	P-I-P-K-P-T-P-E-P-A-P-K-P
Sequence length:	13
Hydrophobicity:	18.6
Mw average:	1368.6533 g/mol
Mw monoisotopic:	1367.7814
Theoretical pI:	pH 9.9

Synthesis/Purification:
Difficult — Easy

SRM/MRM compatibility:
Bad — Good

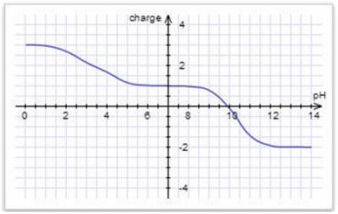

C) TPR2A peptide

Input Sequence:	NDAYKKKDFD
Analysed Sequence:	N-D-A-Y-K-K-K-D-F-D
Sequence length:	10
Hydrophobicity:	10.37
Mw average:	1243.3473 g/mol
Mw monoisotopic:	1242.5881
Theoretical pI:	pH 6.9

Synthesis/Purification:
Difficult — Easy

SRM/MRM compatibility:
Bad — Good

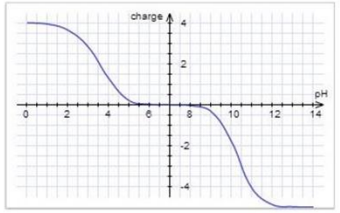

D) TPR2A peptide scrambled

Input Sequence:	KDFYKNDDKA
Analysed Sequence:	K-D-F-Y-K-N-D-D-K-A
Sequence length:	10
Hydrophobicity:	12.46
Mw average:	1243.3473 g/mol
Mw monoisotopic:	1242.5881
Theoretical pI:	pH 6.9

Synthesis/Purification:
Difficult — Easy

SRM/MRM compatibility:
Bad — Good

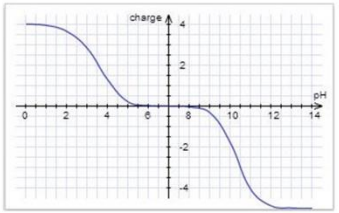

Figure 3.3 - Analysis of designed peptides to bind TPR1 and TPR2A putative actin binding sites

The results of the peptide predictions using the Peptide Analysing Tool (Thermo Fisher Scientific Biopolymers) showing sequence length, hydrophobicity, average molecular weight, monoisotopic molecular weight, theoretical pI, ease of synthesis and purification and SRM/MRM compatibility for A) PP1 peptide, B) PP1 scrambled peptide, C) TPR2A peptide and D) TPR2A scrambled peptide.

3.4 Pairwise sequence alignment and sequence analysis of human and murine STI1

As full length and truncated murine STI1 (mSTI1) protein expression constructs were readily available in the laboratory, a pairwise sequence alignment was completed to determine whether the use of mSTI1 would be a viable option for the replacement of hSTI1 in *in vitro* binding assays. The alignment of the mSTI1 and hSTI1 amino acid sequences was performed using MAFFT (Figure 3.4). Using the BLOSUM62 matrix, the sequence identity and similarity between hSTI1 and mSTI1 was calculated to be 97.4% and 98.9%. All three TPR domains were conserved between the two species, with fewer than 10 residues differing. The same was true for the two DP regions of the proteins. We have also previously demonstrated that mSTI1 can bind to Hsp70 and Hsp90 from human cell lysates, suggesting that mSTI1 can participate in similar interactions to hSTI1 (Contu, 2014). Importantly, the two putative actin binding motifs share a high identity (Figure 3.4). The highlighted PP1 peptide only has one conservative amino acid replacement at the N-terminal of the murine STI1. The amino acids against which the TPR2A peptides have been designed were completely conserved. The high identity and similarity between the two species, particularly within the two putative actin binding motifs, suggested that the existing mSTI1 constructs would be suitable for use in actin binding studies.

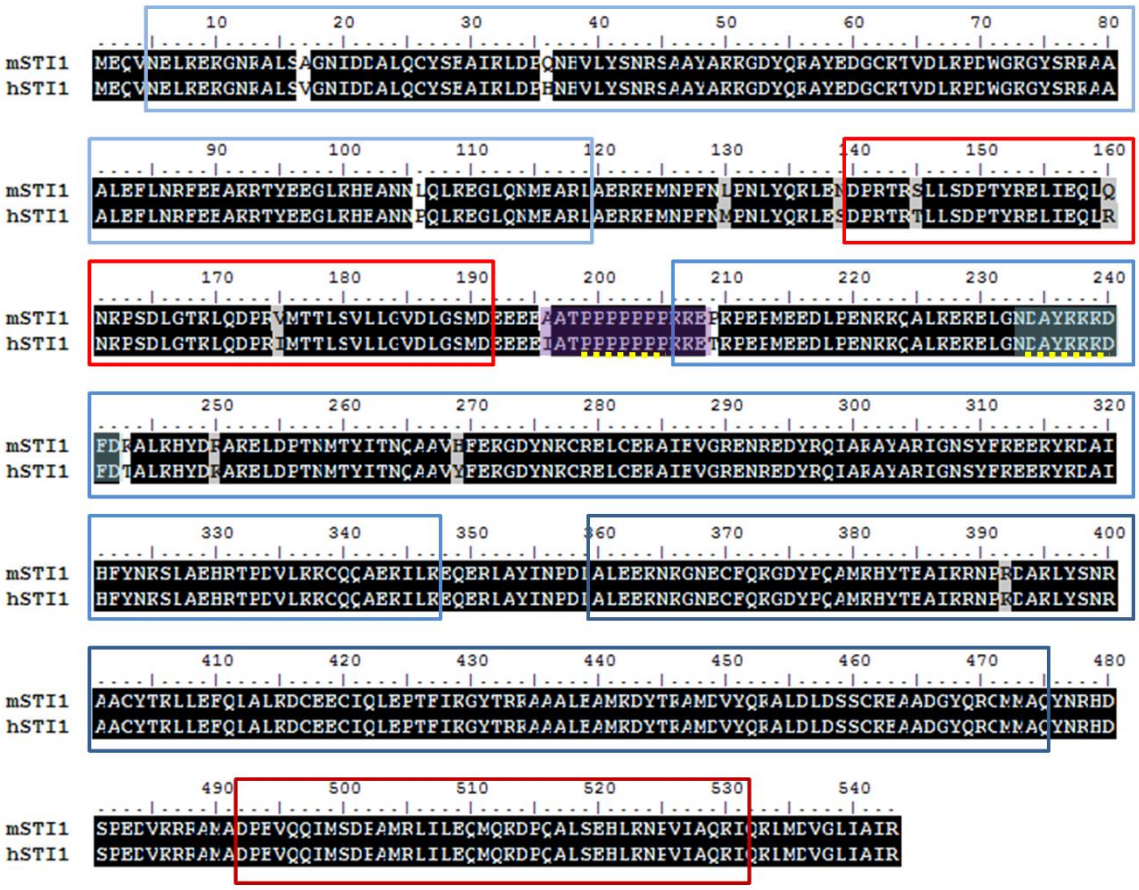

Figure 3.4 - Pairwise sequence alignment of the STI1 protein from the *Homo sapiens* and *Mus musculus* organisms

Amino acids with black shading represent identical residues and those with a grey shading are considered to be similar. The light blue, blue, and dark blue boxes represent the TPR1, TPR2A and TPR2B domains respectively. The red and dark red boxes represent the DP1 and DP2 regions respectively. The dashed yellow lines demonstrate the putative actin binding sites. The amino acids highlighted in purple and light blue show the synthesised peptide sequences.

3.5 Confirmation of correctly isolated plasmids using *Pst*I digestion

The plasmids encoding GST-N217, a C-terminal truncated mSTI1, GST-C334, a N-terminal truncated mSTI1 and GST-FL543, full length GST-tagged mSTI1, were developed as part of a previous study (Lässle et al., 1997; Odunuga et al., 2003). The plasmid identity was confirmed by restriction endonuclease digestions and sequencing (Figure 3.5). The plasmids pGEX4T-1, pGEX3X700, pGEX3X1400 and pGEX3X2000 were digested using *Pst*I. The pGEX4T-1 vector, which encodes the GST tag, is 4952 bp in size, contains only one *Pst*I site and therefore resulted in a single band of ±5000 bp (Figure 3.5A and B, lane 2). The pGEX3X700 vector encodes C-terminal truncated mSTI1, GST-N217, comprising TPR1 and DP1 (residues 1-217), and has an expected size of 5268 bp. The vector contains four *Pst*I sites, and therefore digestion should result in four band sizes of 152, 341, 1141 and 3994 bp. The digestion resulted in two visible bands of 4000 and 1000 bp (Figure 3.5C and D, lane 2). Due to the small size of the additional two fragments it was not possible to visualise them on the agarose gel. The pGEX3X1400 plasmid encodes GST-C334, N-terminal truncated mSTI1, this includes TPR2A, TPR2B and DP2 (residues 208-543). The vector has an expected size of 6385 bp and has one *Pst*I site. The digestion of this vector resulted in a single band of ±5900 bp (Figure 3.5E and F, lane 2). The pGEX3X2000 vector encodes full length mSTI1 and contains four *Pst*I sites. Digestion should therefore result in four bands of sizes 152, 341, 2528 and 3994 bp. Only two bands were large enough to be visible on the agarose gel at ±2600 and ±4300 bp (Figure 3.5G and H, lane 2). The digestion patterns of the four plasmids were equivalent to the predicted patterns suggesting the correct plasmids were isolated. This was confirmed by sequencing (data not shown).

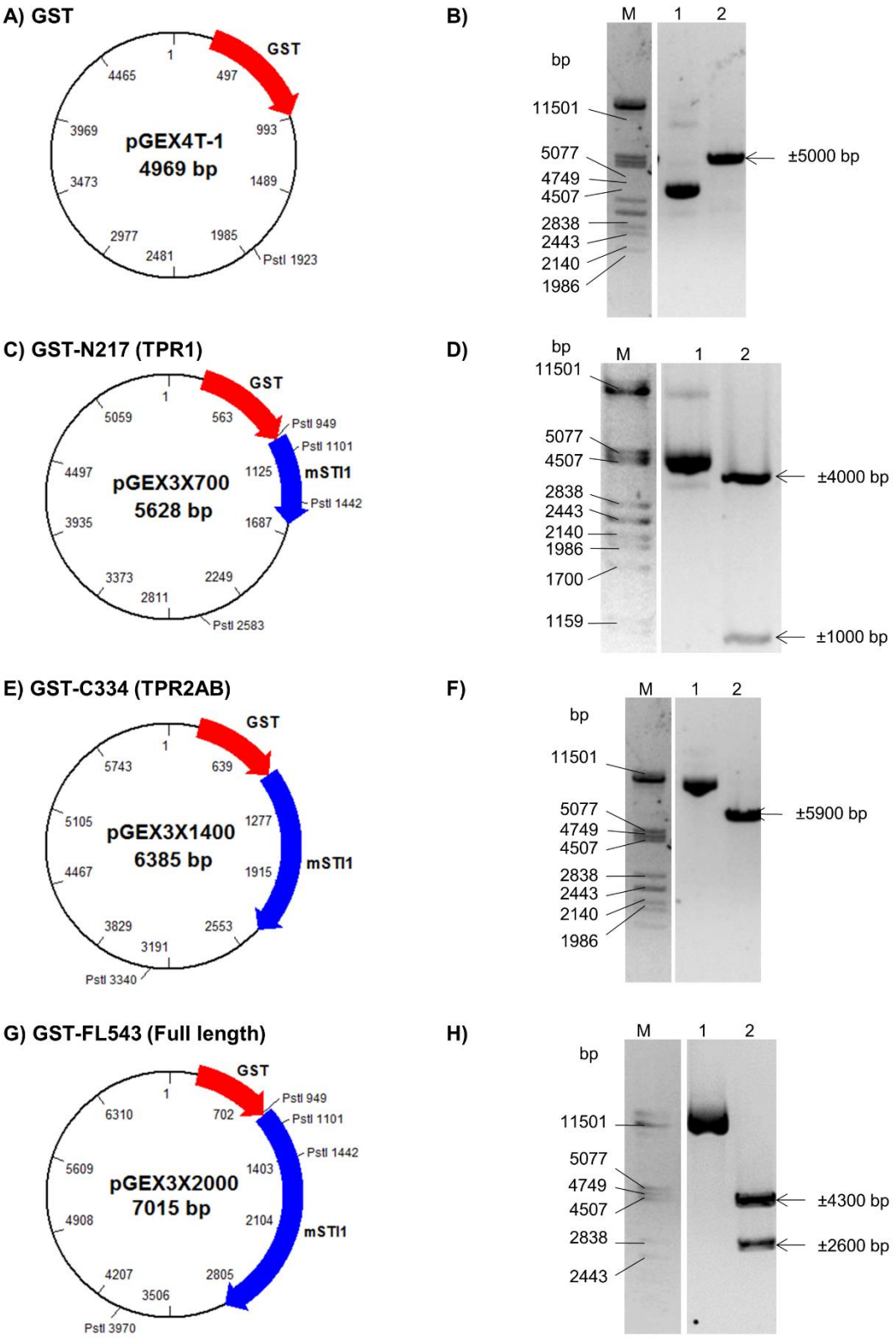

Figure 3.5 - Restriction endonuclease digests and plasmid maps of pGEX4T-1, pGEX3X700, pGEX3X1400 and pGEX3X2000

Restriction endonuclease digestion products were separated using a 1% (w/v) agarose gel in TAE at 80 V for 1 hour 45 minutes. Lane M indicates *Pst*I digestion of λ DNA, lane 1 indicates uncut plasmid and lane 2 indicates *Pst*I digestion of the plasmid. Plasmid maps were created using BioEdit. The GST coding region is shown in red, while the mSTI1 coding region is shown in blue. Plasmid maps and digestions shown for A-B) pGEX4T-1, C-D) pGEX3X700, E-F) pGEX3X1400, G-H) pGEX3X2000.

3.6 Protein induction study

The proteins, GST, GST-N217, GST-C334 and GST-FL543 (Figure 3.6A) were various mSTI1 truncations which contained differing domains of mSTI1 used to determine domains responsible for binding and functionality. GST-N217 and GST-FL543 have previously been shown to bind Hsp70 (Lässle et al., 1997; Odunuga et al., 2003). Additionally, GST-C334 and GST-FL543 have been shown to bind Hsp90 (Lässle et al., 1997). The molecular weight of each of the proteins was determined using the ExPASy online tool for computation of molecular weight (Gasteiger et al., 2005). Each of the amino acid sequences for the proteins was entered and the molecular weights of the proteins were calculated. Each of the GST fusion proteins contained a Factor Xa site, which allowed the cleavage of the GST tag in future purifications (Figure 3.6A).

Expression of proteins in *E.coli* cells transformed with the pGEX vectors encoding GST, GST-N217, GST-C334 and GST-FL543 was induced by 1 mM IPTG for a period of approximately 24 hours during which hourly samples were taken for the first 6 hours with an additional overnight (O/N) sample. Samples were analysed using SDS-PAGE and Coomassie staining (Figure 3.6).

All induction studies were successful and showed a definite induction of a protein of the correct size over the 24 hour period. GST alone showed an increased amount of protein of approximately 26 kDa, the expected size of GST (Figure 3.6B). The intensity of the band relative to the background did not increase after 5 hours post induction. The GST-N217 samples showed an increased expression of a ±48 kDa protein over time, corresponding to the predicted 50 kDa size of GST-N217. The greatest amount of induced protein was present in the 5 hours post induction sample, after which the amount of GST-N217 did not increase (Figure 3.6C). The expected size of GST-C334 is 65 kDa; the induced protein appeared slightly

below the 66.5 kDa mark. The greatest intensity of GST-C334 occurred at 5 hours post induction (Figure 3.6D). The GST-FL543 samples showed an induced protein of ±80 kDa corresponding with the expected size for GST-FL543 of 85kDa. The amount of the induced protein increased up until the 3 hours post induction sample and remained the same until the 5 hour sample and decreased again after this point (Figure 3.6E). Notably, the expression levels of GST-FL543 were much lower in comparison to the other proteins. Based on the induction study, the optimal time for subsequent inductions was selected to be 3 hours of induction as this was the minimum amount of time required to generate high levels of all proteins tested.

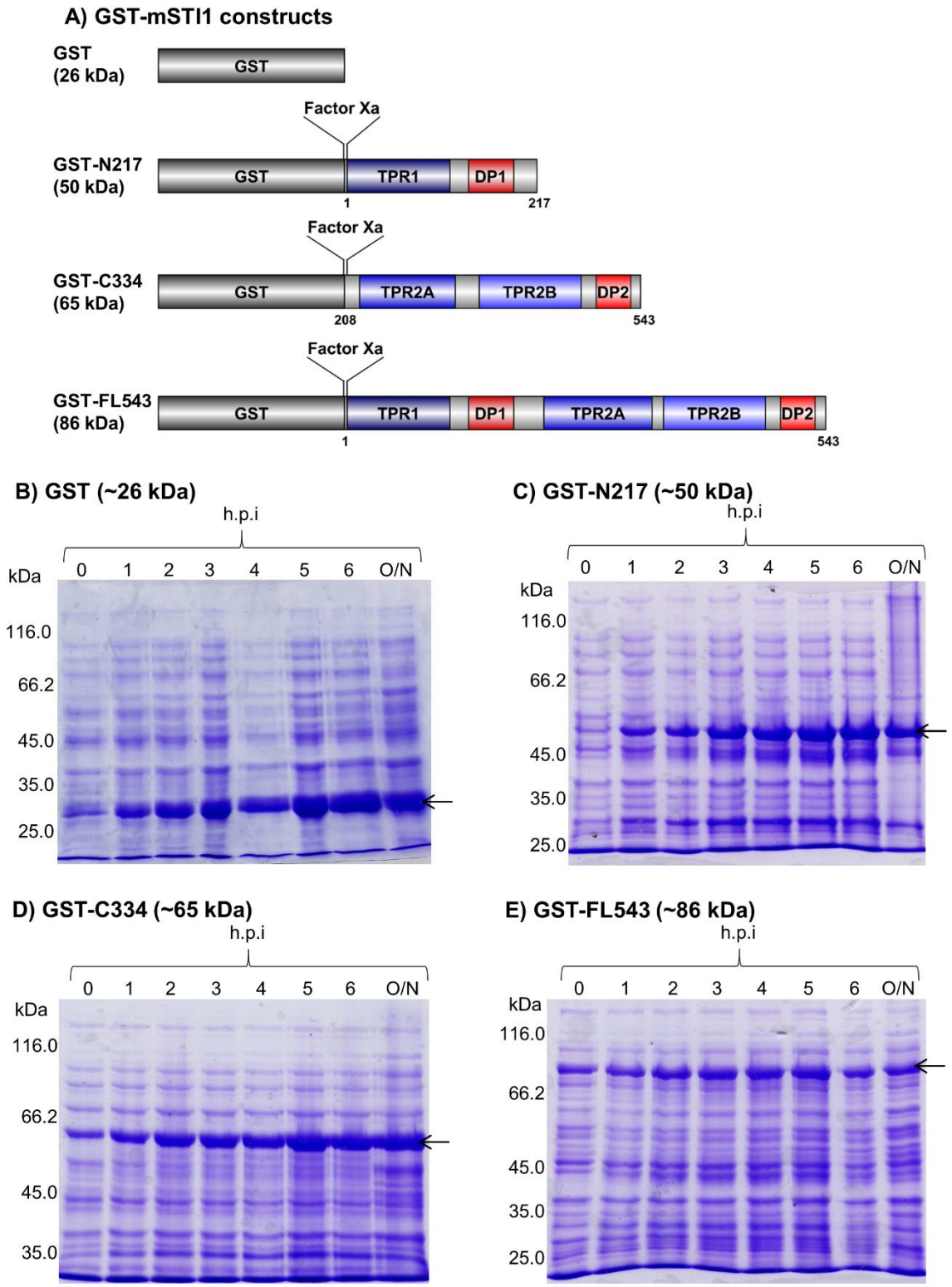

Figure 3.6 - Protein induction study of GST, GST-N217, GST-C334 and GST-FL543

A) Schematic representations of the GST and GST tagged proteins, GST-N217, GST-C334 and GST-FL543 showing domains present. B-E) Protein expression was induced in 50 ml 2 x YT broth with ampicillin by the addition of IPTG (1 mM). Samples were taken hourly at 0-6 hours post induction (h.p.i) as well as an overnight (O/N) sample. These were analysed using SDS-PAGE and Coomassie staining. B) GST C) GST-N217 D) GST-C334 E) GST-FL543. The arrow indicates the expressed protein.

3.7 Purification of GST and GST-tagged mSTI1 proteins

Prior to purification, expression of the GST, GST-N217, GST-C334 and GST-FL543 proteins were induced for 3 hours with IPTG (1 mM), after which samples were taken from each step in order to determine whether the purification was successful. The samples were analysed using SDS-PAGE and Coomassie Blue staining (Figure 3.7A – D). The first elutions from each protein were also analysed by Western blot analysis (Figure 3.7F).

The SDS-PAGE gels for the purifications of GST, GST-N217, GST-C334 and GST-FL543, a band of the relevant protein was present in the pellet (Figure 3.7A-D, lane P) representative of insoluble protein or incomplete lysis of the host cells. The cleared lysate (Figure 3.7A-D, lane CL) contained a thick band of the GST-tagged proteins at their respective sizes, 26, 50, 65, and 86 kDa. This indicated that sufficient soluble protein was available for purification. A lighter band was present at the same molecular weight in the flow through sample (Figure 3.7A-E, lane FL) which suggested that the beads were saturated and therefore small amounts of the protein were lost. The subsequent wash steps removed the majority of the non-specific proteins. The first wash contained most of the non-specific proteins and the next two wash steps mostly showed small amounts of unbound GST-tagged protein (Figure 3.7A-D, lanes W1-3). The GST elution steps produced intense bands at 26 kDa with a clear background which indicated few contaminants and degradation products were present (Figure 3.7A). In the case of GST-N217, GST-C334 and GST-FL543, the elution samples show bands at the expected sizes with a number of lighter bands below this (Figure 3.7B-D). The presence of bands of a lower weight than the purified protein, suggest the bands are likely to be degradation products (which was subsequently confirmed during Western blot analysis) (Figure 3.7F).

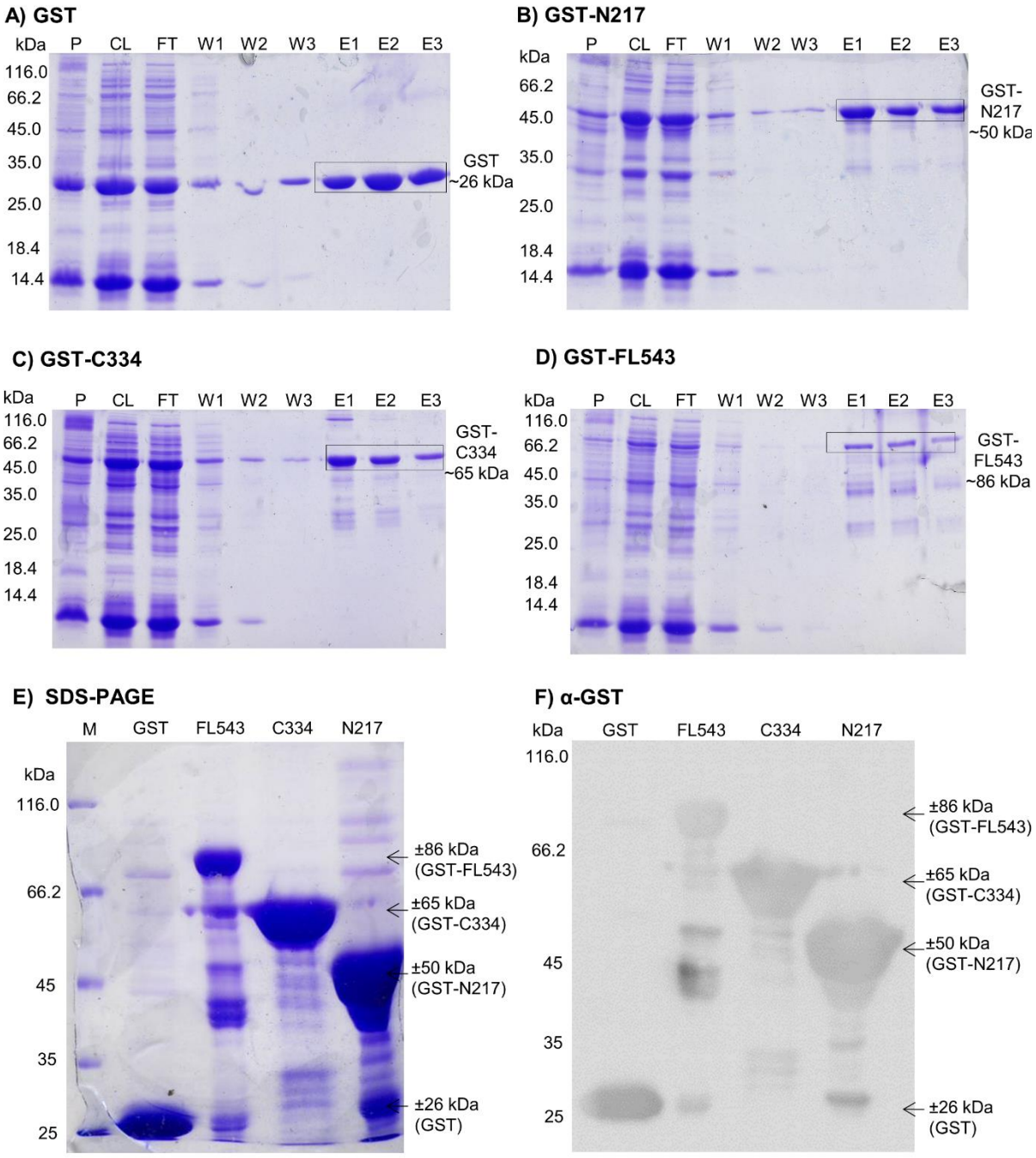

Figure 3.7 - SDS-PAGE analysis of glutathione affinity chromatography purification of GST and GST-mSTI1 proteins with western analysis of first elutions

Samples were taken during the purifications of the pellet (P), cleared lysate (CL), flow through (FT), three washes (W1, W2, W3), and three elutions (E1, E2, E3). A) GST purification. B) GST-N217 purification. C) GST-C334 purification. D) GST-FL543 purification. E) SDS-PAGE of the first elutions from each of the purifications. F) Western analysis of the first elutions using α-GST antibody with donkey α-goat IgG-HRP secondary antibody to probe for GST. All samples were separated using a 8% - 12% reducing SDS-PAGE gel. Data shown are representative of multiple independent purifications.

The first elution of each sample was analysed by SDS-PAGE and Coomassie staining as well as Western blot analysis. In addition to identifying the GST-tagged protein, Western blot analysis was used to determine whether other bands present in the elution were non-specific proteins or degradation products (Figure 3.7E and F). Western blot analysis with an anti-GST antibody confirmed that the fusion proteins were successfully purified. The smaller, lighter bands below the expected protein size shown in the Western blot correlate with the bands seen using Coomassie staining this is indicative of GST-tagged degradation products. A thin band was present above GST-N217 in the western blot analysis, this is likely to be a product of overload of the GST-C334 lane as it is of the correct size.

Independent purifications resulted in high yields for all proteins particularly with respect to the GST, GST-N217 and GST-C334 (Table 3.1). The high protein yields together with the high relative purity of the samples suggested a successful purification of all four proteins.

3.8 Optimisation of Factor Xa concentration and incubation time for GST cleavage of GST-tagged mST1 protein and truncations

For certain experiments the GST-tag was cleaved using the Factor Xa protease from all mSTI1 proteins after purification. Initially, optimisation was required to determine the best incubation time and Factor Xa concentration (Figure 3.8). The GST-N217 protein was used for the purpose of the optimisation. The GST-N217 protein had an expected size of 50 kDa. The GST tag when cleaved and released has an expected size of 26 kDa and the untagged N217 had an expected size of 25 kDa. Although, in the SDS-PAGE gel seen in Figure 3.8, the two bands representing GST and untagged N217, could not be distinguished due to the similar sizes of the proteins. A Western blot analysis using anti-GST would be necessary in order to identify the two bands. The purified GST-N217 was bound to GSH agarose beads after purification and incubated with increasing concentrations of the Factor Xa enzyme, in order to mimic the conditions this would

be performed after GST-tagged protein purification. During the optimisation, the negative control lacked the Factor Xa enzyme (Figure 3.8, 0 µg/ml). In this control some degradation occurred, which resulted in the loss GST-N217 as well as small amounts of release of the GST-tag or N217 over the incubation period (Figure 3.8A). This degradation is a common occurrence of GST fusion proteins (Magdeldin and Moser, 2012). The levels of GST-N217 decreased slightly over time, while the protein at a slightly lower molecular weight (26 kDa) had increased levels, but no increase of the protein with a higher molecular weight (28 kDa) alone was visible. When GST-N217 was incubated with 4 µg/ml Factor Xa a similar pattern was seen to the negative control, with only a slight increase in the levels of the 28 kDa protein at 6 h and 16 h. The results of incubation with 10 and 20 µg/ml Factor Xa were almost identical, whereby the levels of GST-N217 decreased throughout the incubation period and by 16 h the levels have nearly completely diminished (Figure 3.8B). There was a concomitant increase in the 28 kDa protein levels until 6 h, after which little change was seen. Therefore, for all further GST cleavage of GST-mSTI1 proteins, a concentration of 10 µg/ml of Factor Xa was used with an incubation period of 16 h.

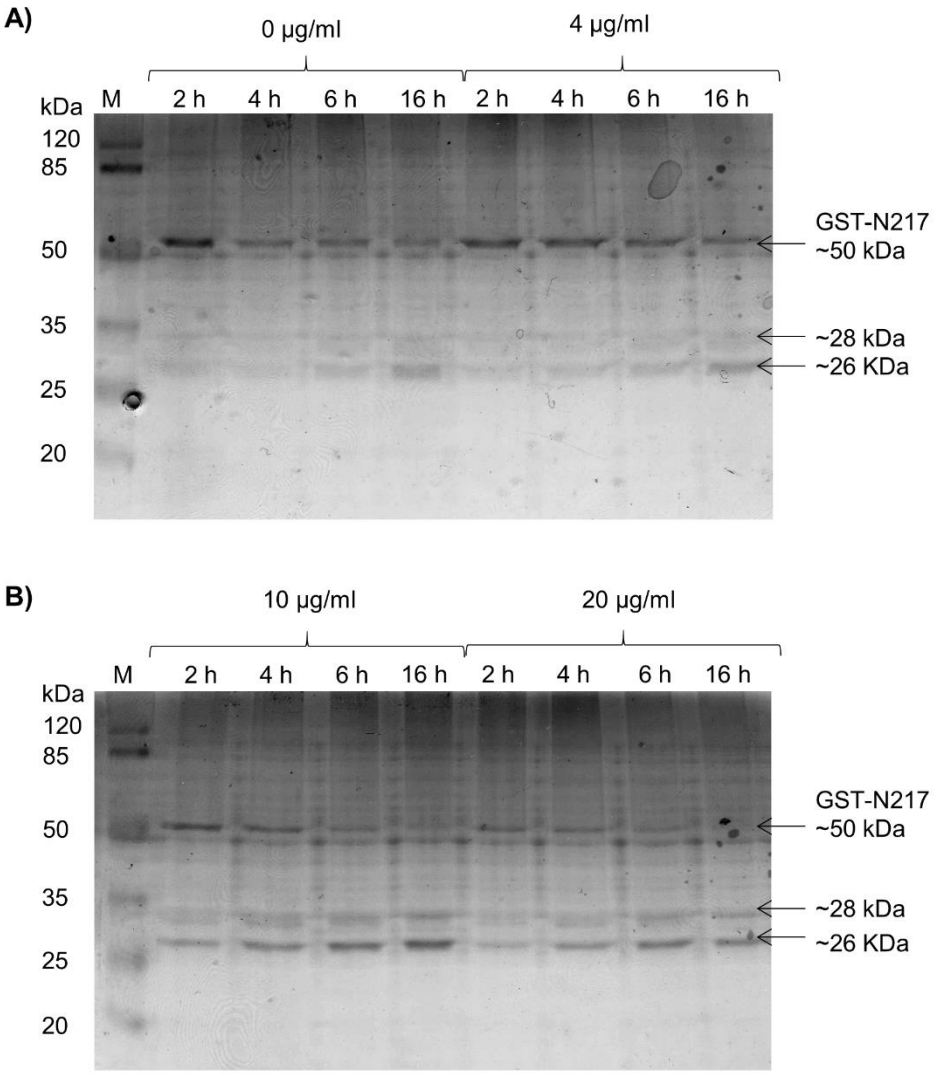

Figure 3.8 - Optimisation of the Factor Xa protease concentration and incubation time for the cleavage of the GST tag from the GST-mSTI1 fusion proteins using GST-N217

GST-N217 (10 µg) bound to GSH agarose was incubated with increasing concentrations of Factor Xa. Samples were taken at 2 h, 4 h, 6 h and 16 h. The samples were analysed using a 8% - 12% reducing SDS-PAGE gel and Coomassie staining. A) Incubation with 0 µg/ml and 4 µg/ml Factor Xa B) 10 µg/ml and 20 µg/ml Factor Xa. M – Prestained protein molecular marker.

3.9 GST-cleavage and capture of purified mSTI1 full length and truncated proteins

In order to obtain purified untagged proteins, all purification steps preceding the elution were carried out as previously described. Factor Xa (10 μg/ml) was subsequently added to the washed GSH agarose beads bound to the GST-tagged mSTI1 proteins and incubated overnight at 25°C. After this, the mixture was incubated with Xarrest beads and centrifuged in a spin column, and the supernatant fraction containing the untagged protein released from the GSH agarose was collected. The samples collected from the purification coupled to the GST cleavage were analysed by SDS-PAGE (Figure 3.9). The thick dark smear with undistinguishable bands seen in the pellet, cleared lysate and flow through samples for the N217, C334 and FL543 purifications represents lanes that had been overloaded with protein from lysates (Figure 3.9, A-C, lanes P, CL and FT). This fact, as well the presence of a large amount of GST-tagged mSTI1 proteins in the first wash samples (Figure 3.9, A-C, lane W1), suggested that the GSH agarose beads were saturated with GST-tagged protein. The fifth wash (Figure 3.9, A-C, lane W5) contained a single band correlating to the size of the purified protein together with the GST tag (GST-N217 – 50 kDa, GST-C334 – 65 kDa and GST-FL543 – 86 kDa) showing all unbound proteins had been removed. Each of the elutions (Figure 3.9, A-C, lane E) showed a decrease in size of about 26 kDa suggesting the cleavage of the GST tag was successful.

SDS-PAGE analysis of the elutions shown in Figure 3.10A demonstrated the presence of high concentrations of proteins of the expected size for the untagged proteins (N217 – 25 kDa, C334 – 39 kDa and FL543 – 60 kDa). Similarly to Figure 3.8, N217 and the GST-tag ran at very similar sizes on the gel (Figure 3.10A). The Western blot analysis using GST specific antibody shown in Figure 3.10B showed that small amounts of cleaved GST were present in all three elutions. However, only the N217 elution showed small amounts of uncleaved GST-N217

present. When probed with an antibody specific to STI1 (α-STI1), the presence of the C334 and FL543 protein was confirmed and therefore the cleavage was determined as successful (Figure 3.10C). However, the C-terminal truncated mSTI1 protein, N217, was not detectable. This suggested that the antibody used may be specific to the C-terminal region of the STI1 protein. The GST cleavage was determined to be successful due to the high protein yields (Table 3.1) and the presence of bands of the expected size for the untagged mSTI1 proteins (N217 – 25 kDa, C334 – 39 kDa and FL543 – 60 kDa) in the Coomassie stained SDS-PAGE gel, and the absence of detection of GST in the Western blot analysis (Figure 3.10A-C).

Table 3.1 - Protein yields obtained for GST-tagged and untagged mSTI1 proteins from independent purifications

Protein	Average yield (mg/L)*
GST	127.2 ± 85.8
GST-N217	97.71 ± 67.3
GST-C334	49.11 ± 34.0
GST-FL543	35.67 ± 26.0
N217	1.50 ± 0.4
C334	0.89 ± 0.2
FL543	1.4 ± 0.5

*All protein concentrations were determined by measuring absorbance at 280 nm

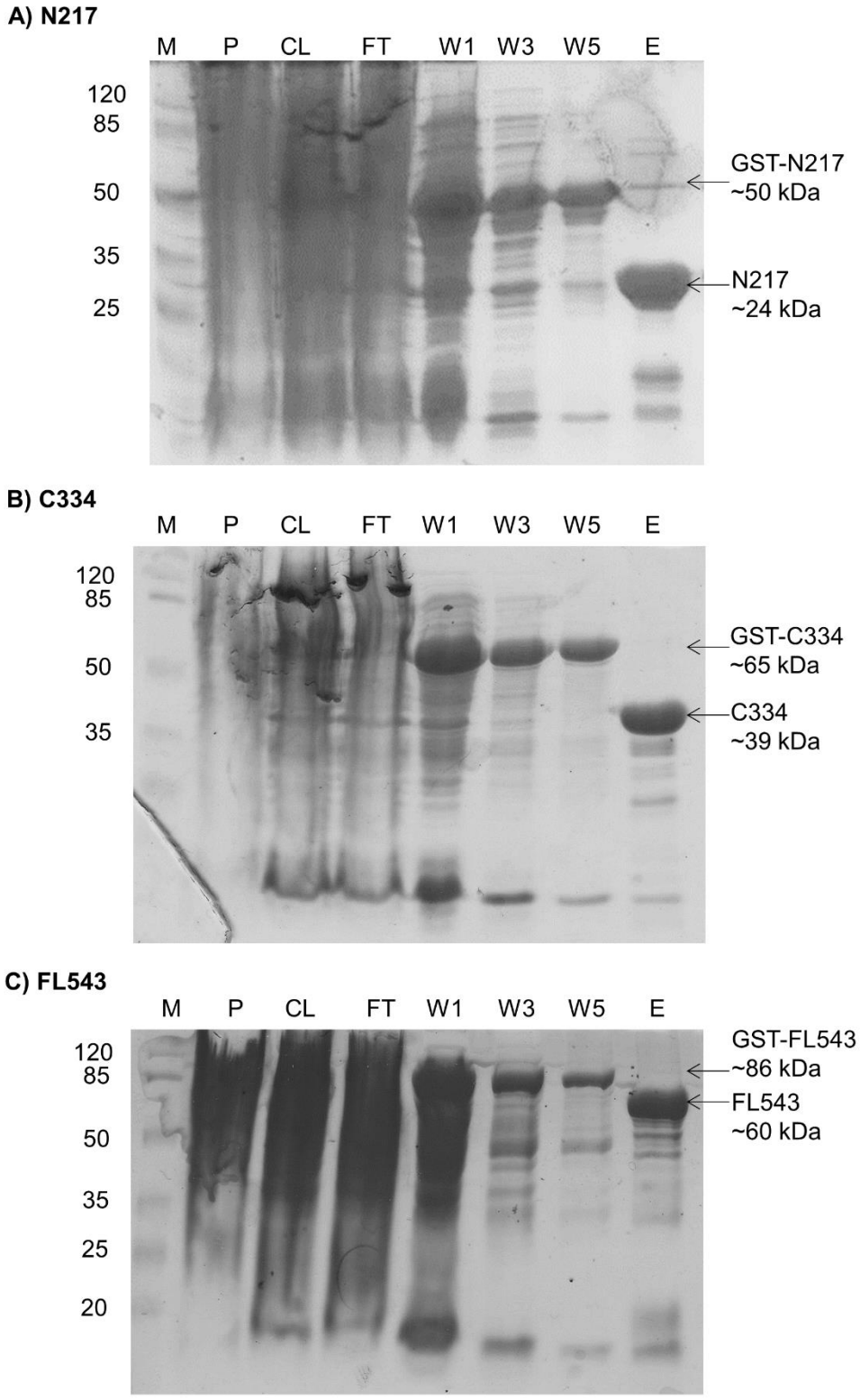

Figure 3.9 - Purification and GST tag cleavage of full length mSTI1 and truncated mSTI1

Samples were taken at various stages of the purification of the expressed GST-tagged mSTI1 and truncated mSTI1 proteins A) GST-N217 B) GST-C334 and C) GST-FL543 from XLI Blue *E. coli* lysate. M – Prestained protein marker, P – pellet, CL – cleared lysate, FT – flow through, W1 – first wash, W3 – third wash, W5 – fifth wash, E – elution after GST cleavage using Factor Xa and Xarrest agarose. Samples were separated using a 8% - 12% reducing SDS-PAGE gel and Coomassie staining. Data shown are representative of multiple independent purifications.

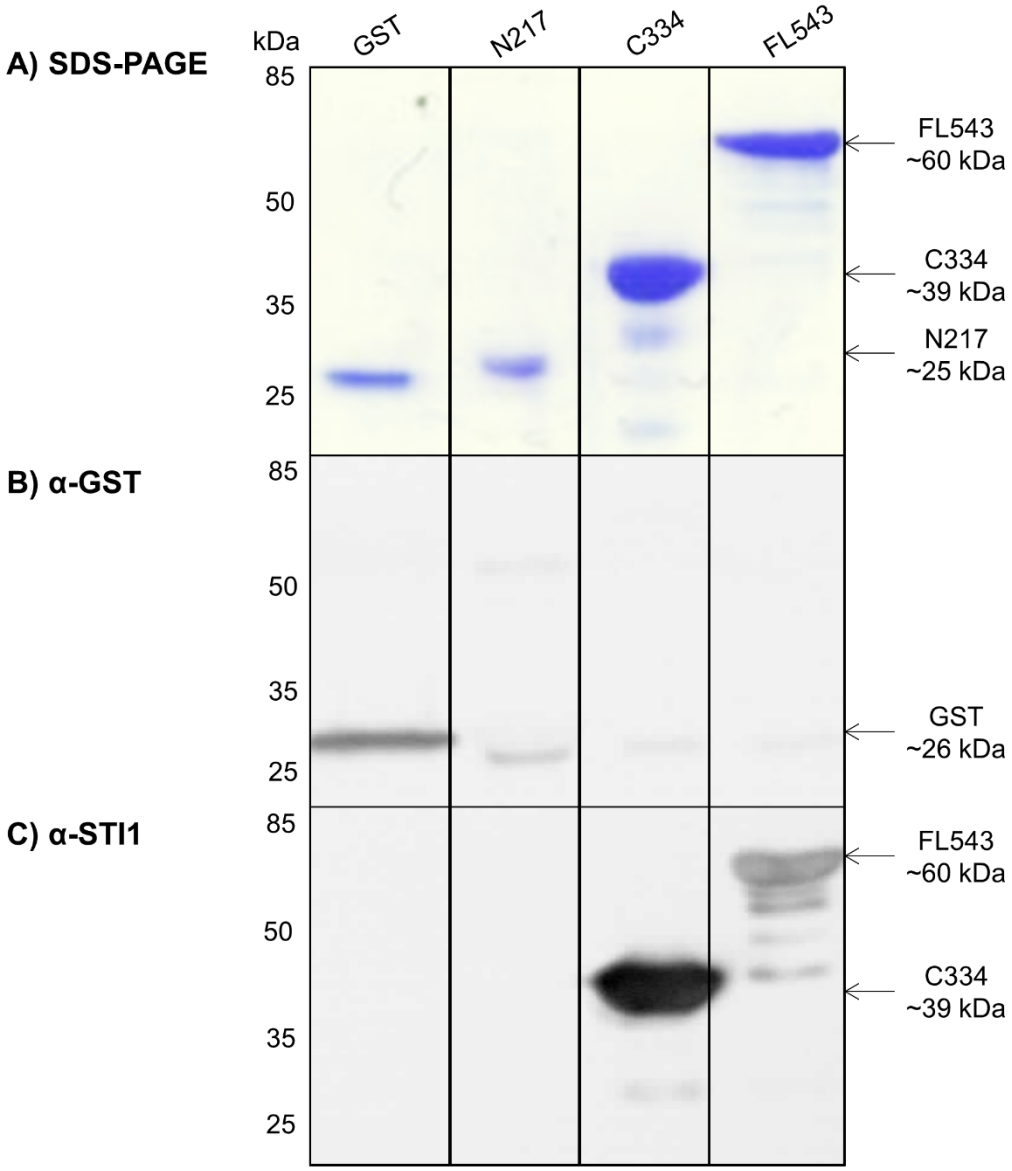

Figure 3.10 - Elutions of N217, C334 and FL543 after GST-tag cleavage using Factor Xa

Samples were taken from each protein elutions (1 µg) and analysed using A) SDS-PAGE (8% - 12%) with Coomassie staining and western blot analysis using B) rabbit anti-GST and donkey anti-rabbit IgG-HRP antibodies and C) mouse anti-STI1, and goat anti-mouse IgG-HRP and protein G-peroxidase antibodies.

3.10 Analysis of endogenous ATPase activity of mSTI1

Earlier this year (Yamamoto et al., 2014) suggested that hSTI1 has ATPase activity. Therefore, to test whether mSTI1 has endogenous ATPase activity and, if so, which domain was responsible for such activity, N217, C334 and FL543 were used in ATPase assays. Neither N217 nor C334 showed detectable ATPase activity (data not shown). On the other hand, FL543 consistently produced free inorganic phosphate (P_i) at an increasing rate in a dose dependent manner. These results were reproducible with relatively low standard deviations (Figure 3.11A). Therefore, only FL543 was used for the remainder of the ATPase experiments.

In order to define the rate at which mSTI1 has the ability to hydrolyse ATP, an ATPase assay was repeated with increasing concentrations of ATP. In order to calculate the kinetic values for mSTI1 it was assumed that mSTI1 is a monomer and contained one active enzyme site per monomer. A Michaelis-Menten plot was used to determine the kinetic values of mSTI1 in order for the obtained kinetic values to be comparable with the hSTI1 values obtained from Yamamoto et al. (2014). The kinetic values were also calculated using the Lineweaver-Burk plot (Appendix, Figure 6.1) in order to ensure the two set of data were similar in order to ensure those obtained from the Michaelis-Menten plot were accurate. The Michaelis-Menten plot in Figure 3.11B produced a V_{max} of 326.4 P_i nM/min. The V_{max} is the maximum theoretical velocity at which mSTI1 hydrolysed ATP when saturated (Dowd and Riggs, 1965). A value of 0.059 mM was determined as the Michaelis constant (K_m). The K_m is the concentration of ATP at half of the maximum velocity of the reaction (Dowd and Riggs, 1965). The k_{cat} was calculated to be 0.1306 min^{-1}, this value is defined as the number of ATP molecules which can be hydrolysed to produce free inorganic phosphate per unit of time (Berry, 1951). Kinetic values obtained from the Lineweaver-Burk plot were similar to those calculated from the Michaelis Menten plot, therefore it was assumed the results were accurate and reliable.

In order to ensure calculated ATPase activity rates of FL543 were not as the result of contaminating DnaK, FL543 elutions were probed for DnaK contamination by Western blot analysis. An *E. coli* cleared lysate was used as a positive control for the presence of DnaK. A thick dark band could be seen in the cleared lysate sample confirming the presence of DnaK (Figure 3.11C). The FL543 elution contained a thin band indicating DnaK was present in the sample but at a much lower level to that of the cleared lysate. Therefore, DnaK was present in FL543 elutions used in the ATPase activity assays. However, it is unlikely that this would have affected the ATPase results due to the absence of an Hsp40 co-chaperone required to stimulate DnaK ATPase (Laufen et al., 1999). High performance liquid chromatography (HPLC) purified DnaK had a low basal ATPase activity rate at 37°C with a turnover number (k_{cat}) of 0.087 ± 0.007 min^{-1} and prior to HPLC purification higher levels of 0.42 ± 0.02 min^{-1} were reported (Palleros et al., 1993). Neither of these values are comparable to our reported values and therefore it is unlikely that DnaK was contributing to ATPase activity.

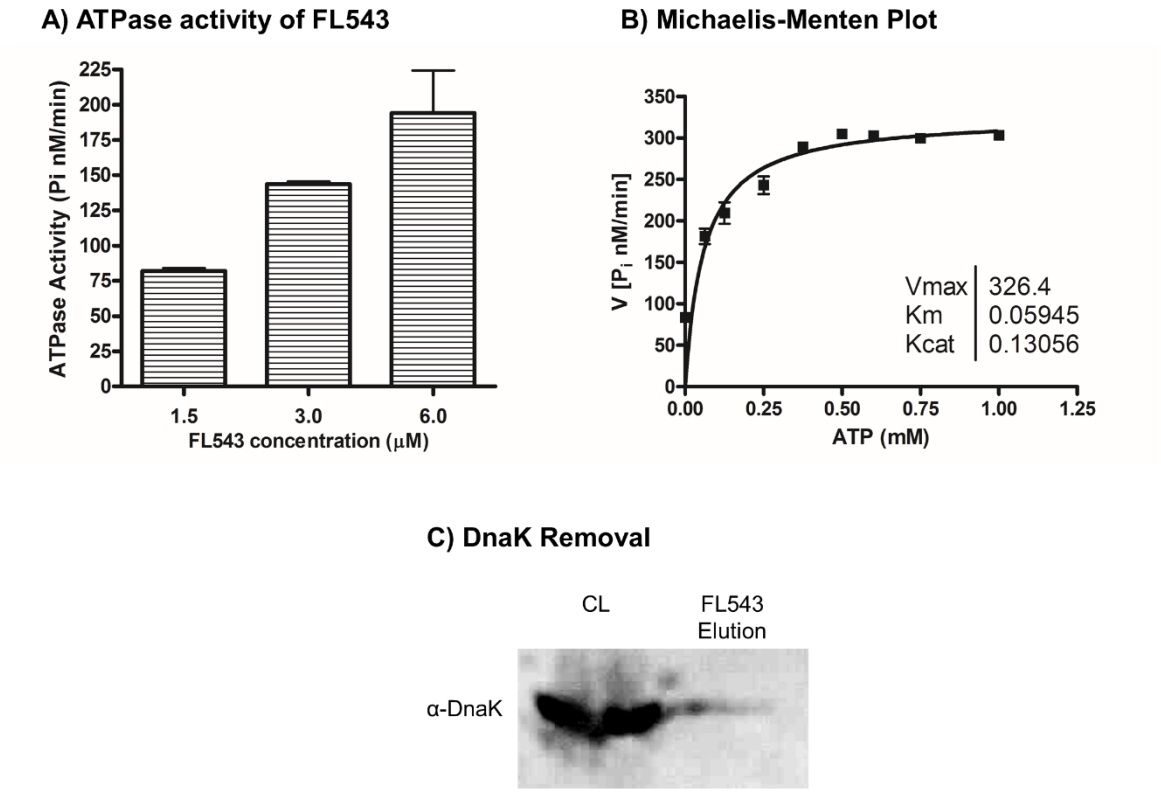

Figure 3.11 - mSTI1 has ATPase activity

FL543 (2.5 μM) was incubated at 37°C in the presence of ATP (0.5 mM), $MgCl_2$ (2 mM) and $CaCl_2$ (50 mM). In order to determine the inorganic phosphate (Pi) production the EnzChek phosphate assay kit was used. UV absorbance was monitored and used to determine the rate of Pi production with the use of a phosphate standard curve. A) FL543 at increasing concentrations B) 2.5 μM FL543 with increasing ATP concentrations. Data are representative of experiments completed in triplicate. C) Detection of DnaK in a cleared expression lysate (CL) and FL543 elution after GST cleavage(1 μg loaded) by Western blot analysis using mouse anti-DnaK antibody.

3.11 Analysis of binding of mSTI1 and actin by surface plasmon resonance (SPR) spectroscopy

Surface plasmon resonance (SPR) spectroscopy was used to determine the interaction of GST-N217, GST-C334 and GST-FL543 with immobilised actin (Figure 3.12). Actin (rabbit muscle) was immobilised on the sensor chip surface while GST, GST-N217, GST-C334 and GST-FL543 at increasing concentrations were flowed over and sensorgrams were collected.

No kinetic data could be obtained from the SPR results as the kinetic model could not be well fitted to the data. Therefore, the kinetic values would not have been a reliable source of information. Instead, the results were analysed were analysed qualitatively. Although the kinetic could not be obtained, the Req values were plotted against the concentrations of each of the proteins in order to ensure saturation was reached and the binding was specific (Appendix, Figure 6.2).

GST alone was used as a negative control and was found to bind actin weakly with a maximum of 1050 response units (RU) at 1000 nM GST (Figure 3.12A). GST-N217 bound actin more strongly than GST alone where a maximum value of 3270 RU was seen at 1000 nM GST-N217 (Figure 3.12B). However, the binding strength of GST-N217 with actin was substantially below that of GST-C334 and GST-FL543. The C-terminal portion of mSTI1, GST-C334, bound actin in a dose-dependent manner. The binding between GST-C334 and actin was dramatically stronger than that between GST-N217 and actin, particularly at the higher concentration of 1000 nM (Figure 3.12C). GST-FL543 bound actin in a dose dependent manner at the lower concentrations. At a concentration of 1000 nM, GST-FL543 bound actin with a maximum value of 5125 RU. The sudden drop in the curve at 90 seconds indicated that GST-FL543 dissociated from actin more quickly than any of the domains tested (Figure 3.12E). This trend was particularly seen at the higher concentrations of 250 nM to 1000 nM (Figure 3.12D). Figure 3.12E shows a direct comparison of actin binding for equivalent concentrations of the

GST and GST-tagged mSTI1 proteins. All GST-tagged mSTI1 proteins associated with actin within the first 60 seconds, after which the proteins began to dissociate. GST-FL543 associated with actin more strongly than GST-C334 and GST-N217. GST-C334 had a weaker association with actin but dissociated from actin more slowly and steadily where a total difference of 542 RU was seen over the 60 – 700 seconds period. Similarly over this time GST-N217 showed a total difference of 330 RU. These data suggested that GST-C334 and GST-FL543 had robust actin binding capabilities, but that the kinetics of mSTI1-actin interactions may be different for the two proteins.

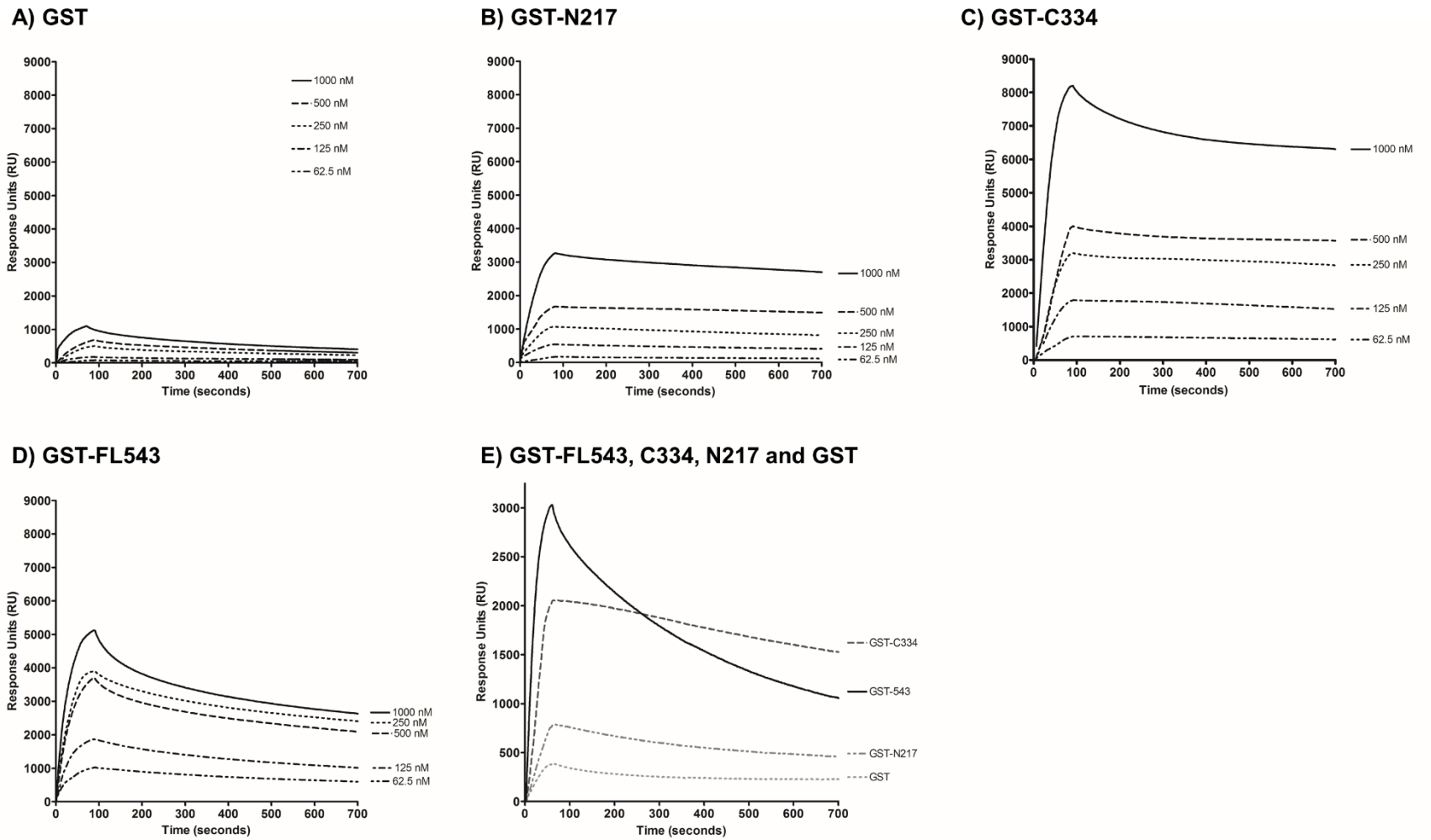

Figure 3.12 - Surface plasmon resonance spectroscopy analysis of GST-tagged mSTI1 and truncations binding actin

SPR analysis showing concentration dependant binding of A) GST, B) GST-N217, C) GST-C334 and D) GST-FL543 to immobilised actin (100 μg/ml). E) Comparative binding of GST--FL543, GST-C334, GST-N217 and GST (160 nM) to actin, y-axis maximum is 3000 RU, compared to 9000 RU in A)-D). Data shown are representative of two independent experiments repeated in completed in triplicate.

3.12 Analysis of binding of mSTI1 to filamentous actin (F-actin) by co-sedimentation analysis

A high speed centrifugation assay (co-sedimentation assay) was used to determine which domain of the mammalian STI1 binds filamentous actin (F-actin) using a protocol adapted from Srivastava and Barber (2008). This was done using the GST-tagged truncations as well as full length untagged mSTI1 and polymerised actin.

Actin (from rabbit muscle) incubated alone was used as a standard for comparison with the test samples. As shown in Figure 3.13A the majority of the actin was seen in the pellet, indicating the actin did in fact polymerise. GST was used as a negative control when testing the binding of GST-tagged proteins. GST was found in both the supernatant and the pellet when centrifuged without actin. There was no change in the sedimentation profile of GST or actin when sedimented alone or together (Figure 3.13A). Therefore the GST was unlikely to be found in the pellet due to an interaction with F-actin. All GST-tagged mSTI1 proteins incubated alone were found mostly in the supernatant with only small quantities found in the pellet. In the case of GST-N217 this result was unchanged when combined with actin suggesting that the GST-N217 did not bind F-actin. When GST-C334 was incubated with F-actin there was a shift of the GST-C334 into the pellet, but no obvious change in the actin distribution between pellet and supernatant. The presence of GST-C334 in the pellet suggested this mSTI1 domain (TPR2AB) had the ability to bind F-actin. Furthermore, this trend was repeated with GST-FL543 with a band seen in the pellet when incubated with F-actin. Therefore, this would indicate the full length mSTI1 can also bind F-actin. These data were consistent with the results of the SPR analysis (Figure 3.12).

The experiment was repeated with the untagged mSTI1 proteins in order to determine whether the GST-tag had an effect on the outcome of the experiment. In this experiment, bovine serum

albumin (BSA) was used as a negative control. Without actin, BSA was only in the supernatant. When combined with actin, the BSA distribution remained largely unchanged, with only a very small amount seen in the pellet (Figure 3.13B). The FL543, C334 and N217 proteins alone were only present in the supernatant. When combined with actin, no obvious shifts of N217 or C334 into the pellet were seen, as well as no obvious change in the amounts of actin in the supernatant and pellet. As seen in the previous experiment (Figure 3.13A), FL543 was found in the pellet when combined with actin but there were no changes in the distribution of actin levels in the supernatant or pellet. This suggested that untagged full length mSTI1, but not the untagged TPR2AB domain, had the ability to bind F- actin.

FL543 was incubated at increasing concentrations with a constant actin concentration in order to obtain an estimation of the binding affinity (Figure 3.13C). When FL543 was incubated without actin, at all concentrations, a greater amount of the protein was found in the supernatant. When incubated with actin, at 5 μg a greater proportion of the FL543 was found in the pellet compared to the supernatant. Between 10 - 20 μg FL543 was evenly distributed between the supernatant and pellet fractions. When the amount of FL543 was increased beyond 10 μg, the proportion of FL543 in the supernatant increased indicating saturation in binding of FL543 to F-actin in the pellet.

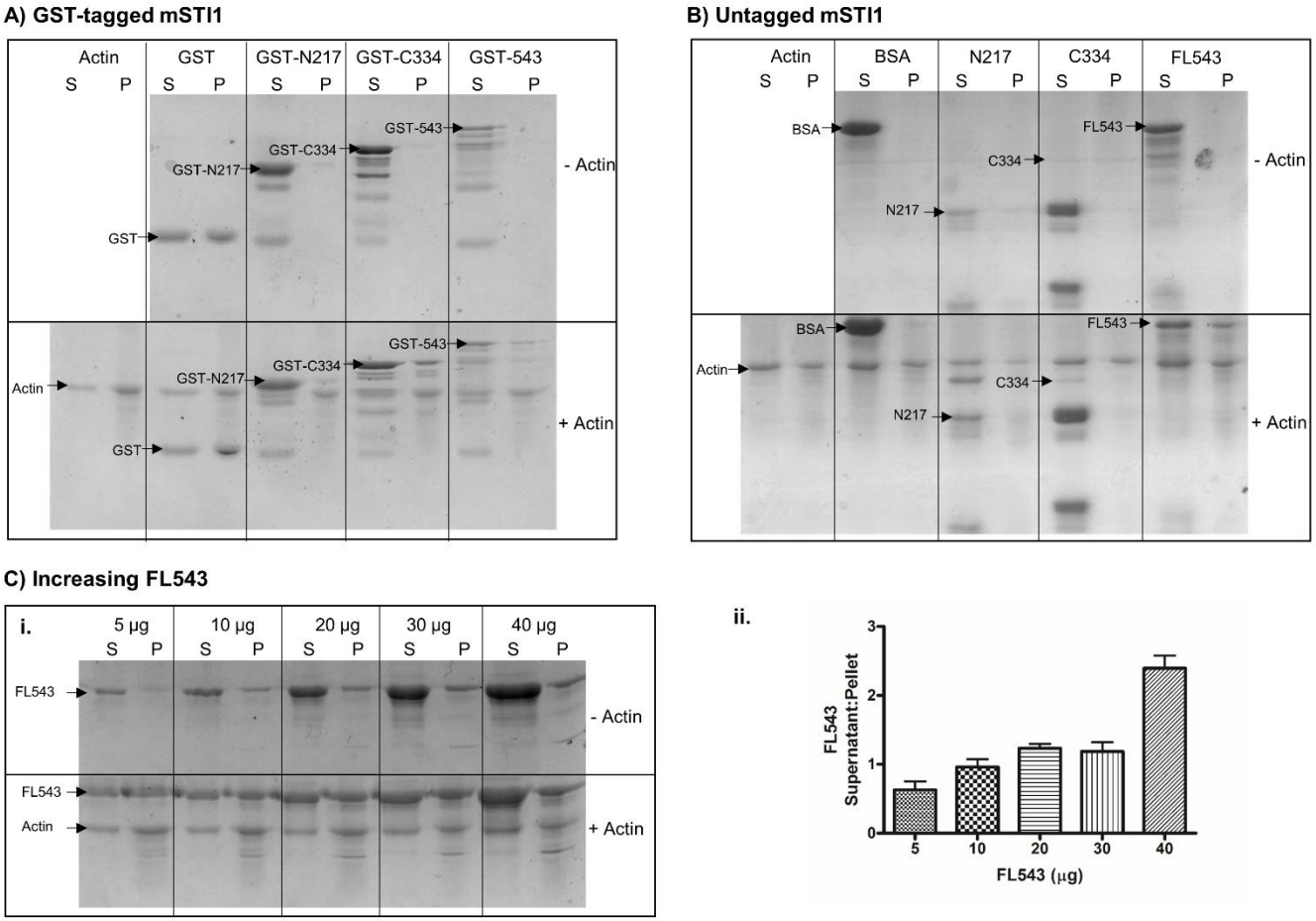

Figure 3.13 - F-actin binding activity of mSTI1 at high speed determined using a co-sedimentation assay

Actin (20 µg) was incubated in polymerisation buffer (500 mM KCl, 20 mM $MgCl_2$, 10 mM ATP, 100 mM Tris-HCl pH 7.5) for 1 hour at 25°C prior to the addition of the test proteins (20 µg), after which the mixture was incubated for a further 30 minutes. Samples were made up to equal volumes and spun down at 150 000 x *g*. Supernatants were collected and pellets resuspended in an equal volume to that of the supernatant in ddH_2O. Samples were mixed with 5 x SDS-PAGE sample buffer and were analysed using a 8% - 12% reducing SDS-PAGE gel with Coomassie staining. Test proteins included A) GST-tagged mSTI1 and truncations with GST alone as a negative control, B) GST-cleaved mSTI1 and truncations with BSA as a negative control, and C)i. Increasing FL543 concentrations (5 µg - 40 µg), ii. Densitometry of FL543 when incubated with actin. BSA was used as a negative control. Data are representative of experiments completed in three independent replicates.

To test whether full length mSTI1 enhanced the formation of F-actin, FL543 was combined with G-actin prior to polymerisation (Figure 3.14A). BSA was used as a negative control. No changes could be seen in the proportions of BSA in the supernatant and pellet when combined with actin in comparison to BSA alone. The proportions of actin in the supernatant and pellet remained unchanged in comparison to actin alone. FL543 alone was present in both the supernatant and pellet, but a greater proportion was seen in the supernatant. When combined with actin, FL543 increased in the pellet. However, no changes could be seen in the sedimentation profile of actin when compared to the profiles when incubated alone or with the non-specific protein, BSA.

To confirm whether mSTI1 plays a role in the formation of F-actin bundles, a low speed co-sedimentation assay was used (Figure 3.14B) (Okamoto et al., 2007). BSA was used as a negative control. In the absence of actin, a dark BSA band was seen in the supernatant, with only a thin band in the pellet. This same pattern was seen with the test proteins, N217, C334 and FL543 without actin. When BSA was incubated with actin, the distribution of the BSA remained unchanged in comparison to the sample without actin. The distribution of N217, C334 and FL543 also remained unchanged, as did the actin profile, indicating that mSTI1 did not promote the bundling action of actin.

A) Globular actin and mSTI1

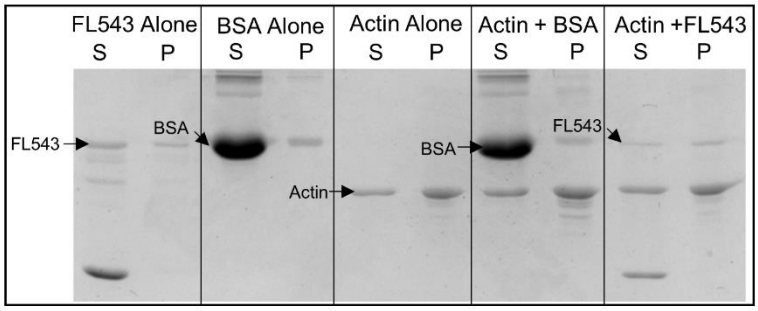

B) Low speed cosedimentation

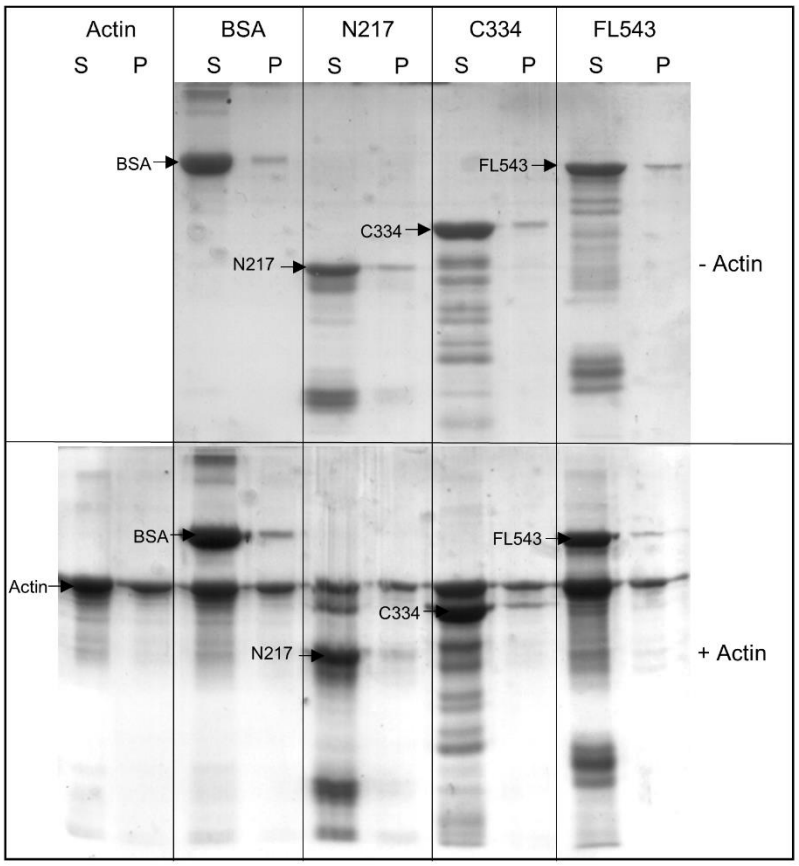

Figure 3.14 - mSTI1 does not stimulate formation of actin filaments or bundling of F-actin

A) FL543 (20 µg) and actin (20 µg) were incubated for 30 minutes at 25°C, actin polymerisation buffer (500 mM KCl, 20 mM $MgCl_2$, 10 mM ATP, 100 mM Tris-HCl pH 7.5) was added and the mixture was incubated another 30 minutes. Samples were made up to equal volumes and spun at 150 000 x *g*. B) Actin (20 µg) was incubated in polymerisation buffer for 1 hour at 25°C prior to the addition of the test proteins (20 µg), after which the mixture was incubated for a further 30 minutes. Samples were made up to equal volumes and spun at 14 000 x *g*. BSA was used as a negative control for both experiments. Supernatants were collected and pellets resuspended in an equal volume to that of the supernatant in ddH_2O. Samples were mixed with 5 x SDS-PAGE sample buffer and were analysed using a 8% - 12% reducing SDS-PAGE gel with Coomassie staining. A) was representative of a single replicate and B) was representative of three independent replicates.

3.13 Analysis of the effect of designed peptides on the ability of mSTI1 to bind F- actin

In an attempt to identify the binding site for actin on mSTI1, the F-actin binding assay was conducted with FL543 (20 µg) in the presence of the mSTI1-derived peptides (PP1 or TPR2A) or controls (PP1Scr and TPR2AScr, respectively) (20 µg) with actin (20 µg). Figure 3.15A shows the results for the assay including each of the individual peptides in combination with FL543 alone, actin alone and FL543 and actin together. The c-myc peptide (EQKLISEEDL) was used as an additional negative control. In the presence of the c-myc peptide, the majority of the FL543 was found in the supernatant with only a faint band visible in the pellet. When the c-myc peptide was combined with actin, the distribution of actin between the pellet and supernatant appeared even (Figure 3.15A). When the c-myc peptide, FL543 and actin were combined together no obvious changes could be seen in the actin distribution. The FL543 had shifted into the pellet as seen in the previous high speed co-sedimentation assays indicating an interaction with F-actin (Figure 3.13A-C). In the presence of the PP1 and PP1Scr peptides, the distribution of the actin of FL543 remained unchanged in comparison to those of the negative control. In combination with the TPR2A and TPR2AScr peptides a small shift was seen into pellet in the case of FL543 alone, but this seemed to make no change to FL543 or actin distribution profile when these were combined with actin.

The experiment shown in Figure 3.15B was similar to the previous experiment with the exception of FL543 alone (20 µg), actin alone (20 µg) and FL543 and actin together were combined with both test peptides and both scrambled peptides (20 µg each) as opposed to testing each peptide separately. This was done to determine whether binding with just one of the putative binding sites was sufficient for mSTI1 to remain bound to F-actin. This would be indicated by an increase in the amount of FL543 in the supernatant and a decrease in the pellet.

The c-myc peptide (40 µg) was used as a negative control. When the c-myc peptide was combined with FL543 alone, most of the protein was found in the supernatant and with a minor fraction present in the pellet. When combined with actin only, the actin was evenly distributed between the supernatant and the pellet. On combination of the c-myc peptide, FL543 and actin, the two proteins were evenly distributed between the supernatant and pellet. The test peptides did not have an effect on the FL543 alone, as the supernatant to pellet distribution was comparable to that of the c-myc peptide, negative control. Likewise, the test peptides had no effect on sedimentation profile of the actin alone. However, when the test peptides were combined with both the FL543 and actin, there was a reduction in the FL543 and the actin in the pellet in comparison to results of the negative control with the c-myc peptide (Figure 3.15B). Statistical analysis of the densitometry from replicate assays however indicated this result was not statistically significant (Figure 3.15B i-ii). The scrambled peptides did not affect the distribution of either actin or FL543 or the actin and FL543 together and were more similar to the results of the negative control c-myc peptide (Figure 3.15B). These results suggested that the region spanning the polyproline region and the DAYKKK motif, may play a role in the mSTI1 interaction with F-actin and this is as a consequence of the motif sequences and not the overall charge of the peptides.

A) Single peptides

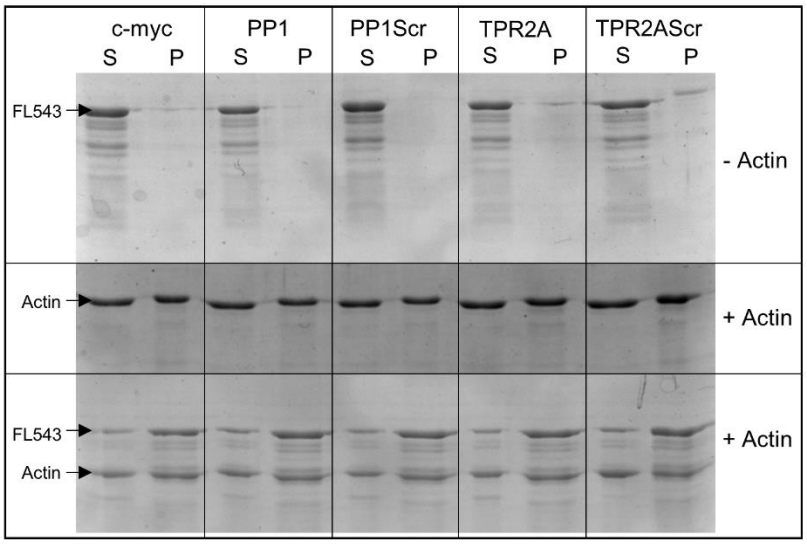

B) Combined peptides

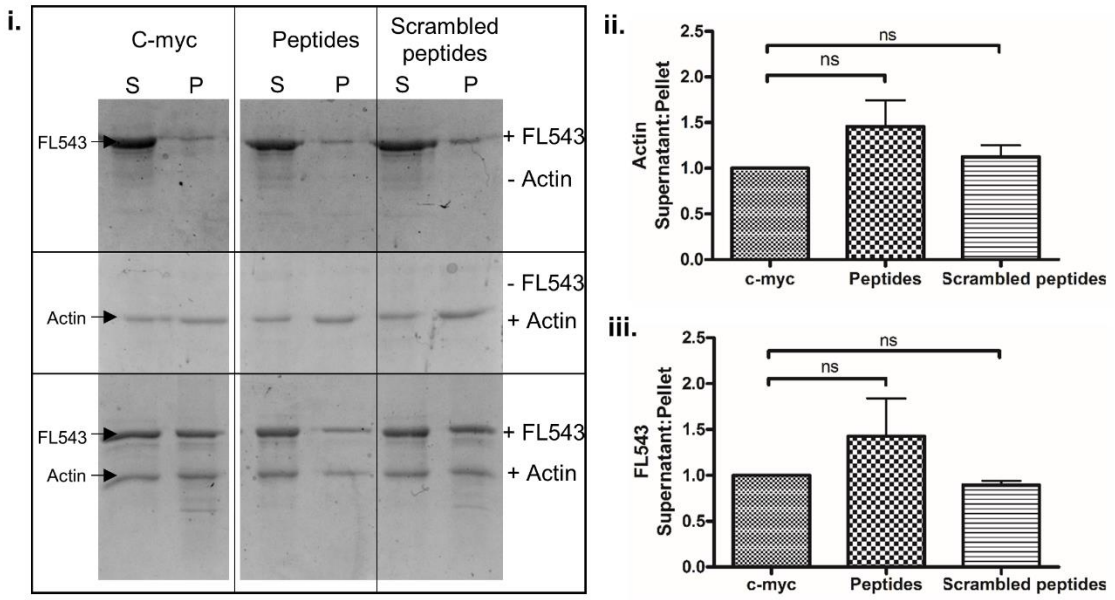

Figure 3.15 - PP1 and TPR2A peptides do not inhibit the mSTI1-F-actin interaction

Actin (20 µg) was incubated in polymerisation buffer (500 mM KCl, 20 mM $MgCl_2$, 10 mM ATP, 100 mM Tris-HCl pH 7.5) for 1 hour at 25°C prior to the addition of FL543 (20 µg) and/or the peptides (20 µg each), after which the mixture was incubated for a further 30 minutes. Samples were made up to equal volumes and centrifuged at 150 000 x *g*. Supernatants were collected and pellets resuspended in an equal volume to that of the supernatant in ddH_2O. Samples were mixed with 5 x SDS-PAGE sample buffer and were analysed using a 8% - 12% reducing SDS-PAGE gel with Coomassie staining. A) Single peptides. B) i. Combined peptides, ii. Densitometry of actin bands when combined with FL543 and peptides, iii. Densitometry of FL543 bands when combined with actin and peptides. Densitometry was determined using ImageJ software. Ratios of the supernatant to the pellet were calculated by the division of the determined supernatant band area by the pellet band area of the corresponding proteins. Statistical analysis by one way ANOVA and Tukey's multiple comparison showed ratio differences to be non-significant (ns). Data are representative of three independent replicates.

3.14 Effect of mSTI1 on the ATPase activity of actin

ATP hydrolysis is associated with the actin treadmilling process, which in turn controls the length of actin filaments (Pantaloni et al., 1985). In order to determine whether mSTI1 may play a role in this process, optimisation experiments were performed and consistent results were obtained when FL543 was incubated with actin at submolar concentrations (data not shown). Therefore, for these experiments, actin was incubated with FL543 at submolar to equimolar concentrations in the presence of $MgCl_2$ (2 mM), KCl (50 mM) and ATP (0.5 mM) to initiate polymerisation and determine the effect of mSTI1 on the rate of ATP hydrolysis by actin. As it was earlier determined that mSTI1 has ATPase activity (Figure 3.11), the data were normalised for any endogenous activity from FL543. This was done in order to observe whether an increase in ATPase activity occurs and to ensure this was not as a result of an additive effect. Included as a control, the "no protein" sample was used to ensure there were no inorganic phosphate contaminants in the components of the kit or any of the buffers resulting in ATPase activity, and in order to deduct any ATPase activity which was not as a result of either of the proteins. An increase in the rate of ATP hydrolysis was seen in a dose dependent manner (Figure 3.16). In comparison to actin alone (5 μM), the increase became significant ($p < 0.01$) at a concentration of 1.5 μM FL543. This suggested that mSTI1 has the ability to stimulate the rate of production of inorganic phosphate by F-actin. This outcome was unlikely due to the contaminating DnaK (Figure 3.11), as in order for a substrate to effectively stimulate the ATPase activity of DnaK, the co-chaperone DnaJ must also be present (Laufen et al., 1999).

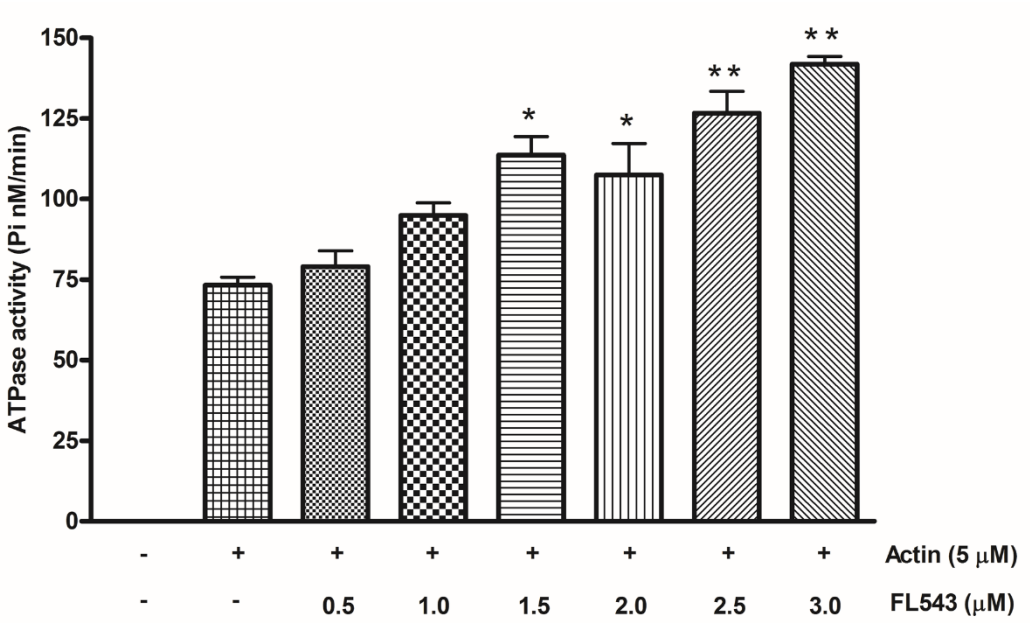

Figure 3.16 - ATPase assay with increasing mSTI1 concentrations with or without actin

FL543 at increasing submolar concentrations was incubated with or without 5 μM actin in the presence of ATP (0.5 mM), $MgCl_2$ (2 mM) and $CaCl_2$ (50 mM). In order to determine the inorganic phosphate (Pi) produced, EnzChek phosphate assay kit was used. UV absorbance was monitored and used to determine the rate of Pi production with the use of a phosphate standard curve. Data was normalised for ATPase activity of endogenous mSTI1. Statistical analysis by one way ANOVA and Tukey's multiple comparison showed statistical differences of *($p<0.01$) and **($p<0.001$). Data are representative of a single experiment run in triplicate.

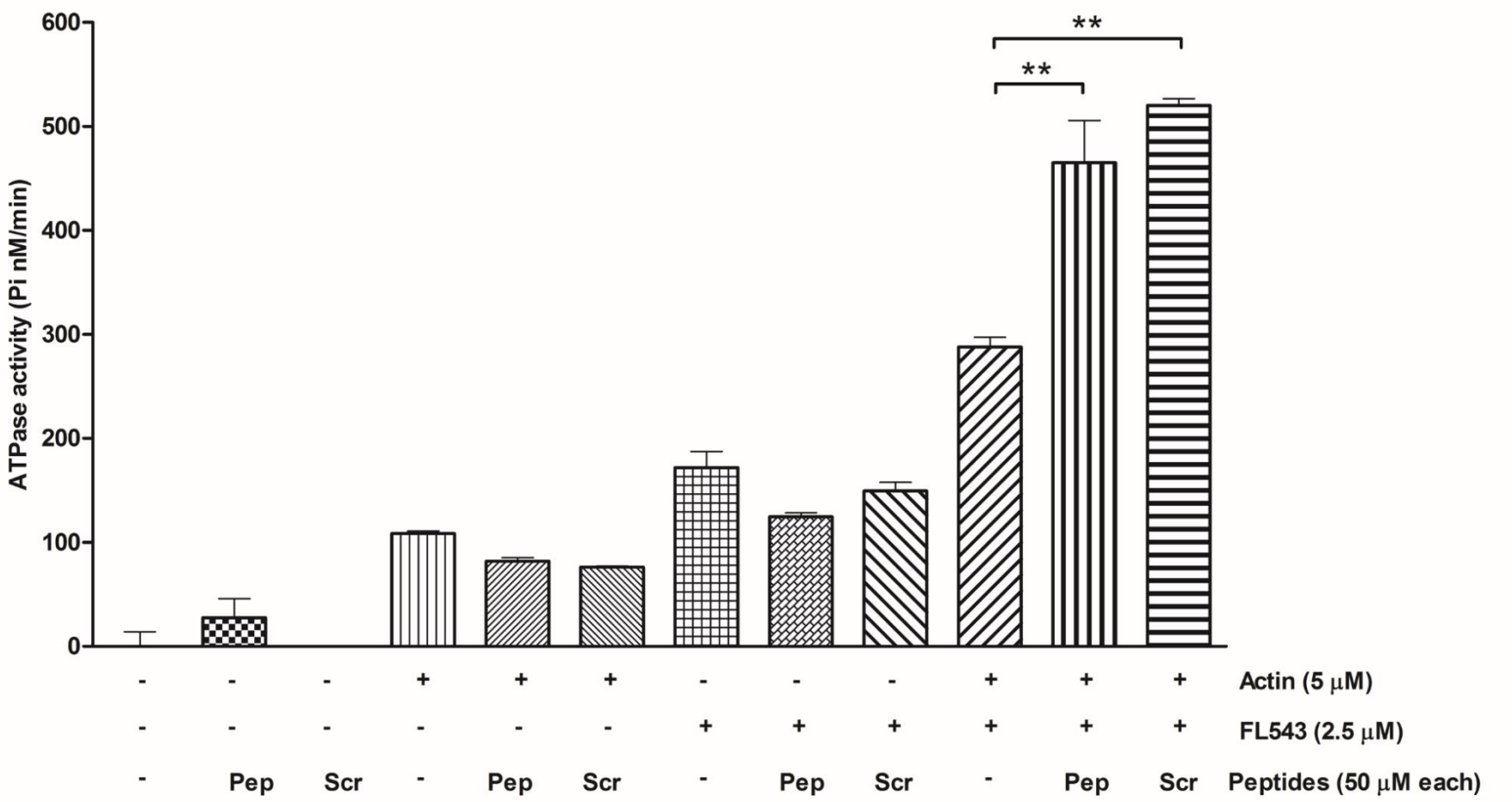

Figure 3.17 - Presence of test or scrambled peptides stimulated combined FL543 and actin ATPase activity

A concentration of 2.5 μM FL543 was incubated with or without 5 μM actin and with or without the test (PP1 and TPR2A) and scrambled peptides (PP1Scr and TPR2AScr) using 50μM each in the presence of ATP (0.5 mM), $MgCl_2$ (2 mM) and $CaCl_2$ (50 mM). In order to determine the inorganic phosphate (Pi) produced, EnzChek phosphate assay kit was used. UV absorbance was monitored and used to determine the rate of Pi production with the use of a phosphate standard curve. The experiment was run once as a triplicate. Statistical analysis by one way ANOVA and Tukey's multiple comparison showed statistical differences of **($p<0.001$) when peptides were included with FL543 and actin, in comparison to FL543 and actin alone.

To determine whether the two putative actin binding motifs played a role in the enhancement of ATPase activity, the experiment was repeated with the inclusion of the mSTI1 derived peptides or their scrambled derivatives (Figure 3.17). The test peptides and scrambled peptides were incubated alone to ensure the peptides contained no ATPase activity. The test and scrambled peptides were also incubated with FL543 and actin to ensure the peptides had no effect on these proteins alone. Fluctuations were seen in these controls but no significant changes were observed. When the test peptides were combined with FL543 and actin together, a significant ($p<0.001$) increase in the ATPase activity was observed. Unexpectedly, similar results were seen when the scrambled peptides were combined with FL543 and actin, with a slightly higher average ATPase activity than that of the FL543, actin and test peptides. These observations together suggested that combined test peptides together with FL543 had the ability to stimulate the ATPase activity of F-actin. As both the test and scrambled peptides stimulated the ATPase activity of actin, this would suggest that the stimulation was not as a result of the amino acid sequence but rather due to some other feature, such as the overall charge. Though peptides have been shown to stimulate the ATPase activity of DnaK this is unlikely the case in these data as no stimulation was seen when FL543 alone and the peptides were combined (Laufen et al., 1999).

3.15 Analysis of the change in F-actin morphology as a result of hSTI1 depletion

Having identified that mSTI1 could bind actin and possibly stimulate its ATPase activity *in vitro*, we next examined the effect of hSTI1 in actin dynamics in cell lines. The morphology and intensity of F-actin staining was examined using NT and hSTI1 shRNA HEK293T cells. These cells lines were previously established in our laboratory (Contu, 2014). The NT shRNA HEK293T cells were HEK293T cells stably transfected with a TRIPZ plasmid containing a

non-targeting short hairpin RNA (shRNA) control sequence. The hSTI1 shRNA HEK293T cells were HEK293T cells stably transfected with a pTRIPZ plasmid which contains a shRNA sequence specific for the knockdown of hSTI1 (Contu, 2014). Cells were induced with doxycycline (1 μg/ml) for 72 hours which results in expression of the shRNA and the subsequent depletion of hSTI1 in the hSTI1 shRNA HEK293T cell line. After this induction period, cells were serum starved for 30 minutes and placed back in normal serum containing medium for 15 minutes in order to induce actin polymerisation. The images were captured with identical laser settings and the F-actin levels compared using the 2.5D and profile tools available on ZEN 2012 software (Zeiss).

The F-actin morphology seen in the NT shRNA HEK293T cells typically had strong F-actin structures around the borders of cells (Figure 3.18). This was particularly seen in the intercellular junctions of cells (Figure 3.18, A-C i, NT shRNA). These strong borders were qualified by the examination of the F-actin staining intensity. Along these borders the intensity peaked at values above 250 units. The 2.5D image (Figure 3.18A-C ii, NT shRNA) showed the presence of these strong borders surrounding all of the cells. On the other hand, in the STI1 shRNA HEK293T cells, the F-actin structures appeared to be less predominant and thinner. The 2.5D image (Figure 3.18A-C ii) showed more scattered fibres with less structure and weaker intensities, as opposed to thicker and more defined and organised fibres seen in the control cells. Strong bundles of F-actin fibres would result in long intense bands but these structures were not seen in cells which were depleted of hSTI1 (Figure 3.18A-C i-ii) (Lazarides, 1975). The intensity value of the F-actin fibres were below 250, even across the cell borders (Figure 3.18A-C i.). In areas where the intensities peaked, it was over a shorter distance than those of the control cells. This suggested that the F-actin borders of the STI1 shRNA HEK293T cells were thinner than those of the non-targeting cell line. Together, these data suggested that hSTI1 may play a role in the distribution and organisation of F-actin across the cell.

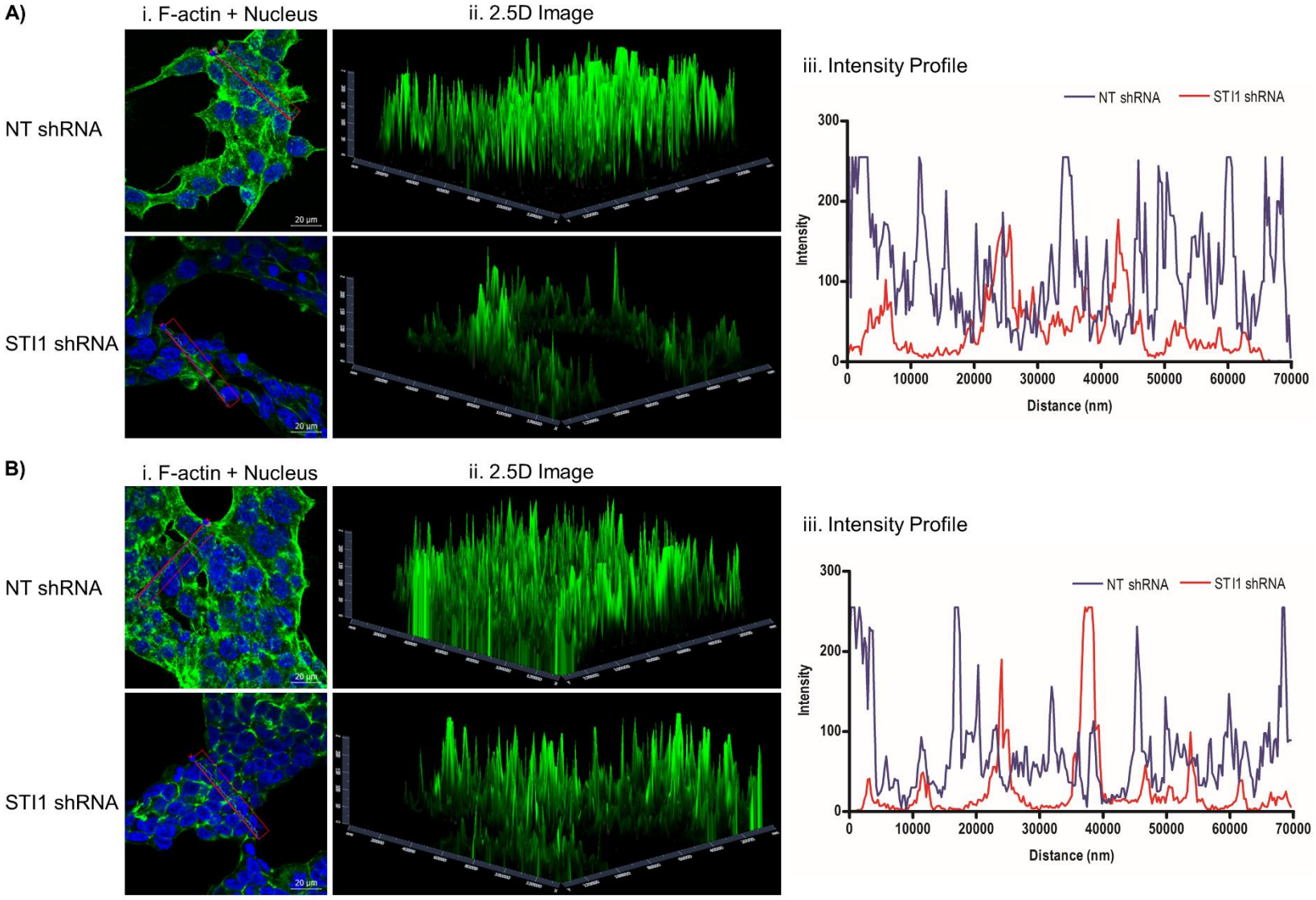

Figure 3.18 - Decrease in thick F-actin bundles and lack of organisation in STI1 depleted cells

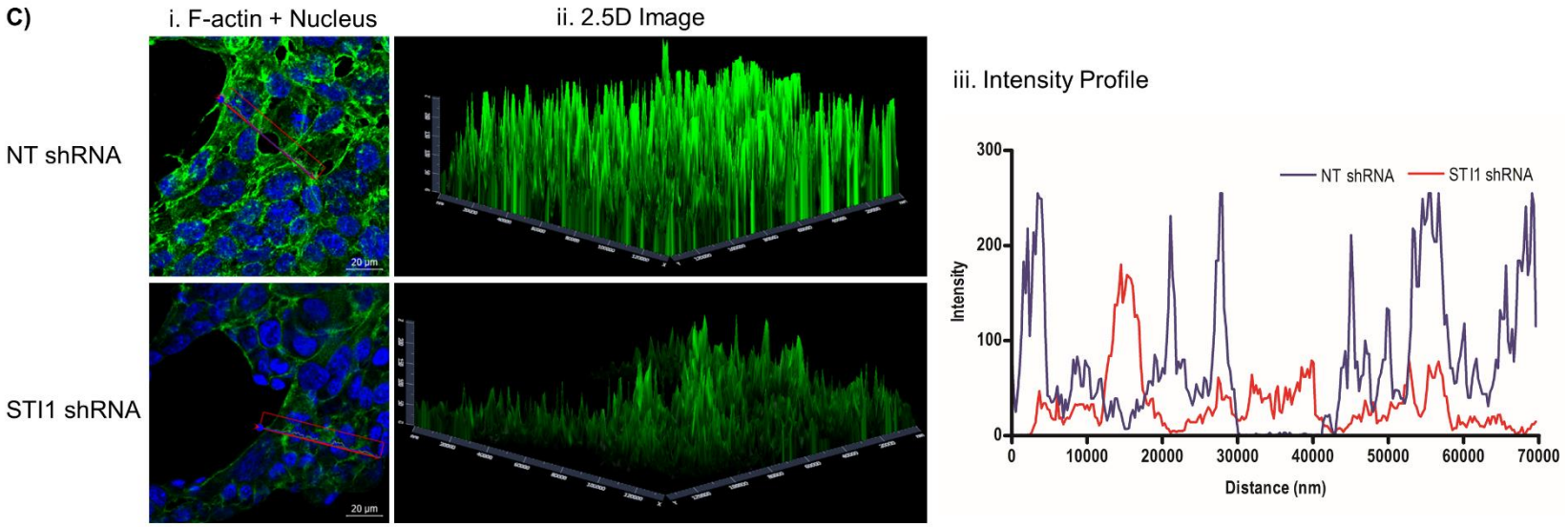

Figure 3.18 - Decrease in thick F-actin bundles and lack of organisation in STI1 depleted cells

F-actin morphology and organisation was analysed using ZEN 2012 software (Zeiss). A-C) show various examples representing F-actin and nuclear staining using ActinGreen™ 488 ReadyProbes® and Hoechst (1 µg/ml) respectively in NT and STI1 shRNA HEK293T cells. The columns show the i. F-actin staining with the analysed profile shown by a red arrow and box, ii. Intensity of staining in seen in i. using a 2.5D image, and iii. the comparison of intensity profiles in NT and STI1 shRNA HEK293T cells. Three images incorporating multiple cells were selected from both cell lines as representative of the general actin structure and morphology.

3.16 Analysis of levels and subcellular localisation of actin binding proteins in hSTI1 knockdown cell lines

In order to gain a better understanding of the mechanism by which actin distribution and organisation were being affected by hSTI1 depletion, levels of actin binding proteins, cofilin and profilin, as well as the cytoskeletal proteins, actin and tubulin, were assessed in lysates prepared from the non-targeting (NT) and STI1 shRNA HEK293T cell lines. Western blot analysis was used to detect the protein levels of hSTI1, actin, cofilin, profilin and tubulin in lysates derived from the equivalent number of cells (Figure 3.19A). The densitometry was determined using ImageJ software and the protein levels were normalised against the non-targeting control levels. The protein levels were statistically analysed using two way ANOVA and a Bonferroni post-test (Figure 3.19B) with Prism 4 (Graphpad Software). The hSTI1 levels were significantly reduced ($p<0.001$) in the STI1 shRNA HEK293T cells in comparison to the non-targeting control (Figure 3.19). No changes were seen in the actin protein levels between the two cell lines (Figure 3.19). Reduced protein levels of the actin binding proteins, cofilin and profilin were seen in hSTI1 depleted cells (Figure 3.19A). This reduction was only statistically significant ($p<0.05$) for the profilin protein levels (Figure 3.19B). A reduction in the levels of tubulin was also seen with hSTI1 knockdown, although this decrease was not statistically significant (Figure 3.19).

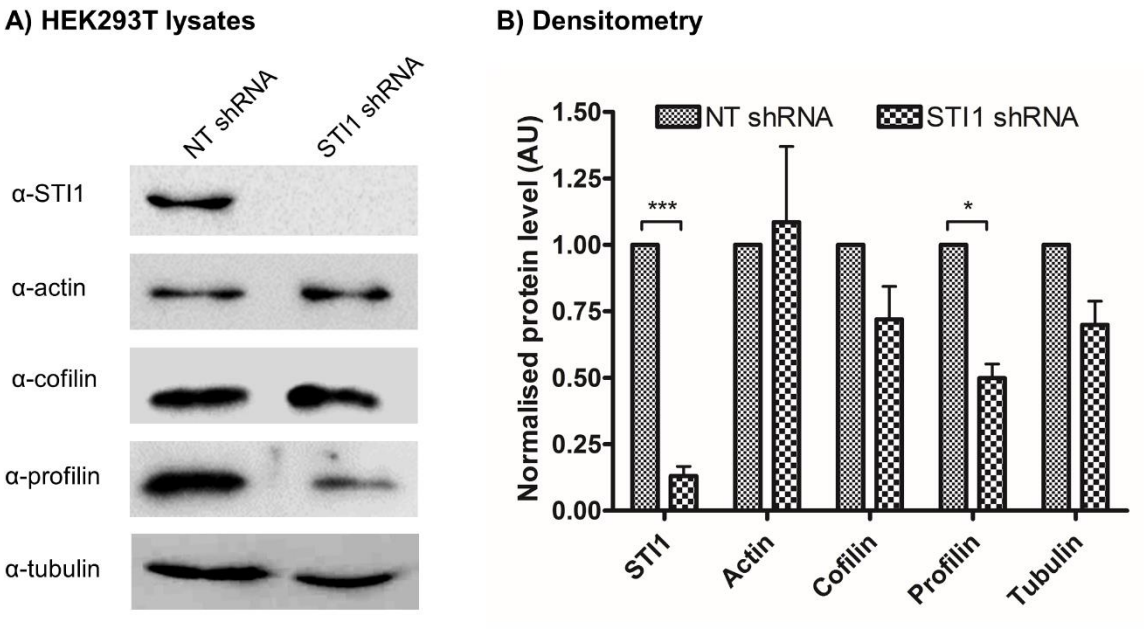

Figure 3.19 - hSTI1 depletion results in decreased levels of cytoskeletal and actin binding proteins

Lysates were made from NT and STI1 shRNA HEK293T cells which were induced with 1 µg/ml doxycycline for a period of 72 hours. The NT HEK293T cells were used as a control and had normal levels of hSTI1 and the STI1 shRNA HEK293T cells had reduced levels of hSTI1. A) Proteins were separated by SDS-PAGE and protein levels were determined by Western blot analysis. B) Densitometry was performed using ImageJ software and levels of hSTI1, actin, profilin, cofilin and tubulin were compared using Prism 4 (Graphpad software). Equal cell numbers were loaded per lane and proteins levels were normalised against the non-targeting control levels. Statistical analysis was done using two way ANOVA and a Bonferroni post-test (*=$p<0.05$,***=$P<0.001$). Data are representative of three independent experiments.

Earlier results in Hs578T cells showed the colocalisation of cofilin and profilin with hSTI1 and Hsp90 (Figure 3.1). Therefore it was investigated whether the depletion of hSTI1 would have an effect on the colocalisation of the cofilin and profilin with F-actin and Hsp90. All comparisons between the control and hSTI1 knockdown cell lines were made on the basis of images captured using identical laser settings. The NT and hSTI1 shRNA HEK293T cells were probed for tubulin, total actin, F-actin, cofilin, profilin and Hsp90 and analysed by confocal microscopy (Figures 3.20-3.23). In the control non-targeting cells, tubulin was seen mostly in the outer parts of the cytoplasm, where the staining brightened towards the edges of the cells. The merged and PDM images demonstrated that tubulin mostly colocalised (Rr = 0.728 ±0.038) with F-actin at the leading edges of the cell (Figure 3.20, NT shRNA). Previous research has suggested that there is an interaction between actin filaments and tubulin (Dent and Kalil, 2001). The tubulin staining was not as defined in HEK293T cells in which hSTI1 had been depleted (Figure 3.20, STI1 shRNA, cofilin). Colocalisation of tubulin and F-actin were seen in similar areas of the cell in control and knockdown HEK293T cells, including along long filaments extending to other cells, but levels of intensity correlation decreased in comparison to the NT shRNA HEK293T cells (Rr = 0.603 ± 0.060). This decrease in Pearson's coefficient values was found to be significant and suggested that hSTI1 may play a role in the colocalisation of F-actin and tubulin.

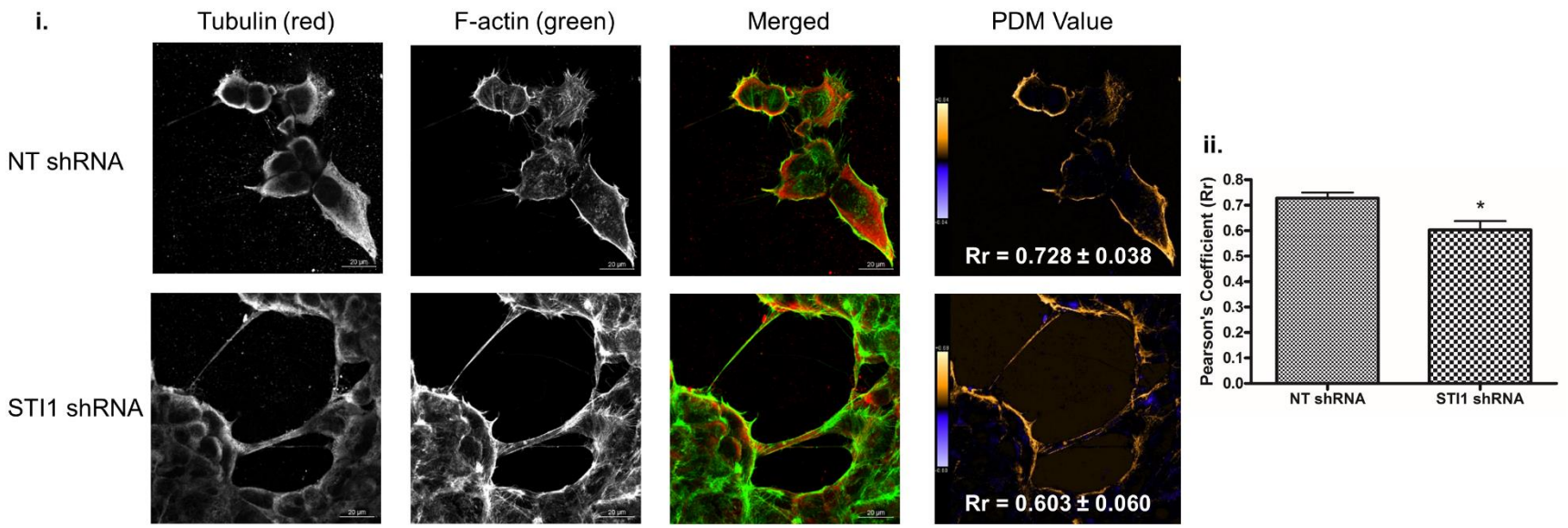

Figure 3.20 - STI1 depletion results in decreased tubulin F-actin colocalisation

NT and STI1 shRNA HEK293T cells were seeded onto glass coverslips and incubated for 24 hours. NT HEK293T cells were used as a control and had normal levels of hSTI1, while the STI1 shRNA HEK293T cells had reduced levels of hSTI1. Cells were induced with doxycycline (1 µg/ml) for 72 hours. Actin polymerisation was induced by serum starvation for 30 minutes followed by serum replenishment. The cells were washed with PBS, fixed with ice cold ethanol and permeabilized with 0.1 % (v/v) Triton-X in PBS. The cells were stained with the appropriate primary and secondary antibodies for tubulin (red). F-actin was stained using ActinGreen™ 488 ReadyProbes®. Cells were visualised using the Zeiss LSM 780 confocal microscope and all images captured using the equivalent laser settings. Images were processed and analysed using the intensity correlation analysis plugin on ImageJ software (Li et al., 2004). The top row of images represents NT shRNA HEK293T cells and the bottom represents STI1 shRNA HEK293T. i. The first column represents the tubulin staining, the second column shows the F-actin staining, the third column represents the merged images. Colours refer to merged images, proteins alone are shown in black and white. The fourth column displays the PDM image with the calculated Pearson's coefficient (Rr). ii. Differences in Pearson's coefficient values were statistically analysed by an unpaired t test (*=$p<0.05$). Data shown are representative of three independent fields of view.

In cells with normal levels of hSTI1, little actin was detectable in the nucleus (Figure 3.21, NT shRNA, total actin). This was quantitatively confirmed as negative values were calculated for the Pearson's coefficient (Rr = -0.232 ± 0.076) (Figure 3.21, NT shRNA, PDM image). Cells with depleted levels of hSTI1 showed an apparent decrease in the actin signal, but an increase in the actin signal in the nucleus (Figure 3.21, STI1 shRNA, total actin). The increase in nuclear actin signal was confirmed by a significant increase of the Pearson's coefficient for the actin signal compared to the nuclear stain (Rr = 0.147 ± 0.171) (Figure 3.21, NT shRNA, PDM image). These data suggested that hSTI1 depletion may change the localisation of actin.

In the non-targeting control cells, cofilin was primarily found in the cytoplasm with punctate staining visible in the nucleus (Figure 3.22A-C). When hSTI1 was depleted the cofilin staining was less defined, as the nucleus-cytoplasm border became less clear in comparison to the control cell line (Figure 3.22A). Furthermore, the colocalisation between cofilin and the nucleus increased, whereby, the Pearson's coefficient significantly increased from a negative value (Rr = -0.239 ± 0.035) to a positive value (Rr = 0.397 ± 0.196) (Figure 3.22 i-ii). These data suggested that hSTI1 may play a role in the localisation of cofilin. F-actin and cofilin demonstrated colocalisation (Rr = 0.599 ± 0.085) in the control cell line. The PDM image in Figure 3.22B showed that colocalisation particularly occurred at the intercellular junctions. In the hSTI1 knockdown cells, the colocalisation became more diminished as the Pearson's coefficient decreases (Rr = 0.385 ± 0.108). The colocalisation of cofilin and F-actin appeared to solely occur at the edges of the cells. This decrease in colocalisation was visible between the cell lines but was not significant (Figure 3.22B i-ii). Cofilin and Hsp90 colocalised in the non-targeting and knockdown cell lines which correlated with our earlier data (Figure 3.1C) in the Hs578T cell line. The depletion of hSTI1 did not appear to have an effect on the colocalisation of Hsp90 and cofilin, as the Pearson's coefficient value remained similar between non-targeting

and knockdown cells lines (Rr = 0.775 ± 0.011 and 0.700 ± 0.047 respectively) (Figure 3.22C i-ii). This suggested that hSTI1 does not play a role in the colocalisation of cofilin and Hsp90.

Profilin was distributed evenly across the cell in the NT shRNA cell line, with the exception being within some of the intercellular junctions, where concentrated areas of profilin staining were found along the cell edges (Figure 3.23B, profilin, shown by arrow 1). In the case of cells depleted of hSTI1, the profilin appeared to be more concentrated in the nucleus of the cells (Figure 3.23A-C). The PDM image of the control cells demonstrates areas of colocalisation in the nucleus with a speckled appearance, whereas the hSTI1 knockdown cells show more concentrated and brighter regions of colocalisation in nuclei (Figure 3.23A, PDM image). This change in the distribution of profilin in the cell upon hSTI1 depletion is further qualified by the increase in the intensity correlation of the profilin and nucleus channels (from Rr = 0.334 ± 0.062 to 0.542 ± 0.167) which suggested a greater amount of profilin colocalised with the nuclear staining in the hSTI1 depleted cells. This change, however, was not determined to be significant (Figure 3.23 i-ii). Profilin colocalised with F-actin in the non-targeting control cells as the channel intensities showed moderate levels of correlation (Rr = 0.600 ± 0.032) (Figure XB i, PDM image). This level of intensity correlation decreased in hSTI1 depleted cells (Rr = 0.469 ± 0.080) (Figure 3.23B i, PDM image). Therefore, profilin and F-actin show lower levels of colocalisation when hSTI1 is depleted (Figure 3.23B ii). Contrarily, hSTI1 seems to have no effect on the colocalisation of profilin and Hsp90, as the Pearson's coefficient is identical between the non-targeting control and the hSTI1 depleted cells (Rr = 0.520 ± 0.118 and 0.520 ± 0.118, respectively) (Figure 3.23C i-ii). Furthermore, the areas where colocalisation between profilin and Hsp90 was seen remained unchanged when hSTI1 was depleted (Figure 3.23C, PDM image).

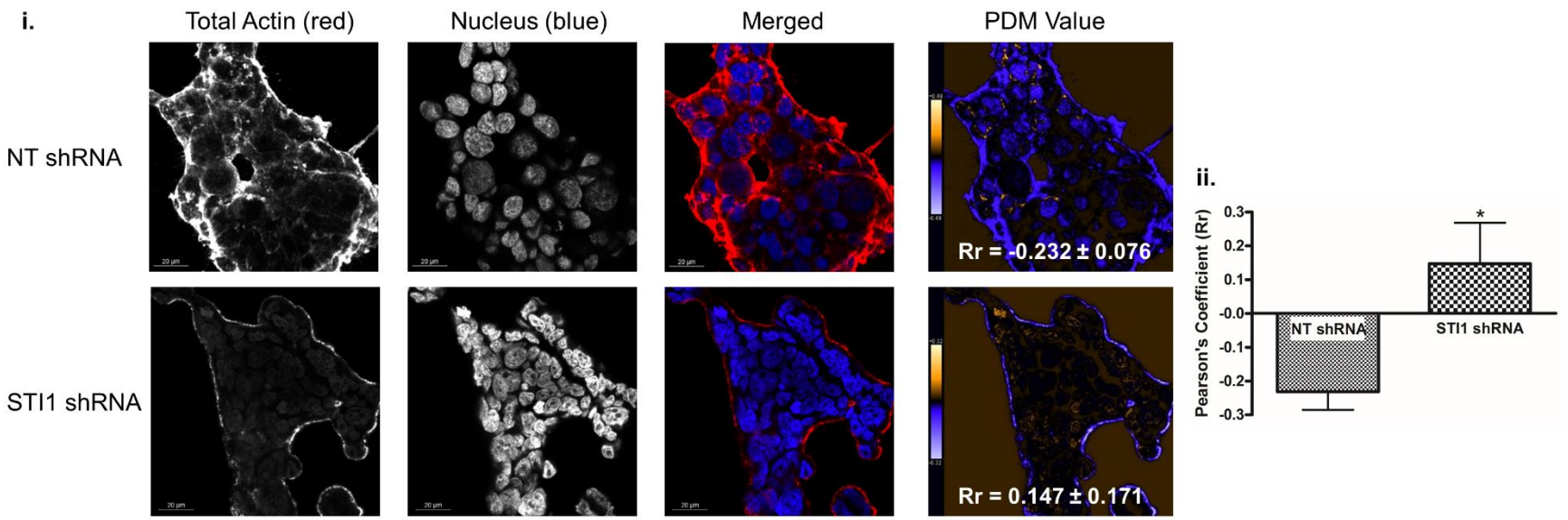

Figure 3.21 - STI1 depletion results in an increase in colocalisation of actin and the nucleus

NT and STI1 shRNA HEK293T cells were seeded onto glass coverslips and incubated for 24 hours. NT HEK293T cells were used as a control and had normal levels of hSTI1 and the STI1 shRNA HEK293T cells had reduced levels of hSTI1. Cells were induced with doxycycline (1 µg/ml) for 72 hours. Actin polymerisation was induced by serum starvation for 30 minutes followed by serum replenishment. The cells were washed with PBS, fixed with ice cold ethanol and permeabilized with 0.1 % (v/v) Triton-X in PBS. The cells were stained with the appropriate primary and secondary antibodies for total actin (red). The nucleus was stained by washing the cells with Hoechst (1 µg/ml). Cells were visualised using the Zeiss LSM 780 confocal microscope and all images captured using the equivalent laser settings. Images were processed and analysed using the intensity correlation analysis plugin on the ImageJ software. i. The top row of images represents NT shRNA HEK293T cells and the bottom represents STI1 shRNA HEK293T. The first column represents the total actin staining, the second column shows the nuclear staining. The third column represents the merged images. Colours refer to merged images, proteins alone are shown in black and white. The fourth column displays the PDM image with the calculated Pearson's coefficient (Rr). ii. Differences in Pearson's coefficient values were statistically analysed by an unpaired t test. (*=$p<0.05$). Data shown are representative of three independent fields of view.

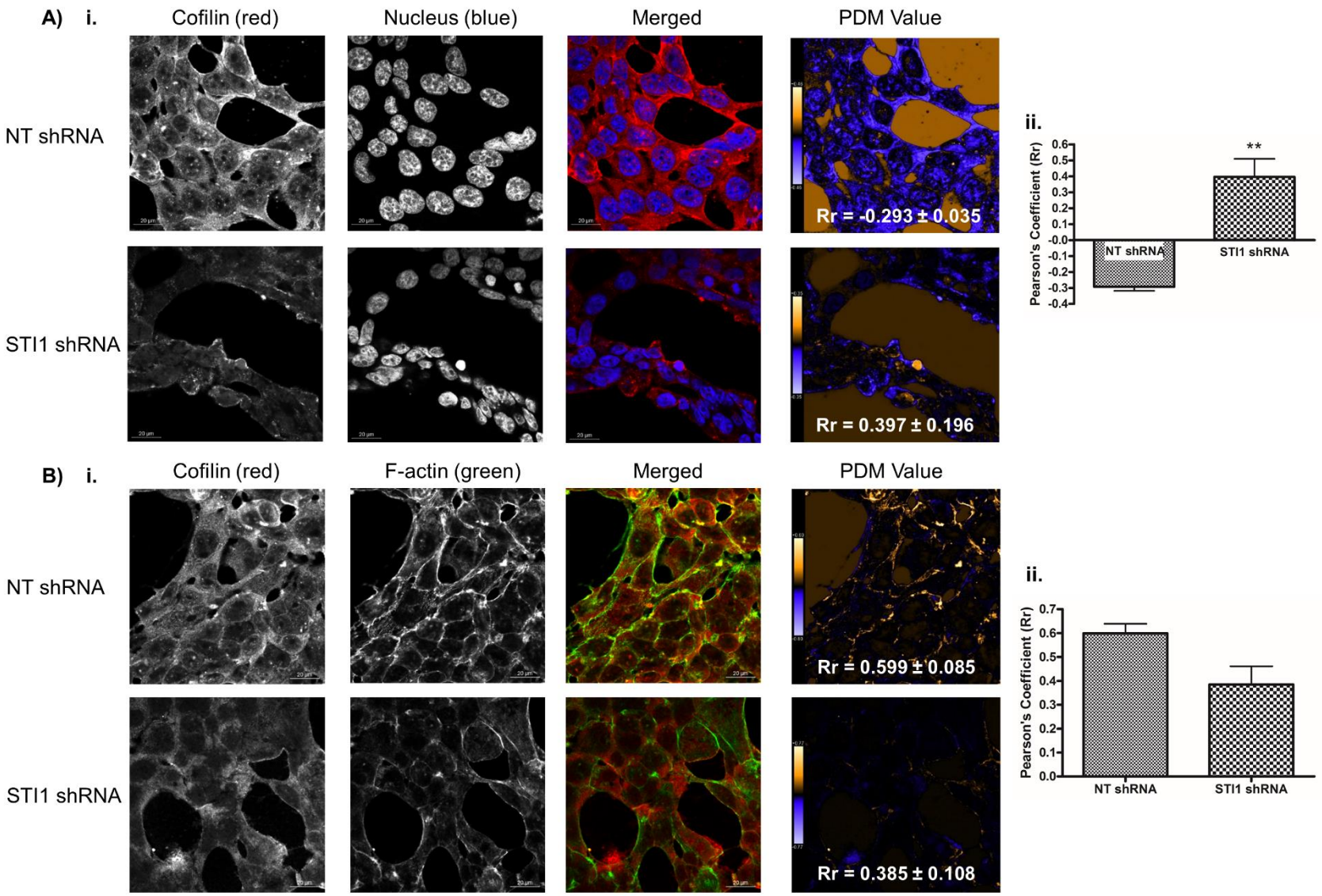

Figure 3.22 - STI1 plays a role in the subcellular localisation of cofilin

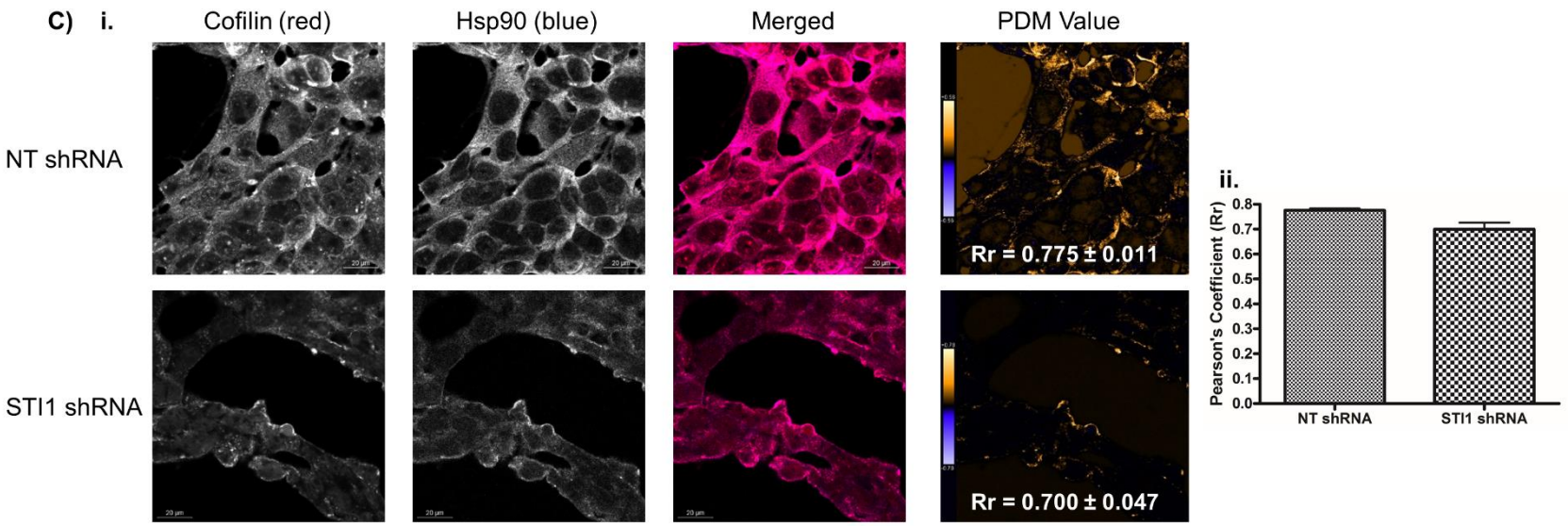

Figure 3.22 - STI1 plays a role in the subcellular localisation of cofilin

NT and STI1 shRNA HEK293T cells were seeded onto glass coverslips and incubated for 24 hours. NT HEK293T cells were used as a control and had normal levels of hSTI1 and the STI1 shRNA HEK293T cells had reduced levels of hSTI1. Cells were induced with doxycycline (1 µg/ml) for 72 hours. Actin polymerisation was induced by serum starvation for 30 minutes followed by serum replenishment. The cells were washed with PBS, fixed with ice cold ethanol and permeabilized with 0.1 % (v/v) Triton-X in PBS. The cells were stained with the appropriate primary and secondary antibodies for cofilin (red) and Hsp90 (purple). F-actin was stained using ActinGreen™ 488 ReadyProbes® and the nucleus was stained by washing the cells with Hoechst (1 µg/ml). Cells were visualised using the Zeiss LSM 780 confocal microscope and all images captured using the equivalent laser settings. Images were processed and analysed using the intensity correlation analysis plugin on the ImageJ software (Li et al., 2004). The top row of images represents NT shRNA HEK293T cells and the bottom represents STI1 shRNA HEK293T. The first column represents the cofilin staining, the second column shows the second channel of A) Nucleus, B) F-actin and C) Hsp90. The third column represents the merged images of the two analysed channels. Colours refer to merged images, proteins alone are shown in black and white. The fourth column displays the PDM image with the calculated Pearson's coefficient (Rr). Differences in Pearson's coefficient values were statistically analysed by an unpaired t test (**=$p<0.01$). Data shown are representative of three independent fields of view.

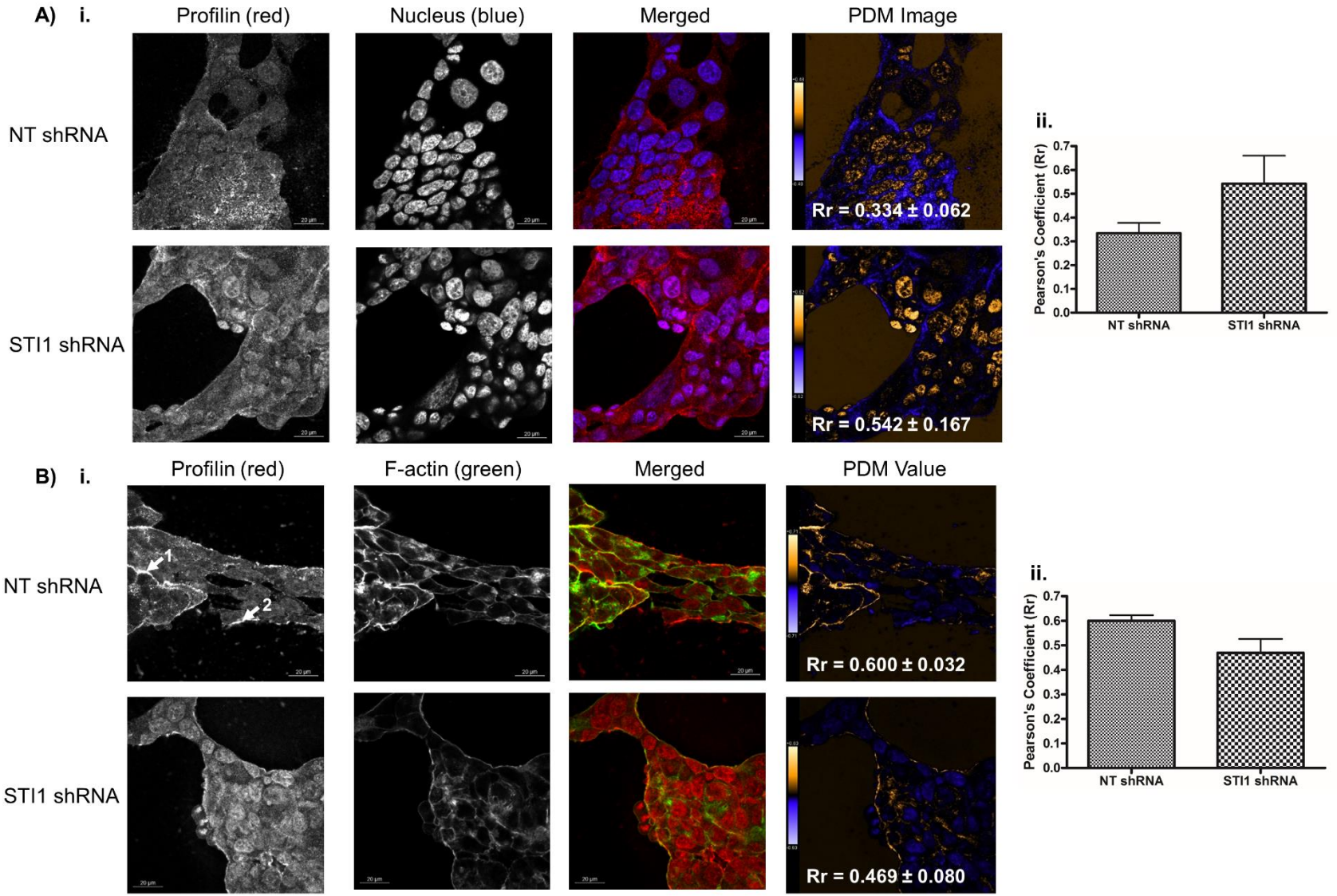

Figure 3.23 - STI1 depletion results in change of profilin subcellular localisation in HEK293T cells

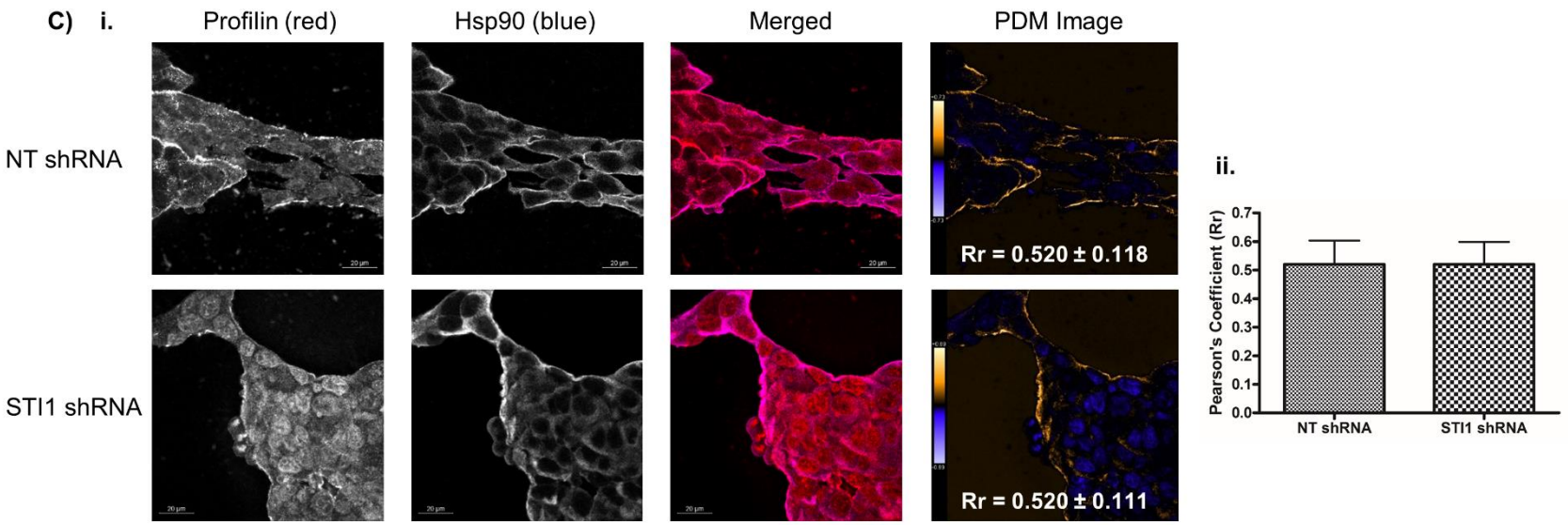

Figure 3.23 - STI1 depletion results in change of profilin subcellular localisation in HEK293T cells

NT and STI1 shRNA HEK293T cells were seeded onto glass coverslips and incubated for 24 hours. NT HEK293T cells were used as a control and had normal levels of hSTI1 and the STI1 shRNA HEK293T cells had reduced levels of hSTI1. Cells were induced with doxycycline (1 µg/ml) for 72 hours. Actin polymerisation was induced by serum starvation for 30 minutes followed by serum replenishment. The cells were washed with PBS, fixed with ice cold ethanol and permeabilized with 0.1 % (v/v) Triton-X in PBS. The cells were stained with the appropriate primary and secondary antibodies for profilin (red) , Hsp90 (purple). F-actin was stained using ActinGreen™ 488 ReadyProbes® and the nucleus was stained by washing the cells with Hoechst (1 µg/ml). Cells were visualised using the Zeiss LSM 780 confocal microscope and all images captured using the equivalent laser settings. Images were processed and analysed using the intensity correlation analysis plugin on the ImageJ software. The top row of images represent NT shRNA HEK293T cells and the bottom represents STI1 shRNA HEK293T. The first column represents the profilin staining, the second column shows the second channel of A) Nucleus, B) F-actin and C) Hsp90. The third column represents the merged images of the two analysed channels. Colours refer to merged images, proteins alone are shown in black and white. The fourth column displays the PDM image with the calculated Pearson's coefficient (Rr). Differences in Pearson's coefficient values were statistically analysed by an unpaired t test, no statistical differences were found. Data shown are representative of three independent fields of view.

Chapter 4: Discussion

4.1 Introduction

A growing amount of evidence is linking the co-chaperone of Hsp70 and Hsp90, STI1, to cell migration (Chao et al., 2013; Fonseca et al., 2012; de Souza et al., 2014; Willmer et al., 2013). Research in our laboratory has shown the colocalisation of hSTI1 with actin in breast cancer cells, as well as direct binding of hSTI1 and F-actin by co-sedimentation *in vitro*. Additionally, the knockdown of STI1 resulted in reduced formation of pseudopodia as well as decreased cell migration (Willmer et al., 2013). Actin is an important component of the cytoskeleton as it makes up the microfilaments (Theriot and Mitchison, 1991). Our research herein has suggested that mSTI1 directly binds F-actin *in vitro*. Although the specific domain(s) required for this interaction could not be determined, it was determined that TPR1 or TPR2AB domains alone were not sufficient for actin binding. Full length mSTI1 displayed ATPase activity and could potentially stimulate the ATPase activity of actin. In mammalian cells hSTI1 colocalised with the cytoskeletal proteins actin and tubulin as well as actin binding proteins, cofilin and profilin. The depletion of hSTI1 using RNA interference resulted in a change in actin morphology, reduction in the total levels of profilin and decreased colocalisation of actin with profilin and cofilin. There was also an observed increase in levels of colocalisation of actin, cofilin and profilin with the nucleus upon hSTI1 depletion.

4.2 mSTI1 is also an ATPase

Previous studies have demonstrated that hSTI1 has ATPase activity (Yamamoto et al., 2014). In Figure 3.11, mSTI1 was shown to have ATPase activity. Although low amounts of the *E. coli* chaperone, DnaK (*E. coli* Hsp70) were detected in the mSTI1 elution (Figure 3.11C), it is unlikely that this chaperone was influencing the rate of ATP hydrolysis. This conclusion is based on the literature stating that HPLC purified DnaK had a low basal ATPase activity rate

with a turnover number of 0.087 ± 0.007 /min, although higher levels of 0.42 ± 0.02 min^{-1} were reported before HPLC purification, both at 37°C (Palleros et al., 1993). Prior to this, high rates of ATP hydrolysis by DnaK were also reported in literature between a range of 0.28 – 0.9 /min at 20 °C (Richarme and Kohiyama, 1993). It was speculated that these higher activities were as a result of the presence of contaminating proteins in the DnaK elutions (Palleros et al., 1993). Our ATPase assays were carried out at 37°C and the turnover values were not comparable with either of the earlier reported DnaK ATPase activity values at this temperature. STI1 has only been reported to stimulate the ATPase activity of one Hsp70. In *Saccharomyces cerevisiae* (yeast), yeast STI1 (ySTI1) was shown to stimulate one yHsp70 isoform Ssa1. As there has been no report of STI1 present in *E. coli*, it is unlikely that mSTI1 is able to stimulate DnaK. Therefore, due to the low basal ATPase rate of the contaminating DnaK, the kinetic values determined were more likely as a result of the ATPase activity of mSTI1. The apparent k_{cat} = 0.131 min^{-1} determined from our research is substantially higher than the k_{cat} reported by Yamamoto et al. (2014). This may be a true difference in ATPase activity rate or as a result of our purification methods. Ultimately, in order to determine more true kinetic values for the hydrolysis of ATP by mSTI1, a more rigorous purification process including an additional step like fast protein liquid chromatography (FPLC) using size exclusion is necessary in order to remove any other potential contaminating ATPases. Furthermore, more research is needed in order to determine whether the ATPase activity of mSTI1 results in a similar conformational change of the protein to that observed by Yamamoto et al. (2014) as well as determination of which specific domain of mSTI1 is responsible for this ATPase activity.

4.3 The ability of mSTI1 to stimulate actin ATP hydrolysis

Figure 3.16 showed a stimulation of ATPase activity when mSTI1 and actin were combined together. Once again, the possibility of contaminating DnaK affecting these results cannot be

completely excluded, although this is improbable. The stimulation of DnaK by only a substrate is poor and inefficient. In order for the ATPase activity to be stimulated efficiently, it is necessary for the DnaK co-chaperone, DnaJ to be present (Laufen et al., 1999). Furthermore, as the endogenous ATPase activity of mSTI1 was subtracted from the values, it suggested that stimulation of the ATPase activity was as a result of combining mSTI1 and actin. However, from the current data it is still theoretically possible that actin was stimulating mSTI1 ATPase activity. To our knowledge, no actin binding protein have been reported in the literature to increase the hydrolysis of ATP by actin. Ideally the actin ATPase experiments should be conducted with a dominant negative mSTI1 protein that lacks ATPase activity (as has been done for Hsp90) (Miao et al., 2008). This is not possible at present as the domains and functional residues required for the ATPase activity of hSTI1 or mSTI1 are currently unknown.

Unexpectedly, the hSTI1-derived test and scrambled peptides resulted in an enhanced stimulation of ATPase activity when mSTI1 and actin were combined (Figure 3.17). This stimulation cannot be as a result of the stimulation of the mSTI1 or the contaminating DnaK as no stimulation was seen when full length mSTI1 and the peptides were incubated alone. Similarly, when incubated with actin alone, no stimulation was seen. As the test and scrambled peptides resulted in a similar stimulation, this suggested that it was not the sequence of the amino acids which resulted in the stimulation of ATPase activity, but possibly that the overall charge of the combined amino acids resulted in the stimulation. Previous data has shown the ATPase activity of SecA to be dependent on hydrophobicity, as well as N-terminal charge of functional signal sequences (Wang et al., 2000). Peptides which are very hydrophobic were able to stimulate the ATPase activity of SecA and the N-terminal charge did not influence this stimulation. Peptides which had an intermediate hydrophobicity were also able to stimulate SecA ATP hydrolysis, but the N-terminal charge of the peptide influenced this stimulation, whereby, the more positive amino acids present at the N-terminal, the greater the stimulation

of SecA ATPase activity (Wang et al., 2000). To our knowledge there are no published reports supporting the ability of the overall charge of a peptide to stimulate ATP hydrolysis.

4.4 Domains of mSTI1 involved in the actin interaction

Figure 3.12 demonstrates the capacity of the full length mSTI1 and mSTI1 truncation proteins to bind actin. These data would suggest that one or more of the TPR2AB-DP2 domains play a role in the actin-mSTI1 interaction as this region of the protein bound to actin more strongly than others. Similarly, this GST-tagged mSTI1 truncation lacking TPR1 and DP1 was able to bind F-actin. However, the untagged version of this mSTI1 truncation did not co-sediment with actin. This suggested that the GST tag affected the binding capabilities of the protein. This may be through the formation of dimers, as GST forms homodimers (Kaplan et al., 1997). This would therefore result in a dimerized version of TPR2AB-DP2 domains of mSTI1. There have been reports of mSTI1 and hSTI1 occurring as both a monomer and dimer, but the most recent study on STI1 oligomerisation found STI1 to only occur as a monomer (Yi et al., 2010). Some F-actin binding proteins have two actin binding sites present on the protein and some rely on the formation of homodimers to create the two actin binding sites (Stevenson et al., 2012). Therefore, the dimerization of mSTI1 via the GST may create two sites to which F-actin can bind, and therefore allowing the N-terminal truncated protein to bind. In order to determine which of the proteins occurred as monomer, dimers or both, protocols such as gel filtration and native SDS-PAGE analysis can be used (Flom et al., 2007; Lee et al., 2005). In order to determine more accurate binding capabilities of the mSTI1 truncation with actin, the SPR analysis should be repeated with the untagged mSTI1 proteins.

The SPR data in Figure 3.12B suggested that TPR1-DP1 had weak affinity for actin. As seen with the N-terminal truncated mSTI1, the GST tag may have affected the binding affinity of the TPR1-DP1 domains for actin.

Both truncated versions of the mSTI1 proteins have been used in previous studies and have been shown to be functional as both were able to bind their corresponding murine chaperones, Hsp70 and Hsp90 (Lässle et al., 1997; Odunuga et al., 2003), as well as human Hsp70 and Hsp90 in our laboratory (Contu, 2014). Therefore, the inability of the separated domains TPR1-DP1 and TPR2AB-DP2 to bind F-actin was not likely to be as a result of misfolded, non-functional proteins.

The GST tagged and untagged full length mSTI1 consistently co-sedimented with F-actin (Figure 3.13). This correlates with previous literature providing evidence that hSTI1 binds F-actin (Willmer et al., 2013). Further supporting this evidence, full length mSTI1 showed a relatively high capacity to bind actin by SPR analysis. Interestingly, although mSTI1 strongly associated to actin, it also dissociated quickly from actin (Figure 3.12). It can be speculated the N-terminal portion of mSTI1 has a particular role when binding actin, as the TPR2AB-DP2 portion of mSTI1 bound actin strongly and dissociated slowly, but the inclusion of the TPR1-DP1 domains resulted in a faster dissociation. Although the SPR analysis did not show the TPR1-DP1 region itself to bind actin strongly (Figure 3.12), this region may account for the quick dissociation of mSTI1 from actin. It is within the N-terminal portion that the seven consecutive proline residues are present. Polyproline regions are associated with weaker binding than globular domains, as well as quick dissociation from the bound protein (Kay et al., 2000). Therefore, this region may result in faster dissociation of the full length mSTI1 (Kay et al., 2000).

Inclusion of the mSTI1-derived peptides in the co-sedimentation assay in Figure 3.15 suggested that the individual motifs are not solely involved in actin binding, as the peptides did not completely block the interaction between full length mSTI1 and actin (den Hartigh et al., 1992). However, the combined effect of these peptides on the mSTI1-actin interaction, although not significant, might suggest that the polyproline and DAYKKK motifs are part of a larger actin

binding motif contained within the region between the DP1 and TPR2A domains. A more robust method which may have been used to determine whether these the polyproline and DAYKKK motif are involved in actin binding is the use of antibodies raised against the designed peptides in binding assays. An advantage of such an approach is these antibodies can also be used in *ex vivo* experimentation (Maeshima et al., 2000). On further inspection of the mSTI1 amino acid sequence, the region encompassing Asp_{191} - $Asp_{240,}$ (which precedes the polyproline region and reaches the second putative actin binding motif, DAYKKK) contains a high percentage of charged amino acids resulting in an overall hydrophilic region (Figure 4.1A). A number of actin binding motifs contain a number of charged residues, as seen in Table 1.1 (Cravchik et al., 1994). Furthermore, hydrophilic portions of an α-helix in the N-terminal of actin binding proteins, Cobl and JMY, have been found to bind a hydrophilic cleft located between subdomain 3 and 4 on the actin monomer (Chen et al., 2013). These hydrophilic regions are part of WH2 domains which have only recently been determined to be of importance in the actin interaction. This recent discovery means therefore, that little is known of the consensus residues for the hydrophilic region (Chen et al., 2013). It may be possible that both these regions are necessary for the binding of actin. In order to determine this, previously described *in vitro* experiments used for this research would be repeated with truncations including the DP1 and TPR2A domains together (Figure 4.1B). Interestingly, this region also contains the nuclear localisation signal (NLS) of mSTI1 (residues 222-239), as well as the sites of phosphorylation which regulate the localisation of mSTI1 (Longshaw et al., 2004). The phosphorylation of other actin binding proteins such as cofilin, regulate its binding affinity for actin (Agnew et al., 1995). Therefore it would be interesting to determine whether the phosphorylation of mSTI1 would affect its F-actin binding affinity. Another feature which has been predicted to be present within this region of mSTI1 was the motif responsible for ATPase activity (Yamamoto et al., 2014). As our results suggest that the combination of mSTI1 and

actin results in increased ATPase activity of one or both of the proteins, it would be of interest to see whether similar results are seen with the incubation of actin and the DP1-TPR2A domains of mSTI1.

A) i.

DEEEEIATPPPPPPPKKETKPEPMEEDLPENKKQALKEKELGNDAYKKKD

ii.

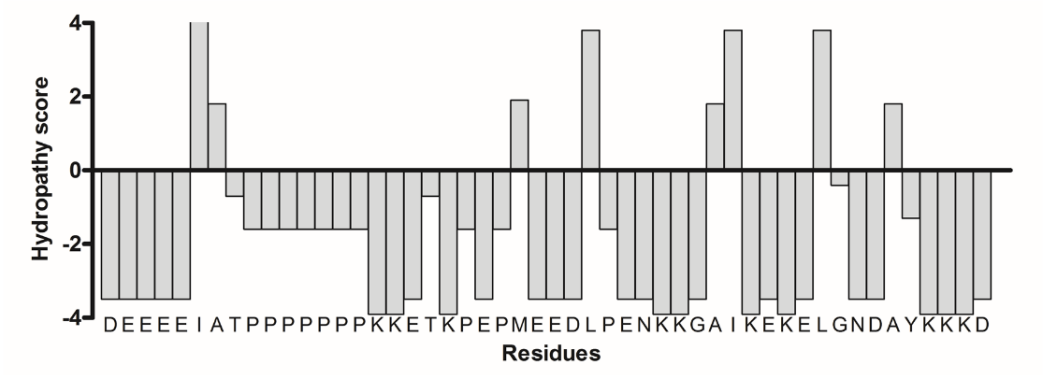

B)

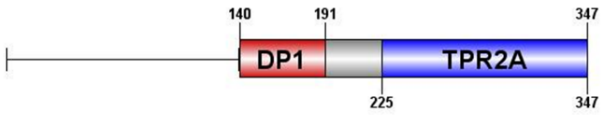

Figure 4.1 - A charged and hydrophilic region exists between the DP1 and TPR2A domains of mSTI1

A) i. The residues between the DP1 and TPR2A domains of hSTI1 consist of many charged amino acids most of which are negatively charged, acidic residues (shown in blue) with some positively charged, basic residues (shown in red). ii. A hydropathy plot shows that the majority of the amino acids between DP1 and TPR2 are hydrophilic. The hydrophathy plot is generated by plotting each of the hydropathy scores of the amino acids (Kyte and Doolittle, 1982). B) mSTI1 truncation required for further determination of actin binding domains. Schematic diagrams were generated using DOG 2.0 software.

4.5 The role of STI1 in cytoskeletal dynamics in mammalian cells

The depletion of STI1 resulted in a change in the morphology and distribution of F-actin in the HEK293T cells (Figure 3.18). The F-actin structures appeared to be less well organised with thinner F-actin filaments (Figure 3.18). Furthermore, hSTI1 depletion resulted in decreased protein levels of another cytoskeletal protein, tubulin, as well as the actin binding proteins cofilin and profilin. In addition, a loss of colocalisation was seen between F-actin and the three proteins tubulin, cofilin and profilin; as well as increased colocalisation between the nucleus and actin, cofilin and profilin. This change in F-actin morphology may therefore be as a result of the direct interaction of hSTI1 and F-actin or as a result of changes in protein levels and subcellular localisation of cofilin and profilin.

Previous work by Li et al. (2012) has shown hSTI1 to bind tubulin *in vitro* and colocalise with microtubules in human umbilical vein endothelial cells (HUVECs). The same study also demonstrated a role for STI1 in angiogenesis via cell migration, as STI1 depletion resulted in decreased cell polarisation and formation of membrane ruffling which consequently reduced cell migration. It was therefore suggested that STI1 influences these processes via its interaction with tubulin (Li et al., 2012). Reduced tubulin levels have been related to a decrease in cell migration (Schaefer et al., 2007). Therefore the reduction of tubulin protein levels seen in our study may suggest a way in which STI1 regulates cell dynamics via an interaction with tubulin.

The same cannot be said for the role of hSTI1 in cell migration via the interaction with F-actin as hSTI1 depletion seemed to have no influence on total levels of actin (Figure 3.19). This indicates that STI1 must have another mechanism by which it regulates cell migration via the actin cytoskeleton.

An interaction between actin filaments and tubulin has previously been described (Griffith and Pollard, 1978; Pollard et al., 1984). Our results showed a colocalisation between F-actin and tubulin, but hSTI1 depletion in the HEK293T cells resulted in a significant decrease in the colocalisation of actin and tubulin. Colocalisation between F-actin and tubulin protein has been shown in neuronal and dividing cells but has not been shown in epithelial cells to our knowledge (Cande et al., 1977; Dent and Kalil, 2001). The interaction between F-actin and tubulin has been shown to be dependent on microtubule-associated proteins (MAPs) (Griffith and Pollard, 1978). hSTI1 has been shown to bind both actin and tubulin (Li et al., 2012; Willmer et al., 2013). More research is required in order to determine the manner in which STI1 affects the colocalisation of F-actin and tubulin. It is tempting to speculate that STI1 may be acting similarly to a MAP and supporting the interaction between F-actin and tubulin. Although it is feasible that either the change in actin morphology and distribution alone has affected the colocalisation of F-actin and tubulin, or the decreased protein levels of tubulin has simply resulted in the decrease in colocalisation.

The role of actin binding proteins is to regulate actin dynamics (Winder and Ayscough, 2005). Cofilin influences the rate of polymerisation and depolymerisation via its actin severing abilities, as well as plays a role in actin nucleation (Andrianantoandro and Pollard, 2014; Carlier et al., 1997; Pavlov et al., 2007). It has been previously suggested that reduced levels of cofilin result in the inhibition of cell motility (Hotulainen et al., 2005). In studies where cofilin-1 and/or actin depolymerising factor (ADF) were knocked down in B16F1 and NIH3T3 cells, abnormal actin stress fibres were formed, these were described to be very long and thin actin fibres. The cells also lost the morphology of small lamellipodia with membrane ruffles and instead exhibited large smooth lamellipodia with no membrane ruffles, and consequently, cell motility was inhibited (Hotulainen et al., 2005). The STI1 depleted HEK293T cells also exhibited an abnormal actin morphology, actin fibres appeared to be predominantly short and

thin with a small number of long, thin filaments extending from the cells (Figure 3.18). The differences between our results and those of Hotulainen et al. (2005) may be explained by a smaller reduction in cofilin levels, and by the use of different cell lines, as the B16F1 and NIH 3T3 have fibroblast-like morphologies whereas the HEK293T cell line has an epithelial morphology. The cofilin pathway has been shown to play a major role in the metastasis and invasiveness of breast cancer cells. Therefore, it may be beneficial to determine whether STI1 plays a role in this pathway in future research (Wang et al., 2007).

The effects of reduced levels of profilin on the actin cytoskeleton are far less clear than those of cofilin. The silencing of profilin in HUVECs resulted in diminished cell migration in wound healing assays (Ding et al., 2006). In Swiss 3T3 (mouse embryonic fibroblast) cells, the co-injection of Cdc42 and mutated profilin (deficient in actin binding) supressed the formation of microspikes typically associated with Cdc42 (Suetsugu et al., 1999b). Similarly, when the mutant profilin was co-injected with Rac, a lack of membrane ruffling was seen which is normally associated with Rac (Suetsugu et al., 1999b). On the other hand, co-injection of mutant profilin and Rho resulted in little change in stress fibre formation; which were seen when Rho was microinjected alone, but reduced upon co-injection of Rho and wild type profilin (Suetsugu et al., 1999b). Although not directly part of this study, RhoC was previously shown in our laboratory to decrease in protein levels when hSTI1 was depleted (Contu, 2014; Willmer et al., 2013). Most isoforms of Rho are involved in cell migration, RhoC has been associated with stress fibre formation, and the knockdown of RhoC in MEFs resulted in an abnormal actin morphology (Golen et al., 2000; Hakem et al., 2005). Interestingly, the actin morphology of the cells in which RhoC had been knocked out is similar to the actin morphology seen in our results of the STI1 shRNA HEK293T cells, whereby the thick actin borders were reduced and smaller less organised F-actin structures were seen. Therefore, changes in actin morphology may be due to decreased levels of profilin together with RhoC. The expression of profilin is

suppressed in cancer cells (Janke et al., 2000). In breast cancer cells the overexpression of profilin resulted in reduced cell migration in response to epidermal growth factor (EGF) (Roy and Jacobson, 2004). Furthermore, lower levels of profilin at the mRNA and protein level were found in the tumorigenic CAL51 cell line in comparison to its matched nontumorigenic cell line CAL/17-5. The CAL51 cells were described to have thin actin filaments bundles with short F-actin aggregates distributed throughout the cytoplasm, whereas the CAL/17-5 cells have thick bundles of F-actin forming stress fibres as well as peripheral belts (Janke et al., 2000). The actin morphology described in the CAL/17-5 cells was more comparable with that seen in the control HEK293T cells from our results. The actin morphology of the CAL51 cells was more similar to the actin morphology seen in the HEK293T cells depleted of STI1 with reduced protein levels of profilin. Together, these results appear contradictory as the knockdown of STI1 in HEK293T cells resulted in decreased levels of profilin whereas, in cancer cells, STI1 expression was increased and profilin levels decreased (Janke et al., 2000; Kubota et al., 2010). It would appear that the role of profilin may be highly context specific and therefore, future experiments of knockdown of STI1 in cancerous cells, with detection of profilin levels, would be beneficial in determining the role of STI1 in regulation of profilin in cancer cells.

Although, to our knowledge, no work has been done on the simultaneous knockdown of cofilin and profilin, research has been done on the increased expression of PIP_2 in CV1 cells by the overexpression of phosphatidylinositol-4-phosphate 5-kinase type 1 (PIP5KI) (Yamamoto et al., 2001). PIP_2 inhibits the binding of both cofilin and profilin to actin. The overexpression of PIP5KI resulted in reduced profilin-actin binding and although it could not be shown, it was thought to inhibit cofilin as well. The overexpression of PIP5KI resulted in more robust actin stress fibres in comparison to the control cells. This differs from our results of the control cell line with normal expression levels of STI1 as well as cofilin and profilin which have more robust fibres (Yamamoto et al., 2014). It would be of interest to determine whether STI1

depletion affects molecules such as PIP_2 and Rho-associated protein kinase (ROCK) which regulate actin dynamics upstream of profilin and cofilin, in order to gain a better understanding of the mechanism in which STI1 affects actin morphology as well as the levels of the actin binding proteins.

STI1 depletion also increased the amount of actin, profilin and cofilin in the nucleus in the HEK293T cells (Figure 3.21-3.23). Ongoing work in our laboratory has also shown that, on the depletion of STI1 in HEK293T cells, there were levels of residual STI1 predominantly located in the nucleus (Wingate, 2014).

Actin levels have been shown to increase in the nucleus during cellular stress (Fukui and Katsumaru, 1979). As phalloidin staining is typically unable to detect this actin, it has been speculated that the majority of the actin present in the nucleus is in the monomeric form or an "unconventional" conformation (Jockusch et al., 2006). Serum starvation of the cells in our experiment might have induced a stress response, and therefore it is not unexpected that increased amounts of actin were found in the nucleus in the STI1 shRNA HEK293T cells. Interestingly, the same effect was not seen in the control cells. The increase of actin colocalisation with the nucleus may be as a result of a number of reasons. Firstly, it is possible that on STI1 depletion there is a movement of STI1 into the nucleus, and as this occurs it may assist in the transportation of actin as well. Secondly, the STI1 which has been seen in the nucleus in STI1 depleted cells may be residual hSTI1, in which case, STI1 may have a stabilising effect on actin, and therefore the loss on STI1 in the cytoplasm may have resulted in the loss of the cytoplasmic actin over the nuclear actin. The latter option is less likely due to Western blot analysis showing unchanged protein levels of actin in the control and knockdown cells. Another scenario which must also be considered is that the knockdown cells were under greater cellular stress conditions in comparison to the non-targeting cells, due to the STI1 depletion as well as the serum starvation. This could have resulted in increased levels of actin

in the nucleus in a mechanism which is unrelated to hSTI1. The way in which actin enters the nucleus has not yet been determined as actin does not have an NLS, but it has been speculated that actin may enter the nucleus via another protein that does have an NLS (Vartiainen, 2008). It is therefore an interesting possibility that STI1 may play a role in the localisation of actin, and possibly the transportation of actin to the nucleus. In order to determine whether hSTI1 plays a role in the transportation of actin into the nucleus, an experiment can be conducted whereby cells are transfected with a plasmid for the overexpression on hSTI1 as the control or hSTI1 with a non-functional NLS for the test experiment. Cells would be placed under stress conditions such as heat shock to induce the movement of actin into the nucleus. The cells would be analysed using subcellular fractionation with Western blot analysis. A reduced amount of actin in the cells expressing mutated hSTI1 would suggest hSTI1 may assist the import of actin into the nucleus.

Cofilin is an NLS containing protein and, similarly to actin, has also been found to move into the nucleus upon cellular stress (Iida et al., 1992; Munsie et al., 2012). It has also been suggested that cofilin is required for the movement of actin into the nucleus (Pendleton et al., 2003). When in the nucleus, cofilin promotes the formation of actin rods in the nucleus, the function of these fibres has not been determined (Pendleton et al., 2003). The non-targeting control cells showed that cofilin was primarily found in the cytoplasm (Figure 3.22), whereas, an increase in cofilin colocalisation with nuclear staining was seen when STI1 was depleted in the HEK293T cells (Figure 3.22A). Though the cofilin did not concentrate in the nucleus as seen in the previously mentioned studies, the distribution of cofilin between the nucleus and cytoplasm was more evenly distributed (Figure 3.22). As previously mentioned, residual hSTI1 was primarily found in the nucleus upon hSTI1 knockdown (Wingate, 2014). Therefore, the increased colocalisation of cofilin and the nucleus may be due to the lack of hSTI1 in the cytoplasm which, in turn, resulted in the degradation of cytoplasmic cofilin, thus explaining

the decrease in overall cofilin protein levels. Otherwise, hSTI1 depletion may result in the movement of cofilin into the nucleus. An experiment using subcellular fractionation with Western blot analysis using the NT and STI1 shRNA HEK293T cells would be able to distinguish between these two possibilities.

Profilin has been found in the nucleus, where it functions as a cofactor with exportin-6 in the export of actin out of the nucleus (Stuven et al., 2003). As literature suggests that large pools of G-actin are present in the nucleus, profilin in the nucleus may also play a similar role to its cytoplasmic function of sequestering G-actin and promoting nucleotide exchange (Vartiainen, 2008). In the control HEK293T cells, the majority of profilin was found in the cytoplasm, largely excluded from the nucleus (Figure 3.23A). In the STI1 depleted cells, profilin staining in the nucleus was more prominent and the colocalisation of profilin with the nucleus increased (Figure 3.23A). Similarly to cofilin, the increased colocalisation of profilin with the nucleus may be as a result of degradation of cytoplasmic profilin due to the decreased levels of hSTI1 in the cytoplasm. Alternatively, hSTI1 may also play a role in the subcellular localisation of profilin.

Hsp90 is known to play a role in actin dynamics (Koyasu et al., 1986; Taiyab and Rao, 2011). It has also been shown that it functions in the signalling pathway of cofilin whereby it interacts with LIM kinase 1 (LIMK1), a regulatory protein which inactivates cofilin, whereby it promotes and stabilises the formation of the LIMK1 homodimer (Li et al., 2006). There is no literature existing to our knowledge on the colocalisation or interaction between Hsp90 and profilin. Our results in the Hs578T cells show high levels of colocalisation between Hsp90 and profilin and cofilin (Figure 3.1C-D). The area in which Hsp90 and the two actin binding proteins colocalised was similar to the areas of colocalisation between STI1, cofilin and profilin. However, in the HEK293T cells, the depletion of STI1 did not alter the colocalisation levels between Hsp90 and the actin binding proteins (Figure 3.22 and 3.23). This suggested

that the both hSTI1 and Hsp90 may associate with cofilin and profilin, but hSTI1 may specifically function in the subcellular localisation of profilin and cofilin at least in part independently of Hsp90. In order to confirm that Hsp90 does not have a function in the localisation of these proteins, knockdown studies of Hsp90 could be used in order to observe whether a similar effect is seen in the localisation of cofilin and profilin. Future studies to determine whether there is a direct interaction between hSTI1 and cofilin or profilin would include immunoprecipitation assays using cell lysates as well as recombinant proteins.

4.6 Conclusions

Taken together, our data suggests that STI1 plays a diverse role in the dynamics and organisation of the cytoskeleton, possibly independently from Hsp90. STI1 directly interacts with the cytoskeletal proteins tubulin and actin. Furthermore, it may play a role in the interaction between tubulin microtubules and actin filaments. The loss of actin organisation when STI1 was depleted suggests STI1 plays a role in the organisation of F-actin. This may be via the direct interaction of STI1 and actin, or via actin binding proteins known to affect actin dynamics. Indeed, STI1 depletion modified the localisation of actin, and the levels and localisation of cofilin and profilin, leading to an apparent increase of these proteins in the nucleus upon STI1 depletion. Therefore, it is tempting to speculate that STI1 may also play a role in the dynamics of nuclear cytoskeletal dynamics. These functions of STI1 have only been shown in human embryonic kidney cells, therefore future studies are required in cancer cells in order to determine whether STI1 functions similarly in cancer.

4.7 Future studies

In order gain a greater understanding of the role of mSTI1 in cell migration via its ability to bind actin further experimentation is required. To determine more accurate kinetic values for mSTI1, it is necessary to repeat the ATPase assay protocol using mSTI1 which has been purified by a rigorous purification process such an FPLC, ensuring there is no contaminating DnaK present (Palleros et al., 1993). The exact region of mSTI1 that is involved in actin binding could not be determined in this project and therefore, more research is required in order to do so. This can be done by repeating binding assays with the use of truncated proteins, other designed peptides as well as peptide-directed antibodies raised against the regions thought to be involved in the interaction (Maeshima et al., 2000; Odunuga et al., 2003). After the motif essential for actin binding has been identified, it would be useful to determine the specific residues essential for binding actin. The use of site-directed mutagenesis would be useful for this (Flom et al., 2006).

Ex vivo experiments from our research have suggested hSTI1 may play a role in cell migration by directly or indirectly effecting more than one protein involved in actin dynamics. More research is required to gain a better understanding of the pathways in which hSTI1 may be involved. This would include determining whether hSTI1 plays a role in actin-tubulin interactions, confirming whether hSTI1 pays a role in the cofilin and profilin pathways and whether hSTI1 may be involved in the shuttling of actin between the nucleus and the cytoplasm of the cell. Suggestions of experiments include the use of immunoprecipitation assays using cell lysates or recombinant proteins to determine whether there is a direct interaction between hSTI1 and cofilin or profilin, and whether Hsp90 is involved in either of the possible interactions. Subcellular fractionation using the NT and STI1 shRNA HEK293T cells can also be done to confirm whether hSTI1 plays a role in the cellular localisation of cofilin and profilin. In order to determine whether hSTI1 plays a role in actin regulation further upstream NT and

STI1 shRNA HEK293T lysates can be used to examine whether molecules such as PIP_2 and Rho-associated protein kinase (ROCK) are affected by hSTI1 protein levels. Lastly, the use of cells transfected with a plasmid for the overexpression of hSTI1 or hSTI1 with a non-functional NLS could be used to determine whether hSTI1 plays a role in the transportation of actin to the nucleus (Krauer et al., 2004).

Chapter 5: References

Abraham, V.C., Krishnamurthi, V., Taylor, D.L. and Lanni, F. (1999), "The actin-based nanomachine at the leading edge of migrating cells.," *Biophysical Journal*, Vol. 77 No. 3, pp. 1721–1732.

Agnew, B.J., Minamide, L.S. and Bamburg, J.R. (1995), "Reactivation of Phosphorylated Actin Depolymerizing Factor and Identification of the Regulatory Site," *Journal of Biological Chemistry* , Vol. 270 No. 29 , pp. 17582–17587.

Alexandropoulos, K., Cheng, G. and Baltimore, D. (1995), "Proline-rich sequences that bind to Src homology 3 domains with individual specificities," *Proceedings of the National Academy of Sciences of the United States of America*, Vol. 92 No. April, pp. 3110–3114.

Amiri, A., Noei, F., Feroz, T. and Lee, J.M. (2007), "Geldanamycin anisimycins activate Rho and stimulate Rho- and ROCK-dependent actin stress fiber formation.," *Molecular Cancer Research*, Vol. 5 No. 9, pp. 933–942.

Ampe, C., Markey, F., Lindberg, U. and Vandekerckhove, J. (1988), "The primary structure of human platelet profilin: Reinvestigation of the calf spleen profilin sequence," *FEBS Letters*, Vol. 228 No. 1, pp. 17–21.

Andrianantoandro, E. and Pollard, T.D. (2014), "Mechanism of Actin Filament Turnover by Severing and Nucleation at Different Concentrations of ADF/Cofilin," *Molecular Cell*, Vol. 24 No. 1, pp. 13–23.

Arber, S., Barbayannis, F.A., Hanser, H., Schneider, C., Stanyon, C.A., Bernard, O. and Caroni, P. (1998), "Regulation of actin dynamics through phosphorylation of cofilin by LIM-kinase," *Nature*, Vol. 393 No. 6687, pp. 805–809.

Atilgan, E., Wirtz, D. and Sun, S.X. (2005), "Morphology of the lamellipodium and organization of actin filaments at the leading edge of crawling cells.," *Biophysical Journal*, Vol. 89 No. 5, pp. 3589–3602.

Baek, K., Liu, X., Ferron, F., Shu, S., Korn, E.D. and Dominguez, R. (2008), "Modulation of actin structure and function by phosphorylation of Tyr-53 and profilin binding," *Proceedings of the National Academy of Sciences of the United States of America*, National Academy of Sciences, Vol. 105 No. 33, pp. 11748–11753.

Beraldo, F.H., Soares, I.N., Goncalves, D.F., Fan, J., Thomas, A. a, Santos, T.G., Mohammad, A.H., Roffé, M., Calder, M.D., Nikolova, S., Hajj, G.N., Guimaraes, A.L., Massensini, A.R., Welch, I., Betts, D.H., Gros, R., Drangova, M., Watson, A.J., Bartha, R., Prado, V.F., Martins, V.R. and Prado, M.A.M. (2013), "Stress-inducible phosphoprotein 1 has unique cochaperone activity during development and regulates cellular response to ischemia via the prion protein.," *FASEB Journal*, Vol. 27 No. 9, pp. 3594–3607.

Bercovich, B., Stancovski, I., Mayer, A., Blumenfeld, N., Laszlo, A., Schwartz, A.L. and Ciechanover, A. (1997), "Ubiquitin-dependent Degradation of Certain Protein Substrates in Vitro Requires the Molecular Chaperone Hsc70," *Journal of Biological Chemistry* , Vol. 272 No. 14 , pp. 9002–9010.

Bernard, O., Ganiatsas, S., Kannourakis, G. and Dringen, R. (1994), "Kiz-1, a protein with LIM zinc finger and kinase domains, is expressed mainly in neurons," *Cell growth & differentiation : The Molecular Biology Journal of the American Association for Cancer Research*, Vol. 5 No. 11, pp. 1159–1171.

Berry, W.K. (1951), "The Turnover Number of Cholinesterase," *Biochemical Journal*, Vol. 49 No. 5, pp. 615–620.

Bisi, S., Disanza, A., Malinverno, C., Frittoli, E., Palamidessi, A. and Scita, G. (2013), "Membrane and actin dynamics interplay at lamellipodia leading edge," *Current Opinion in Cell Biology*, Vol. 25 No. 5, pp. 565–573.

Blatch, G.L. and Lässle, M. (1999), "The tetratricopeptide repeat: a structural motif mediating protein-protein interactions.," *BioEssays*, Vol. 21 No. 11, pp. 932–939.

Blatch, G.L., Lässle, M., Zetter, B.R. and Kundra, V. (1997), "Isolation of a mouse cDNA encoding mSTI1, a stress-inducible protein containing the TPR motif.," *Gene*, Vol. 194 No. 2, pp. 277–282.

Bravo-Cordero, J.J., Hodgson, L. and Condeelis, J. (2012), "Directed cell invasion and migration during metastasis.," *Current Opinion in Cell Biology*, Vol. 24 No. 2, pp. 277–283.

Bravo-Cordero, J.J., Magalhes, M.A.O., Eddy, R., Hodgson, L. and Condeelis, J. (2013), "Functions of cofilin in cell locomotion and invasion," *Nature Reviews Molecular Cell Biology*, Vol. 14 No. 7, pp. 1–24.

Buss, F., Temm-Grove, C., Henning, S. and Jockusch, B.M. (1992), "Distribution of profilin in fibroblasts correlates with the presence of highly dynamic actin filaments," *Cell motility and the Cytoskeleton*, Vol. 22 No. 1, pp. 51–61.

Cande, W.Z., Lazarides, E. and McIntosh, J.R. (1977), "A comparison of the distribution of actin and tubulin in the mammalian mitotic spindle as seen by indirect immunofluorescence.," *The Journal of Cell Biology* , Vol. 72 No. 3 , pp. 552–567.

Carlier, M., Laurent, V., Santolini, J., Melki, R., Didry, D., Xia, G., Hong, Y., Chua, N. and Pantaloni, D. (1997), "Actin Depolymerizing Factor (ADF/Cofilin) Enhances the Rate of Filament Turnover: Implication in Actin-based Motility," *The Journal of Cell Biology*, Vol. 136 No. 6, pp. 1307–1322.

Carrigan, P.E., Riggs, D.L., Chinkers, M. and Smith, D.F. (2005), "Functional comparison of human and Drosophila Hop reveals novel role in steroid receptor maturation.," *The Journal of Biological Chemistry*, Vol. 280 No. 10, pp. 8906–8911.

Carrigan, P.E., Sikkink, L.A., Smith, D.F. and Ramirez-alvarado, M. (2006), "Domain:domain interactions within Hop, the Hsp70/Hsp90 organizing protein, are required for protein stability and structure," *Protein Science*, Vol. 15, pp. 522–532.

Casella, J.F., Craig, S.W., Maack, D.J. and Brown, A.E. (1987), "Cap Z(36/32), a barbed end actin-capping protein, is a component of the Z-line of skeletal muscle.," *The Journal of Cell Biology* , Vol. 105 No. 1 , pp. 371–379.

Cavallaro, U. and Christofori, G. (2000), "Molecular Mechanisms of Tumor Angiogenesis and Tumor Progression," *Journal of Neuro-Oncology*, Vol. 50 No. 1-2, pp. 63–70.

Chao, A., Lai, C., Tsai, C., Hsueh, S., Hsueh, C., Lin, C., Chou, H., Lin, Y., Chen, H., Chang, T. and Wang, T. (2013), "Tumor Stress-Induced Phosphoprotein1 (STIP1) as a Prognostic Biomarker in Ovarian Cancer," *PloS ONE*, Vol. 8 No. 2, pp. 1–9.

Chardin, P. (2006), "Function and regulation of Rnd proteins," *Nature Reviews Molecular Cell Biology* , Vol. 7 No. 1, pp. 54–62.

Chaturvedi, V. and Sreedhar, A.S. (2010), "Hsp90 inhibition induces destabilization of actin cytoskeleton in tumor cells: functional significance of Hsp90 interaction with F–actin," *Asian Pacific Journal of Tropical Medicine*, Vol. 3 No. 9, pp. 715–722.

Chen, S. and Smith, D.F. (1998), "Hop as an adaptor in the heat shock protein 70 (Hsp70) and hsp90 chaperone machinery.," *The Journal of Biological Chemistry*, Vol. 273 No. 52, pp. 35194–35200.

Chen, X., Ni, F., Tian, X., Kondrashkina, E., Wang, Q. and Ma, J. (2013), "Structural Basis of Actin Filament Nucleation by Tandem W Domains," *Cell Reports*, Vol. 3 No. 6, pp. 1910–1920.

Le Clainche, C. and Carlier, M.-F. (2008), "Regulation of Actin Assembly Associated With Protrusion and Adhesion in Cell Migration," *Physiological Reviews*, Vol. 88 No. 2, pp. 489–513.

Coitinho, A.S., Lopes, M.H., Hajj, G.N.M., Rossato, J.I., Freitas, A.R., Castro, C.C., Cammarota, M., Brentani, R.R., Izquierdo, I. and Martins, V.R. (2007), "Short-term memory formation and long-term memory consolidation are enhanced by cellular prion association to stress-inducible protein 1.," *Neurobiology of Disease*, Vol. 26 No. 1, pp. 282–290.

Contu, L. (2014), *The effects of extracellular and intracellular Hop on cell migration processes*. MSc dissertation, Rhodes University.

Courson, D.S. and Rock, R.S. (2010), "Actin cross-link assembly and disassembly mechanics for alpha-Actinin and fascin.," *The Journal of Biological Chemistry*, Vol. 285 No. 34, pp. 26350–26357.

Cravchik, A., Reddy, D. and Matus, A. (1994), "Identification of a novel microtubule-binding domain in microtubule- associated protein 1A (MAP1A)," *Journal of Cell Science*, Vol. 107, pp. 661–672.

Dent, E.W. and Kalil, K. (2001), "Axon Branching Requires Interactions between Dynamic Microtubules and Actin Filaments," *The Journal of Neuroscience*, Vol. 21 No. 24, pp. 9757–9769.

de Souza, L.E.R., Moura Costa, M.D., Bilek, E.S., Lopes, M.H., Martins, V.R., Püschel, A.W., Mercadante, A.F., Nakao, L.S. and Zanata, S.M. (2014), "STI1 antagonizes cytoskeleton collapse mediated by small GTPase Rnd1 and regulates neurite growth.," *Experimental Cell Research*, Vol. 324 No. 1, pp. 84–91.

Didry, D., Carlier, M.-F. and Pantaloni, D. (1998), "Synergy between Actin Depolymerizing Factor/Cofilin and Profilin in Increasing Actin Filament Turnover," *Journal of Biological Chemistry* , Vol. 273 No. 40 , pp. 25602–25611.

Ding, Z., Lambrechts, a., Parepally, M. and Roy, P. (2006), "Silencing profilin-1 inhibits endothelial cell proliferation, migration and cord morphogenesis," *Journal of Cell Science*, Vol. 119 No. 20, pp. 4366–4366.

Dominguez, R. (2004), "Actin-binding proteins--a unifying hypothesis.," *Trends in Biochemical Sciences*, Vol. 29 No. 11, pp. 572–578.

Dominguez, R. and Holmes, K.C. (2011), "Actin Structure and Function," *Annual Review of Biophysics*, Vol. 40 No. 3, pp. 169–186.

Dowd, J.E. and Riggs, D.S. (1965), "A Comparison of Estimates of Michaelis-Menten Kinetic Constants from Various Linear Transformations," *The Journal of Biological Chemistry*, Vol. 240 No. 2, pp. 863–869.

Drewes, G., Ebneth, A. and Mandelkow, E.-M. (1998), "MAPs, MARKs and microtubule dynamics," *Trends in Biochemical Sciences*, Vol. 23 No. 8, pp. 307–311.

Finidori, J., Friedrich, E., Kwiatkowski, D.J. and Louvard, D. (1992), "In vivo analysis of functional domains from villin and gelsolin," *The Journal of Cell Biology*, Vol. 116 No. 5, pp. 1145–1155.

Finkel, T., Theriot, J.A., Dise, K.R., Tomaselli, G.F. and Goldschmidt-Clermont, P.J. (1994), "Dynamic actin structures stabilized by profilin.," *Proceedings of the National Academy of Sciences*, Vol. 91 No. 4 , pp. 1510–1514.

Flaherty, K.M., McKay, D.B., Kabsch, W. and Holmes, K.C. (1991), "Similarity of the three-dimensional structures of actin and the ATPase fragment of a 70-kDa heat shock cognate protein.," *Proceedings of the National Academy of Sciences of the United States of America*, Vol. 88 No. 11, pp. 5041–5045.

Flom, G., Weekes, J., Williams, J.J. and Johnson, J.L. (2006), "Effect of mutation of the tetratricopeptide repeat and asparatate-proline 2 domains of Sti1 on Hsp90 signaling and interaction in Saccharomyces cerevisiae.," *Genetics*, Vol. 172 No. 1, pp. 41–51.

Flom, G., Behal, R.H., Rosen, L., Cole, D.G. and Johnson, J.L. (2007), "Definition of the minimal fragments of Sti1 required for dimerization, interaction with Hsp70 and Hsp90 and in vivo functions.," *The Biochemical Journal*, Vol. 404 No. 1, pp. 159–167.

Fonseca, a C.C. Da, Romão, L., Amaral, R.F., Assad Kahn, S., Lobo, D., Martins, S., Marcondes de Souza, J., Moura-Neto, V. and Lima, F.R.S. (2012), "Microglial stress inducible protein 1 promotes proliferation and migration in human glioblastoma cells.," *Neuroscience*, Vol. 200, pp. 130–141.

Fountain, S.T. (2001), "Mass Spectrometry in Drug Discovery," inRossi,D.T. and Sinz,M. (Eds.), CRC Press, pp. 28–31.

Franke, W.W., Schmid, E., Osborn, M. and Weber, K. (1978), "Different intermediate-sized filaments distinguished by immunofluorescence microscopy.," *Proceedings of the National Academy of Sciences*, Vol. 75 No. 10, pp. 5034–5038.

Friederich, E., Vancompernolle, K., Huet, C., Goethals, M., Finidori, J., Vandekerckhove, J. and Louvard, D. (1992), "An actin-binding site containing a conserved motif of charged amino acid residues is essential for the morphogenic effect of villin," *Cell*, Vol. 70 No. 1, pp. 81–92.

Frydman, J. (2001), "Folding Of Newly Translated Proteins In Vivo: The Role of Molecular Chaperones," *Annual Review of Biochemistry*, Vol. 70 No. 1, pp. 603–647.

Fujiwara, I., Vavylonis, D. and Pollard, T.D. (2007), "Polymerization kinetics of ADP- and ADP-Pi-actin determined by fluorescence microscopy.," *Proceedings of the National Academy of Sciences of the United States of America*, Vol. 104 No. 21, pp. 8827–8832.

Fukata, M., Watanabe, T., Noritake, J., Nakagawa, M., Yamaga, M., Kuroda, S., Matsuura, Y., Iwamatsu, A., Perez, F. and Kaibuchi, K. (2002), "Rac1 and Cdc42 Capture Microtubules through IQGAP1 and CLIP-170," *Cell*, Vol. 109 No. 7, pp. 873–885.

Fukui, Y. and Katsumaru, H. (1979), "Nuclear actin bundles in Amoeba, dictyostelium and human HeLa cells induced by dimethyl sulfoxide," *Experimental Cell Research*, Vol. 120 No. 2, pp. 451–455.

Garnier, C., Barbier, P., Gilli, R., Lopez, C., Peyrot, V. and Briand, C. (1998), "Heat-shock protein 90 (hsp90) binds in vitro to tubulin dimer and inhibits microtubule formation.," *Biochemical and Biophysical Research Communications*, Vol. 250 No. 2, pp. 414–419.

Gasteiger, E., Hoogland, C., Gattiker, A., Duvaud, S., Wilkins, M.R., Appel, R.D. and Bairoch, A. (2005), "Protein Identification and Analysis Tools on the ExPASy Server," inWalker,J.M. (Ed.), *The Proteomics Protocols Handbook*, pp. 571–608.

Gebauer, M., Melki, R. and Gehring, U. (1998), "The chaperone cofactor Hop/p60 interacts with the cytosolic chaperonin-containing TCP-1 and affects its nucleotide exchange and protein folding activities.," *The Journal of Biological Chemistry*, Vol. 273 No. 45, pp. 29475–29480.

Goldschmidt-Clermont, P.J., Furman, M.I., Wachsstock, D., Safer, D., Nachmias, V.T. and Pollard, T.D. (1992), "The control of actin nucleotide exchange by thymosin beta 4 and profilin. A potential regulatory mechanism for actin polymerization in cells.," *Molecular Biology of the Cell* , Vol. 3 No. 9 , pp. 1015–1024.

Goldschmidt-Clermont, P.J., Machesky, L.M., Baldassare, J.J. and Pollard, T.D. (1990), "The actin-binding protein profilin binds to PIP2 and inhibits its hydrolysis by phospholipase C," *Science*, Vol. 247 No. 4950, pp. 1575–1578.

Golen, K.L. Van, Wu, Z.-F., Qiao, X.T., Bao, L.W. and Merajver, S.D. (2000), "RhoC GTPase, a Novel Transforming Oncogene for Human Mammary Epithelial Cells That Partially Recapitulates the Inflammatory Breast Cancer Phenotype," *Cancer Research*, Vol. 60, pp. 5832–5838.

Griffith, L.M. and Pollard, T.D. (1978), "Evidence for actin filament-microtubule interaction mediated by microtubule-associated proteins," *The Journal of Cell Biology*, Vol. 18 No. September, pp. 958–965.

Hakem, A., Sanchez-Sweatman, O., You-Ten, A., Duncan, G., Wakeham, A., Khokha, R. and Mak, T.W. (2005), "RhoC is dispensable for embryogenesis and tumor initiation but essential for metastasis.," *Genes & Development*, Vol. 19 No. 17, pp. 1974–1979.

Hall, T.A. (1999), "BioEdit: a user-friendly biological sequence alignment editor and analysis program for Windows 95/98/NT," *Nucleic Acids Symposium Series*, Vol. 41, pp. 95–98.

Hanahan, D., Jessee, J. and Bloom, F.R. (1991), *Bacterial Genetic Systems*, *Methods in Enzymology*, Methods in Enzymology, Elsevier, Vol. 204, pp. 63–113.

Den Hartigh, J.C., van Bergenen Henegouwen, P.M.P., Verkleij, A.J. and Boonstra, J. (1992), "The EGF Receptor is an Actin-binding Protein," *The Journal of Cell Biology*, Vol. 119 No. 2, pp. 349–355.

Hartl, F.U. and Hayer-Hartl, M. (2002), "Molecular chaperones in the cytosol: from nascent chain to folded protein.," *Science*, Vol. 295 No. 5561, pp. 1852–1858.

Hartmann, C.A., Martins, V.R. and Lima, F.R.S. (2013), "High levels of cellular prion protein improve astrocyte development.," *FEBS letters*, Vol. 587 No. 2, pp. 238–244.

Hartwig, J.H., Thelen, M., Rosen, A., Janmey, P.A., Nairn, A.C. and Aderem, A. (1992), "MARCKS is an actin filament crosslinking protein regulated by protein kinase C and calcium-calmodulin.," *Nature*, Vol. 356 No. 6370, pp. 618–622.

Havrylenko, S., Noguera, P., Abou-Ghali, M., Manzi, J., Faqir, F., Lamora, A., Guérin, C., Blanchoin, L and Plastino, J. (2015), "WAVE binds Ena/VASP for enhanced Arp2/3 complex-based actin assembly," *Molecular Biology of the Cell* . doi:10.1091/mbc.E14-07-1200

He, H.J., Wang, X.S., Pan, R., Wang, D.L., Liu, M.N. and He, R.Q. (2009), "The proline-rich domain of tau plays a role in interactions with actin.," *BMC Cell Biology*, Vol. 10, p. 81.

Hessling, M., Richter, K. and Buchner, J. (2009), "Dissection of the ATP-induced conformational cycle of the molecular chaperone Hsp90," *Nature Structural & Molecular Biology*, Vol. 16 No. 3, pp. 287–293.

Higashi, M., Yu, J., Tsuchiya, H., Saito, T., Oyama, T., Kawana, H., Kitagawa, M., Tamaru, J.-I. and Harigaya, K. (2010), "Visualization of the Activity of Rac1 Small GTPase in a Cell," *Acta Histochemica et Cytochemica*, Vol. 43 No. 6, pp. 163–168.

Hitchcock-DeGregori, S.E. and Heald, R.W. (1987), "Altered actin and troponin binding of amino-terminal variants of chicken striated muscle alpha-tropomyosin expressed in Escherichia coli.," *Journal of Biological Chemistry*, Vol. 262 No. 20, pp. 9730–9735.

Holt, M.R. and Koffer, a. (2001), "Cell motility: proline-rich proteins promote protrusions.," *Trends in Cell Biology*, Vol. 11 No. 1, pp. 38–46.

Honore, B., Leffers, H., Madsen, P., Rasmussen, H.H., Vandekerckhove, J. and Celis, J.E. (1992), "Molecular cloning and expression of a transformation-sensitive human protein containing the TPR motif and sharing identity to the stress-inducible yeast protein STI1.," *Journal of Biological Chemistry*, Vol. 267 No. 12, pp. 8485–8491.

Hotulainen, P., Paunola, E., Vartiainen, M.K. and Lappalainen, P. (2005), "Actin-depolymerizing factor and cofilin-1 play overlapping roles in promoting rapid F-actin depolymerization in mammalian nonmuscle cells.," *Molecular Biology of the Cell*, Vol. 16 No. 2, pp. 649–664.

Howard, J. and Hyman, A.A. (2009), "Growth, fluctuation and switching at microtubule plus ends," *Nature Reviews Molecular Cell Biology* , Vol. 10 No. 8, pp. 569–574.

Iida, K., Matsumoto, S. and Yahara, I. (1992), "The KKRKK Sequence is Involved in Heat Shock-Induced Nuclear Translocation of the 18-kDa Actin-Binding Protein, Cofilin.," *Cell Structure and Function*, Vol. 17 No. 1, pp. 39–46.

Insall, R.H. and Machesky, L.M. (2009), "Actin Dynamics at the Leading Edge: From Simple Machinery to Complex Networks," *Developmental Cell*, Vol. 17 No. 3, pp. 310–322.

Ishikawa, H., Bischoff, R. and Holtzer, H. (1968), "Mitosis and intermediate-sized filaments in developing skeletal muscle.," *The Journal of Cell Biology*, Vol. 38 No. 3, pp. 538–555.

Janke, B.J., Schlüter, K., Jandrig, B., Theile, M., Kölble, K., Arnold, W., Grinstein, E., Schwartz, A., Estevéz-Scwarz, L. Schlag, P.M., Jockusch, B.M. and Scherneck, S. (2000), "Suppression of Tumorigenicity in Breast Cancer Cells by the Microfilament Protein Profilin 1," *Journal of Experimental Medicine*, Vol. 191 No. 10, pp. 1675–1685.

Jockusch, B.M., Schoenenberger, C.-A., Stetefeld, J. and Aebi, U. (2006), "Tracking down the different forms of nuclear actin.," *Trends in Cell Biology*, Vol. 16 No. 8, pp. 391–396.

Johnson, B.D., Schumacher, R.J., Ross, E.D. and Toft, D.O. (1998), "Hop Modulates hsp70/hsp90 Interactions in Protein Folding," *Journal of Biological Chemistry*, Vol. 273 No. 6, pp. 3679–3686.

Johnson, J.L. (2012), "Evolution and function of diverse Hsp90 homologs and cochaperone proteins.," *Biochimica et Biophysica Acta*, Vol. 1823 No. 3, pp. 607–613.

Kaiser, D.A. and Pollard, T.D. (1996), "Characterization of Actin and Poly- L -proline Binding Sites of *Acanthamoeba* Profilin with Monoclonal Antibodies and by Mutagenesis," *Journal of Molecular Biology*, Vol. 256, pp. 89–107.

Kaplan, W., Husler, P., Klump, H., Sluis-cremer, N. and Dirr, H. (1997), "Conformational stability of pGEX-expressed *Schistosoma japonicum* glutathione S-transferase : A detoxification enzyme and fusion-protein affinity tag," *Protein Science*, Vol. 6, pp. 399–406.

Kaverina, I. and Straube, A. (2011), "Regulation of cell migration by dynamic microtubules.," *Seminars in Cell & Developmental Biology*, Vol. 22 No. 9, pp. 968–974.

Kay, B.K., Williamson, M.P. and Sudol, M. (2000), "The importance of being proline : the interaction of proline-rich motifs in signaling proteins with their cognate domains ABSTRACT," *FASEB journal*, Vol. 14, pp. 231–241.

Kinley, A.W., Weed, S.A., Weaver, A.M., Karginov, A. V, Bissonette, E., Cooper, J.A. and Parsons, J.T. (2003), "Cortactin Interacts with WIP in Regulating Arp2/3 Activation and Membrane Protrusion," *Current Biology*, Vol. 13, pp. 384–393.

Kirschner, M.W. and Mitchison, T. (1986), "Microtubule dynamics.," *Nature*, Vol. 324 No. 6098, p. 621.

Komarova, Y.A., Vorobjev, I.A. and Borisy, G.G. (2002), "Life cycle of MTs : persistent growth in the cell interior , asymmetric transition frequencies and effects of the cell boundary," *Journal of Cell Science*, Vol. 115 No. 17, pp. 3527–3539.

Koyasu, S., Nishida, E., Kadowaki, T., Matsuzaki, F., Iida, K., Harada, F., Kasuga, M., Sankai, H. and Yahara, I. (1986), "Two mammalian heat shock proteins, HSP90 and HSP100, are actin-binding proteins.," *Proceedings of the National Academy of Sciences of the United States of America*, Vol. 83 No. 21, pp. 8054–8058.

Krauer, K., Buck, M., Flanagan, J., Belzer, D. and Sculley, T. (2004), "Identification of the nuclear localization signals within the Epstein-Barr virus EBNA-6 protein," *Journal of General Virology*, Vol. 85 No. 1, pp. 165-172

Krokhin, O. V, Craig, R., Spicer, V., Ens, W., Standing, K.G., Beavis, R.C. and Wilkins, J.A. (2004), "An Improved Model for Prediction of Retention Times of Tryptic Peptides in Ion Pair Reversed-phase HPLC: Its Application to Protein Peptide Mapping by Off-Line HPLC-MALDI MS ," *Molecular & Cellular Proteomics* , Vol. 3 No. 9 , pp. 908–919.

Kubota, H., Yamamoto, S., Itoh, E., Abe, Y., Nakamura, A., Izumi, Y., Okada, H., Iida, M., Nanjo, H., Itoh, H. and Yamamoto, Y. (2010), "Increased expression of co-chaperone HOP with HSP90 and HSC70 and complex formation in human colonic carcinoma.," *Cell Stress & Chaperones*, Vol. 15 No. 6, pp. 1003–1011.

Kyte, J. and Doolittle, R.F. (1982), "A simple method for displaying the hydropathic character of a protein," *Journal of Molecular Biology*, Vol. 157 No. 1, pp. 105–132.

Laemmli, U.K. (1970), "Cleavage of structural proteins during the assembly of the head of bacteriophage T4," *Nature*, Vol. 227 No. 5259, pp. 680–685.

Lammermann, T., Bader, B.L., Monkley, S.J., Worbs, T., Wedlich-Soldner, R., Hirsch, K., Keller, M., Förster, R., Critchley, D.R., Fässler, R. and Sixt, M. (2008), "Rapid leukocyte migration by integrin-independent flowing and squeezing," Vol. 453 No. 7191, pp. 51–55.

Laskey, R.A., Honda, B.M., Mills, A.D. and Finch, J.T. (1978), "Nucleosomes are assembled by an acidic protein which binds histones and transfers them to DNA," *Nature*, Vol. 275 No. 5679, pp. 416–420.

Lässle, M., Blatch, G.L., Kundra, V., Takatori, T. and Zetter, B.R. (1997), "Characterization of binding domains for heat shock proteins and in vitro phosphorylation by differen kinases," *The Journal of Biological Chemistry*, Vol. 272 No. 3, pp. 1876–1884.

Laufen, T., Mayer, M.P., Beisel, C., Klostermeier, D., Mogk, A., Reinstein, J. and Bukau, B. (1999), "Mechanism of regulation of Hsp70 chaperones by DnaJ cochaperones," *Proceedings of the National Academy of Sciences of the United States of America*, Vol. 96 No. May, pp. 5452–5457.

Lazarides, E. (1975), "Immunofluorescence studies on the structure of actin filaments in tissue culture cells.," *Journal of Histochemistry & Cytochemistry*, Vol. 23 No. 7, pp. 507–528.

Lee, H.-J., Lai, Y.-H., Wu, S.-Y. and Chen, Y.-H. (2005), "The effect of N-terminal truncation on double-dimer assembly of goose delta-crystallin.," *The Biochemical Journal*, Vol. 392 No. Pt 3, pp. 545–554.

Lee, C.-T., Graf, C., Mayer, F.J., Richter, S.M. and Mayer, M.P. (2012), "Dynamics of the regulation of Hsp90 by the co-chaperone Sti1.," *The EMBO Journal*, Vol. 31 No. 6, pp. 1518–1528.

Lee, S.-D., Lai, T.W., Lin, S.-Z., Lin, C.-H., Hsu, Y.-H., Li, C.-Y., Wang, H.-J., Lee, W., Su, C.-Y. and Yu, Y.-L. (2013), "Role of stress-inducible protein-1 in recruitment of bone marrow derived cells into the ischemic brains.," *EMBO molecular medicine*, Vol. 5 No. 8, pp. 1227–1246.

Li, J., Soroka, J. and Buchner, J. (2012), "The Hsp90 chaperone machinery: conformational dynamics and regulation by co-chaperones.," *Biochimica et Biophysica Acta*, Vol. 1823 No. 3, pp. 624–635.

Li, J., Sun, X., Wang, Z., Chen, L., Dengwen, L., Zhou, J. and Liu, M. (2012), "Regulation of vascular endothelial cell polarization and migration by Hsp70/Hsp90-organizing protein.," *PloS ONE*, Vol. 7 No. 4, p. e36389.

Li, R., Soosairajah, J., Harari, D., Citri, A., Price, J., Ng, H.L., Morton, C.J., Parker, M.W., Yarden, Y. and Bernard, O. (2006), "Hsp90 increases LIM kinase activity by promoting its homo-dimerization," *The FASEB Journal* , Vol. 20 No. 8 , pp. 1218–1220.

Liang, P. and MacRae, T.H. (1997), "Molecular chaperones and the cytoskeleton.," *Journal of Cell Science*, Vol. 110, pp. 1431–1440.

Longshaw, V.M., Chapple, J.P., Balda, M.S., Cheetham, M.E. and Blatch, G.L. (2004), "Nuclear translocation of the Hsp70/Hsp90 organizing protein mSTI1 is regulated by cell cycle kinases.," *Journal of Cell Science*, Vol. 117 No. Pt 5, pp. 701–710.

Lopes, M.H., Hajj, G.N.M., Muras, A.G., Mancini, G.L., Castro, R.M.P.S., Ribeiro, K.C.B., Brentani, R.R., Linden, R. and Martins, V. (2005), "Interaction of cellular prion and stress-inducible protein 1 promotes neuritogenesis and neuroprotection by distinct signaling pathways.," *The Journal of Neuroscience*, Vol. 25 No. 49, pp. 11330–11339.

Lorenz, M., Popp, D. and Holmes, K.C. (1993), "Refinement of the F-Actin Model against X-ray Fiber Diffraction Data by the Use of a Directed Mutation Algorithm," *Journal of Molecular Biology*, Vol. 234 No. 3, pp. 826–836.

Machesky, L.M. and Insall, R.H. (1998), "Scar1 and the related Wiskott–Aldrich syndrome protein, WASP, regulate the actin cytoskeleton through the Arp2/3 complex," *Current Biology*, Vol. 8 No. 25, pp. 1347–1356.

Magdeldin, S. and Moser, A. (2012), *Affinity Chromatography: Principles and applications*, (Magdeldin,S.,Ed.), InTech. Rijeka, Croatia.

Mandelkow, E., Song, Y.-H., Schweers, O., Marx, A. and Mandelkow, E.-M. (1995), "On the structure of Microtubules, Tau and Paired Helical filaments," *Neurobiology of Aging*, Vol. 16 No. 3, pp. 347–354.

Maeshima, Y., Colorado, P.C. and Kalluri, R. (2000), "Two RGD-independent $\alpha_v\beta_3$ Intergrin Binding Sites on Tunstatin Regulate Distinct Anti-tumor Properties," *The Journal of Biological Chemistry,* Vol. 275 No. 31, pp. 23754-23750

McGough, A., Pope, B., Chiu, W. and Weeds, A. (1997), "Cofilin Changes the Twist of F-Actin: Implications for Actin Filament Dynamics and Cellular Function," *The Journal of Cell Biology*, Vol. 138 No. 4, pp. 771–781.

McWilliam, H., Li, W., Uludag, M., Squizzato, S., Park, Y.M., Buso, N., Cowley, A.P. and Lopez, R. (2013), "Analysis Tool Web Services from the EMBL-EBI.," *Nucleic acids research*, Vol. 41 No. Web Server issue, pp. W597–600.

Miao, R.Q., Fontana, J., Fulton, D., Lin, M.I., Harrison, K.D. and Sessa, W.C. (2008), "Dominant-Negative Hsp90 Reduces VEGF-Stimulated Nitric Oxide Release and Migration in Endothelial Cells," *Arteriosclerosis, Thrombosis, and Vascular Biology* , Vol. 28 No. 1 , pp. 105–111.

Miki, H., Suetsugu, S. and Takenawa, T. (1998), "WAVE, a novel WASP-family protein involved in actin reorganization induced by Rac.," *The EMBO Journal*, Vol. 17 No. 23, pp. 6932–6941.

Miki, H. and Takenawa, T. (1998), "Direct binding of the verprolin-homology domain in N-WASP to actin is essential for cytoskeletal reorganization.," *Biochemical and Biophysical Research Communications*, Vol. 243 No. 1, pp. 73–78.

Mimori-Kiyosue, Y., Grigoriev, I., Lansbergen, G., Sasaki, H., Matsui, C., Severin, F., Galjart, N., Grosveld, F., Vorobjev, I., Tsukita, S. and Akhmanova (2005), "CLASP1 and CLASP2 bind to EB1 and regulate microtubule plus-end dynamics at the cell cortex," *The Journal of Cell Biology* , Vol. 168 No. 1 , pp. 141–153.

Mitchison, T. and Kirschner, M. (1984), "Dynamic instability of microtubule growth," *Nature*, Vol. 312 No. 5991, pp. 237–242.

Mitchison, T.J. and Cramer, L.P. (1996), "Actin-Based Cell Motility and Cell Locomotion," *Cell*, Vol. 84 No. 3, pp. 371–379.

Morgan, T.E., Lockerbie, R.O., Minamide, L.S., Browning, M.D. and Bamburg, J.R. (1993), "Isolation and characterization of a regulated form of actin depolymerizing factor," *The Journal of Cell Biology* , Vol. 122 No. 3 , pp. 623–633.

Mosser, D.D. and Morimoto, R.I. (2004), "Molecular chaperones and the stress of oncogenesis.," *Oncogene*, Vol. 23 No. 16, pp. 2907–2918.

Mullins, R.D., Heuser, J.A. and Pollard, T.D. (1998), "The interaction of Arp2/3 complex with actin: Nucleation , high affinity pointed end capping, and formation of branching networks of filaments," *Proceedings of the National Academy of Sciences of the United States of America*, Vol. 95 No. 11, pp. 6181–6186.

Munsie, L.N., Desmond, C.R. and Truant, R. (2012), "Cofilin nuclear-cytoplasmic shuttling affects cofilin-actin rod formation during stress.," *Journal of Cell Science*, Vol. 125 No. Pt 17, pp. 3977–3988.

Murphy, M.E. (2013), "The HSP70 family and cancer.," *Carcinogenesis*, Vol. 34 No. 6, pp. 1181–1188.

Nicolet, C.M. and Craig, E.A. (1989), "Isolation and characterization of STI1, a stress-inducible gene from *Saccharomyces cerevisiae*.," *Molecular and Cellular Biology*, Vol. 9 No. 9, pp. 3638–3646.

Niethammer, P., Bastiaens, P. and Karsenti, E. (2004), "Stathmin-Tubulin Interaction Gradients in Motile and Mitotic Cells," *Science* , Vol. 303 No. 5665 , pp. 1862–1866.

Nobes, C.D. and Hall, A. (1995), "Rho, Rac, and Cdc42 GTPases regulate the assembly of multimolecular focal complexes associated with actin stress fibers, lamellipodia, and filopodia," *Cell*, Vol. 81 No. 1, pp. 53–62.

Odunuga, O.O., Hornby, J.A, Bies, C., Zimmermann, R., Pugh, D.J. and Blatch, G.L. (2003), "Tetratricopeptide repeat motif-mediated Hsc70-mSTI1 interaction. Molecular characterization of the critical contacts for successful binding and specificity.," *The Journal of Biological Chemistry*, Vol. 278 No. 9, pp. 6896–6904.

Oinuma, I., Kawada, K., Tsukagoshi, K. and Negishi, M. (2012), "Rnd1 and Rnd3 targeting to lipid raft is required for p190 RhoGAP activation," *Molecular Biology of the Cell* , Vol. 23 No. 8 , pp. 1593–1604.

Okamoto, K.-I., Narayanan, R., Lee, S.H., Murata, K. and Hayashi, Y. (2007), "The role of CaMKII as an F-actin-bundling protein crucial for maintenance of dendritic spine structure," *Proceedings of the National Academy of Sciences* , Vol. 104 No. 15 , pp. 6418–6423.

Oliyai, C. and Borchardt, R.T. (1993), "Chemical pathways of peptide degradation. IV. Pathways, kinetics, and mechanism of degradation of an aspartyl residue in a model hexapeptide.," *Pharmaceutical Research*, Vol. 10 No. 1, pp. 95–102.

Paavilainen, V.O., Bertling, E., Falck, S. and Lappalainen, P. (2004), "Regulation of cytoskeletal dynamics by actin-monomer-binding proteins.," *Trends in Cell Biology*, Vol. 14 No. 7, pp. 386–394.

Palleros, D.R., Reid, K.L., Shi, L. and Fink, A.L. (1993), "DnaK ATPase activity revisited," *FEBS Letters*, Vol. 336 No. 1, pp. 124–128.

Pantaloni, D., Hills, T.L., Carlier, M. and Korn, E.D. (1985), "A model for actin polymerization and the kinetic effects of ATP hydrolysis," *Proceedings of the National Academy of Sciences of the United States of America*, Vol. 82 No. November, pp. 7207–7211.

Park, S.J., Suetsugu, S., Sagara, H. and Takenawa, T. (2007), "HSP90 cross-links branched actin filaments induced by N-WASP and the Arp2/3 complex.," *Genes to cells*, Vol. 12 No. 5, pp. 611–622.

Pavlov, D., Muhlrad, A., Cooper, J., Wear, M. and Reisler, E. (2007), "Actin filament severing by cofilin.," *Journal of Molecular Biology*, Vol. 365 No. 5, pp. 1350–1358.

Pendleton, A., Pope, B., Weeds, A. and Koffer, A. (2003), "Latrunculin B or ATP depletion induces cofilin-dependent translocation of actin into nuclei of mast cells.," *The Journal of Biological Chemistry*, Vol. 278 No. 16, pp. 14394–14400.

Pollard, T.D. and Borisy, G.G. (2003), "Cellular Motility Driven by Assembly and Disassembly of Actin Filaments," *Cell*, Vol. 112, pp. 453–465.

Pollard, T.D., Selden, S.C. and Maupin, P. (1984), "Interaction of Actin Filaments with Microtubules," *The Journal of Cell Biology*, Vol. 99 No. 1, p. 33s–37s.

Pratt, W.B. and Toft, D.O. (2003), "Regulation of Signaling Protein Function and Trafficking by the hsp90/hsp70-Based Chaperone Machinery," *Experimental Biology and Medicine* , Vol. 228 No. 2 , pp. 111–133.

Prodromou, C. and Pearl, L. (2003), "Structure and Functional Relationships of Hsp90," *Current Cancer Drug Targets*, Vol. 3 No. 5, pp. 301–323.

Ressad, F., Didry, D., Xia, G.-X., Hong, Y., Chua, N.-H., Pantaloni, D. and Carlier, M.-F. (1998), "Kinetic Analysis of the Interaction of Actin-depolymerizing Factor (ADF)/Cofilin with G- and F-Actins: comparison of plant and human adfs and effect of phosphorylation ," *Journal of Biological Chemistry* , Vol. 273 No. 33 , pp. 20894–20902.

Richarme, G. and Kohiyama, M. (1993), "Autostimulation of the DnaK (HSP 70) ATPase of *Escherichia coli*," *FEBS Letters*, Vol. 322 No. 3, pp. 277–279.

Ridley, A.J. (2011), "Life at the Leading Edge," *Cell*, Vol. 145 No. 7, pp. 1012–1022.

Ridley, A.J. and Hall, A. (1992), "The small GTP-binding protein rho regulates the assembly of focal adhesions and actin stress fibers in response to growth factors," *Cell*, Elsevier, Vol. 70 No. 3, pp. 389–399.

Rottner, K. and Stradal, T.E.B. (2011), "Actin dynamics and turnover in cell motility," *Current Opinion in Cell Biology*, Vol. 23 No. 5, pp. 569–578.

Roy, P. and Jacobson, K. (2004), "Overexpression of profilin reduces the migration of invasive breast cancer cells.," *Cell Motility and the Cytoskeleton*, Vol. 57 No. 2, pp. 84–95.

Russell, L.C., Whitt, S.R., Chen, M.-S. and Chinkers, M. (1999), "Identification of Conserved Residues Required for the Binding of a Tetratricopeptide Repeat Domain to Heat Shock Protein 90," *Journal of Biological Chemistry*, Vol. 274 No. 29, pp. 20060–20063.

Saksela, K. and Permi, P. (2012), "SH3 domain ligand binding: What's the consensus and where's the specificity?," *FEBS letters*, Vol. 586 No. 17, pp. 2609–2614.

Sanchez, C., Padilla, R., Paciucci, R., Zabala, J.C. and Avila, J. (1994), "Binding of Heat-Shock Protein 70 (hsp70) to Tubulin," *Archives of Biochemistry and Biophysics*, Vol. 310 No. 2, pp. 428–432.

Schaefer, K.L., Takahashi, H., Morales, V.M., Harris, G., Barton, S., Osawa, E., Nakajima, A., and Saubermann, L.J (2007), "PPARgamma inhibitors reduce tubulin protein levels by a PPARgamma, PPARdelta and proteasome-independent mechanism, resulting in cell cycle arrest, apoptosis and reduced metastasis of colorectal carcinoma cells.," *International Journal of Cancer*, Vol. 120 No. 3, pp. 702–713.

Scheufler, C., Brinker, a, Bourenkov, G., Pegoraro, S., Moroder, L., Bartunik, H., Hartl, F.U. and Moarefi, I. (2000), "Structure of TPR domain-peptide complexes: critical elements in the assembly of the Hsp70-Hsp90 multichaperone machine.," *Cell*, Vol. 101 No. 2, pp. 199–210.

Schlüter, K., Schleicher, M. and Jockusch, B.M. (1998), "Effects of single amino acid substitutions in the actin-binding site on the biological activity of bovine profilin I," *Journal of Cell Science*, Vol. 111, pp. 3261–3273.

Schmid, A.B., Lagleder, S., Gräwert, M.A., Röhl, A., Hagn, F., Wandinger, S.K., Cox, M.B., Demmer, O., Richter, K., Groll, M., Kessler, H. and Buchner, J. (2012), "The architecture of functional modules in the Hsp90 co-chaperone Sti1/Hop.," *The EMBO Journal*, Vol. 31 No. 6, pp. 1506–1517.

Schutt, C.E., Myslik, J.C., Rozycki, M.D., Goonesekere, N.C.W. and Lindberg, U. (1993), "The structure of crystalline profilin–[beta]-actin," *Nature*, Vol. 365 No. 6449, pp. 810–816.

Sept, D. and McCammon, J.A. (2001), "Thermodynamics and kinetics of actin filament nucleation.," *Biophysical Journal*, Vol. 81 No. 2, pp. 667–674.

Simard, J.P., Reynolds, D.N., Kraguljac, A.P., Smith, G.S.T. and Mosser, D.D. (2011), "Overexpression of HSP70 inhibits cofilin phosphorylation and promotes lymphocyte migration in heat-stressed cells.," *Journal of Cell Science*, Vol. 124 No. Pt 14, pp. 2367–2374.

Small, J. V, Isenberg, G. and Celis, J.E. (1978), "Polarity of actin at the leading edge of cultured cells.," *Nature*, Vol. 272 No. 5654, pp. 638–639.

Sreedhar, A.S., Kalmár, É., Csermely, P. and Shen, Y.-F. (2004), "Hsp90 isoforms: functions, expression and clinical importance," *FEBS Letters*, Vol. 562 No. 1–3, pp. 11–15.

Srivastava, J. and Barber, D. (2008), "Actin Co-Sedimentation Assay ; for the Analysis of Protein Binding to F-Actin," *Journal of Visualized Experiments*, Vol. 13, pp. 2–3.

Steinmetz, M.O., Stoffler, D., Hoenger, A, Bremer, A and Aebi, U. (1997), "Actin: from cell biology to atomic detail.," *Journal of Structural Biology*, Vol. 119 No. 3, pp. 295–320.

Stevenson, R.P., Veltman, D. and Machesky, L.M. (2012), "Actin-bundling proteins in cancer progression at a glance," *Journal of Cell Science*, Vol. 125 No. 5, pp. 1073–1079.

Stuven, T., Hartmann, E. and Gorlich, D. (2003), "Exportin 6 : a novel nuclear export receptor that is specific for profilin-actin complexes," *The EMBO Journal*, Vol. 22 No. 21, pp. 5928–5940.

Suetsugu, S., Miki, H. and Takenawa, T. (1999a), "Identification of two human WAVE/SCAR homologues as general actin regulatory molecules which associate with the Arp2/3 complex.," *Biochemical and Biophysical Research Communications*, Vol. 260 No. 1, pp. 296–302.

Suetsugu, S., Miki, H. and Takenawa, T. (1999b), "Distinct roles of profilin in cell morphological changes : microspikes , membrane ruffles , stress fibers , and cytokinesis," *FEBS Letters*, Vol. 457, pp. 470–474.

Symons, M., Derry, J.M.., Karlak, B., Jiang, S., Lemahieu, V., McCormick, F., Francke, U. and Abo, A. (1996), "Wiskott–Aldrich Syndrome Protein, a Novel Effector for the GTPase CDC42Hs, Is Implicated in Actin Polymerization," *Cell*, Vol. 84 No. 5, pp. 723–734.

Taiyab, A. and Rao, C.M. (2011), "HSP90 modulates actin dynamics: inhibition of HSP90 leads to decreased cell motility and impairs invasion.," *Biochimica et Biophysica Acta*, Vol. 1813 No. 1, pp. 213–221.

Taylor, D.L. and Condeelis, J.S. (1979), "Cytoplasmic Structure and Contractility in Amoeboid Cells,", *Internation Review if Cytology,* Vol. 56, pp. 57–144.

Theriot, J.A. and Mitchison, T.J. (1991), "Actin microfilament dynamics in locomoting cells," *Nature*, Vol. 352 No. 6331, pp. 126–131.

Tobacman, L.S. and Korn, E.D. (1983), "The Kinetics of Actin Nucleation and Polymerization," *The Journal of Biological Chemistry*, Vol. 258 No. 5, pp. 3207–3214.

Towbin, H., Staehelin, T. and Gordon, J. (1979), "Electrophoretic transfer of proteins from polyacrylamide gels to nitrocellulose sheets: procedure and some applications," *Proceedings of the National Academy of Sciences*, Vol. 76 No. 9 , pp. 4350–4354.

Tsutsumi, S. and Neckers, L. (2007), "Extracellular heat shock protein 90: A role for a molecular chaperone in cell motility and cancer metastasis," *Cancer Science*, Vol. 98 No. 10, pp. 1536–1539.

Ujfalusi, Z., Kovács, M., Nagy, N.T., Barkó, S., Hild, G., Lukács, A., Nyitrai, M. and Bugyi, B. (2012), "Myosin and Tropomyosin Stabilize the Conformation of Formin-nucleated Actin Filaments," *Journal of Biological Chemistry*, Vol. 287 No. 38 , pp. 31894–31904.

Urbanek, A.N., Smith, A.P., Allwood, E.G., Booth, W.I. and Ayscough, K.R. (2013), "A novel actin-binding motif in Las17/WASP nucleates actin filaments independently of Arp2/3," *Current Biology*, Vol. 23 No. 3, pp. 196–203.

Vandekerckhove, J. and Vancompernolle, K. (1992), "Structural relationships of actin-binding proteins," *Current Opinion in Cell Biology*, Vol. 4 No. 1, pp. 36–42.

Vandekerckhove, J.S., Kaiser, D.A. and Pollard, T.D. (1989), "*Acanthamoeba* actin and profilin can be cross-linked between glutamic acid 364 of actin and lysine 115 of profilin," *The Journal of Cell Biology*, Vol. 109 No. 2, pp. 619–626.

Vartiainen, M.K. (2008), "Nuclear actin dynamics--from form to function," *FEBS letters*, Vol. 582 No. 14, pp. 2033–2040.

Vartiainen, M.K., Mustonen, T., Mattila, P.K., Ojala, P.J., Thesleff, I., Partanen, J. and Lappalainen, P. (2002), "The Three Mouse Actin-depolymerizing Factor/Cofilins Evolved to Fulfill Cell-Type–specific Requirements for Actin Dynamics," *Molecular Biology of the Cell*, Vol. 13 No. 1, pp. 183–194.

Wang, C.L., Wang, L.W., Xu, S.A., Lu, R.C., Saavedra-Alanis, V. and Bryan, J. (1991), "Localization of the calmodulin- and the actin-binding sites of caldesmon,"*Journal of Biological Chemistry*, Vol. 266 No. 14, pp. 9166–9172.

Wang, L., Miller, A. and Kendall, D.A. (2000), "Signal Peptide Determinants of SecA Binding and Stimulation of ATPase Activity," *Journal of Biological Chemistry*, Vol. 275 No. 14 , pp. 10154–10159.

Wang, W., Eddy, R. and Condeelis, J. (2007), "The cofilin pathway in breast cancer invasion and metastasis," *Nature Reviews Cancer*, Vol. 7 No. 6, pp. 429–440.

Watanabe, N. and Mitchison, T.J. (2002), "Single-Molecule Speckle Analysis of Actin Filament Turnover in Lamellipodia," *Science*, Vol. 295 No. 5557 , pp. 1083–1086.

Weber, A., Pennise, C.R., Babcock, G.G. and Fowler, V.M. (1994), "Tropomodulin caps the pointed ends of actin filaments," *The Journal of Cell Biology*, Vol. 127 No. 6 , pp. 1627–1635.

Weigt, C., Schoepper, B. and Wegner, A. (1990), "Tropomyosin-troponin complex stabilizes the pointed ends of actin filaments against polymerization and depolymerization," *FEBS Letters*, Vol. 260 No. 2, pp. 266–268.

Weis, F., Moullintraffort, L., Heichette, C., Chrétien, D. and Garnier, C. (2010), "The 90-kDa Heat Shock Protein Hsp90 Protects Tubulin against Thermal Denaturation," *Journal of Biological Chemistry*, Vol. 285 No. 13 , pp. 9525–9534.

Wen, Q. and Janmey, P.A. (2011), "Polymer physics of the cytoskeleton.," *Current pinion in Solid State & Materials Science*, Vol. 15 No. 5, pp. 177–182.

WHO. (2014), “World Health Organisation.” Retrieved December 2, 2014, from http://www.who.int/mediacentre/factsheets/fs297/en/

Willmer, T., Contu, L., Blatch, G.L. and Edkins, A.L. (2013), “Knockdown of Hop downregulates RhoC expression, and decreases pseudopodia formation and migration in cancer cell lines,” *Cancer Letters*, Vol. 328 No. 2, pp. 252–260.

Winder, S.J. and Ayscough, K.R. (2005), “Actin-binding proteins,” *Journal of Cell Science*, Vol. 118, pp. 651–654.

Wingate, I. (2014), *Proteomic analysis of the role of Hop in cancer cell biology*. MSc dissertation, Rhodes University.

Wittenmayer, N., Jandrig, B., Rothkegel, M., Arnold, W., Haensch, W., Scherneck, S. and Jockusch, B.M. (2004), “Tumor Suppressor Activity of Profilin Requires a Functional Actin Binding Site,” *Molecular Biology of the Cell*, Vol. 15 No. April, pp. 1600–1608.

Woodham, E.F. and Machesky, L.M. (2014), “Polarised cell migration: intrinsic and extrinsic drivers,” *Current Opinion in Cell Biology*, Vol. 30C, pp. 25–32.

Yamaguchi, H. and Condeelis, J. (2007), “Regulation of the actin cytoskeleton in cancer cell migration and invasion,” *Biochimica et Biophysica Acta*, Vol. 1773 No. 5, pp. 642–652.

Yamamoto, M., Hilgemann, D.H., Feng, S., Bito, H., Ishihara, H., Shibasaki, Y. and Yin, H.L. (2001), “Phosphatidylinositol 4,5-Bisphosphate Induces Actin Stress-Fiber Formation and Inhibits Membrane Ruffling in Cv1 Cells,” *The Journal of Cell Biology*, Vol. 152 No. 5, pp. 867–876.

Yamamoto, S., Subedi, G.P., Hanashima, S., Satoh, T., Otaka, M., Wakui, H., Sawada, K., Yokota, S., Yamaguchi, Y., Kubota, H. and Itoh, H. (2014), “ATPase activity and ATP-dependent conformational change in the co-chaperone HSP70/HSP90-organizing protein (HOP),” *The Journal of Biological Chemistry*, Vol. 289 No. 14, pp. 9880–9886.

Yamazaki, D., Kurisu, S. and Takenawa, T. (2005), “Regulation of cancer cell motility through actin reorganization.,” *Cancer Science*, Vol. 96 No. 7, pp. 379–386.

Yang, N., Higuchi, O., Ohashi, K., Nagata, K., Wada, A., Kangawa, K., Nishida, E. and Mizuno, A. (1998), “Cofilin phosphorylation by LIM-kinase 1 and its role in Rac-mediated actin reorganization,” *Nature*, Vol. 393 No. 6687, pp. 809–812.

Yi, F., Doudevski, I. and Regan, L. (2010), “HOP is a monomer: investigation of the oligomeric state of the co-chaperone HOP.,” *Protein science*, Vol. 19 No. 1, pp. 19–25.

Yonezawa, N., Homma, Y., Yahara, I., Sakai, H. and Nishida, E. (1991a), “A short sequence responsible for both phosphoinositide binding and actin binding activities of cofilin.,” *Journal of Biological Chemistry*, Vol. 266 No. 26, pp. 17218–17221.

Yonezawa, N., Nishida, E., Iida, K., Kumagai, H., Yahara, I. and Sakai, H. (1991b), “Inhibition of Actin Polymerization by a Synthetic Dodecapeptide Patterned on the Sequence around the Actin-binding Site of Cofilin,” *The Journal of Biological Chemistry*, Vol. 266 No. 16, pp. 10485–10489.

Yonezawa, N., Nishida, E., Iida, K., Yahara, I. and Sakai, H. (1990), “Inhibition of the interactions of cofilin, destrin, and deoxyribonuclease I with actin by phosphoinositides.,” *Journal of Biological Chemistry*, Vol. 265 No. 15, pp. 8382–8386.

Yonezawa, N., Nishida, E., Ohba, M., Seki, M., Kumagai, H. and Sakai, H. (1989), “An actin-interacting heptapeptide in the cofilin sequence.,” *European Journal of Biochemistry / FEBS*, Vol. 183 No. 1, pp. 235–238.

Zanata, S.M., Lopes, M.H., Mercadante, A.F., Hajj, G.N.M., Chiarini, L.B., Nomizo, R., Freitas, A.R.O., Cabral, A.L., Lee, K.S., Juliano, M.A., de Oliveira, E., Jachieri S.G., Burliname A., Huang, L., Linden, R., Breantani, R.R. and Martin, V.R. (2002), "Stress-inducible protein 1 is a cell surface ligand for cellular prion that triggers neuroprotection," *The EMBO Journal*, Vol. 21 No. 13, pp. 3307–3316.

Zhang, Z., Quick, M.K., Kanelakis, K.C., Gijzen, M. and Krishna, P. (2003), "Characterization of a plant homolog of hop, a cochaperone of hsp90.," *Plant Physiology*, Vol. 131 No. 2, pp. 525–535.

Zinchuk, V., Zinchuk, O. and Okada, T. (2007), "Quantitative colocalization analysis of multicolor confocal immunofluorescence microscopy images: pushing pixels to explore biological phenomena.," *Acta Histochemica et Cytochemica*, Vol. 40 No. 4, pp. 101–111.

Chapter 6: Appendix

6.1 Materials

All general reagents were brought from Sigma-Aldrich. The expression plasmid, pGEX4T-1 was available in our laboratory and was supplied by Morgan Hunter. The plasmids encoding the mSTI1 protein and truncations, pGEX3X2000, pGEX1400 and pGEX700 were supplied by the laboratory (Lässle et al., 1997; Odunuga et al., 2003). The antibiotic, ampicillin was purchased from Sigma-Aldrich (Cat #: A9518). The *Pst*I digested lambda bacteriophage DNA ladder was purchased from Life Sciences Advanced Technology Inc (Cat #: LSM-VI-NM2427). The *Pst*I restriction enzyme and the buffer used for the digestion of the plasmids were supplied by Promega (Cat #: R611A). The isopropyl β-D-1-thiogalactopyranoside (IPTG) used to induce protein expression was purchased from Peqlab (Germany). Lysozyme was purchased from Sigma-Aldrich (Cat #: L2879). PMSF was purchased from Roche Applied Science (Cat #: 10837091001). Two protein molecular weight markers were used with SDS-PAGE. The Pierce Prestained Protein Molecular Weight Marker and the Unstained Protein Molecular Weight Marker were both purchased from Thermo Scientific (Cat #: 26612 and 26610). Coomassie brilliant blue R250 was purchased from USB. Supported nitrocellulose membranes were purchased from Bio-Rad (Cat #: 1620097). Adenosine 5'-triphosphate (ATP) was purchased from Sigma-Aldrich (Cat #: A26209). Cytochalasin D was purchased from Sigma-Aldrich (Cat #: C8273).

6.2 Tissue culture materials and reagents

L-Glutamine (Cat #: 21051024), sodium pyruvate (Cat #: S8636), Trypsin solution (Cat #: 59427C), G418 (Cat #: A1720) and puromycin (Cat #: P8833) were purchased from Sigma-Aldrich. Dulbecco's Modified Eagle Medium, DMEM (Cat #: 21063045), MEM non-essential amino acids (Cat #: 1140035) were purchased from Life Technologies. Fetal bovine serum

(FBS) (Cat #: S181H) was purchased from Celtic Molecular Diagnostics. All tissue culture grade plasticware was purchased from NEST Biotechnology Co.

Table 6.1 - Primary antibodies used for Western blot analysis and immunofluorescence

Antibody	Species	Dilution	Application	Catalogue Number	Supplier
α-GST	Rabbit	1:2000	WB	Sc-459	Santa Cruz Biotechnology
α-STI1	Mouse	1:100	IF	Ab56873	Abcam
α-STI1	Rabbit	1:10 000	WB	Ab126724	Abcam
		1:100	IF		
α-DnaK	Mouse	1:2000	WB	Ab69617	Abcam
α-actin	Rabbit	1:1000	WB	A2103	Sigma-Aldrich
		1:100	IF		
α-cofilin	Rabbit	1:500	WB	Ab42824	Abcam
		1:50	IF		
α-profilin	Rabbit	1:1000	WB	3237S	Cell Signalling Technology
		1:100	IF		
α-tubulin	Mouse	1:2500	WB	Ab78078	Abcam
		1:100	IF		
α-GAPDH-HRP	Rabbit	1:5000	WB	Ab185059	Abcam
α-Hsp90	Mouse	1:1000	WB	Sc-13119	Santa Cruz Biotechnology
α-Hsp90	Goat	1:100	IF	Sc-1055	Santa Cruz Biotechnology

* WB: Western blot, IF: Immunofluorescence

Table 6.2: HRP-conjugated secondary antibodies for western blot

Antibody	Species	Dilution	Catalogue Number	Supplier
α-rabbit	Donkey	1:10 000	Ab6802	Abcam
α-mouse	Goat	1:5000	A2304	Sigma-Aldrich

Table 6.3: Fluorescently labelled secondary antibodies for immunofluorescence

Antibody	Species	Fluorescent Dye	Dilution	Catalogue Number	Supplier
α-mouse	Donkey	DyLight® 550	1:1000	Ab96875	Abcam
α-rabbit	Donkey	DyLight® 550	1:1000	Ab56873	Abcam
α-mouse	Donkey	DyLight® 488	1:1000	Ab126724	Abcam
α-rabbit	Donkey	DyLight® 488	1:1000	Ab69617	Abcam
α-goat	Donkey	DyLight® 650	1:1000	A2103	Abcam

6.3 Lineweaver-Burk plot

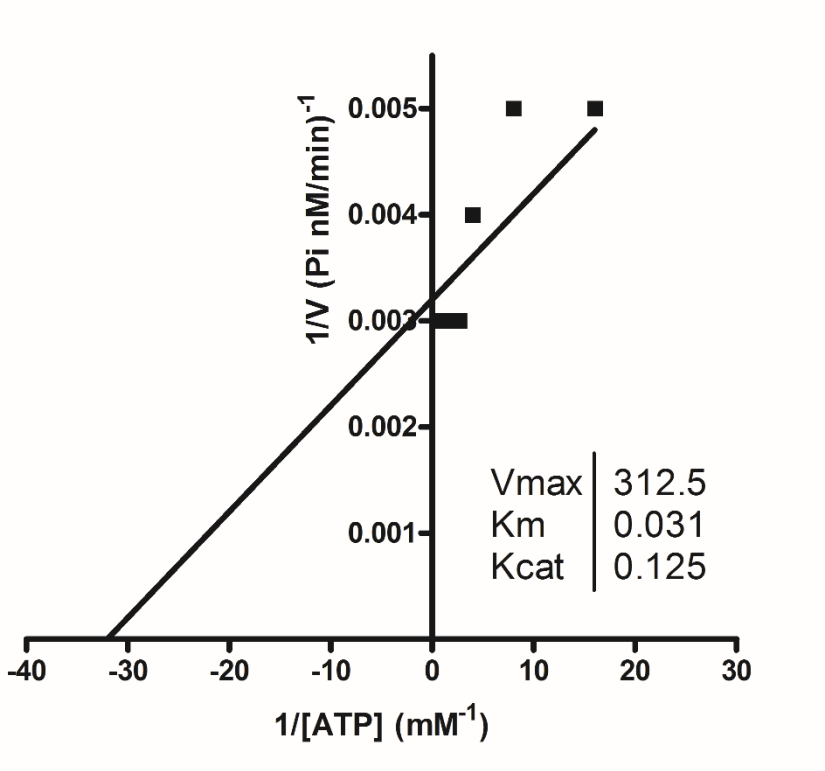

Figure 6.1 - Lineweaver-Burk plot of mSTI1 with increasing ATP concentrations

FL543 (2.5 μM) was incubated at 37°C in the presence of ATP (0.5 mM), $MgCl_2$ (2 mM) and $CaCl_2$ (50 mM). In order to determine the inorganic phosphate (Pi) production the EnzChek phosphate assay kit was used. UV absorbance was monitored and used to determine the rate of Pi production with the use of a phosphate standard curve. A concentration of 2.5 μM FL543 was incubated with increasing ATP concentrations. These data were used to plot a Lineweaver-Burk graph using the inverse of inorganic phosphate production and the inverse of ATP concentrations. Data are representative of experiments completed in triplicate.

6.4 Detection of saturation of binding of GST-tagged mSTI1 and truncated proteins to actin

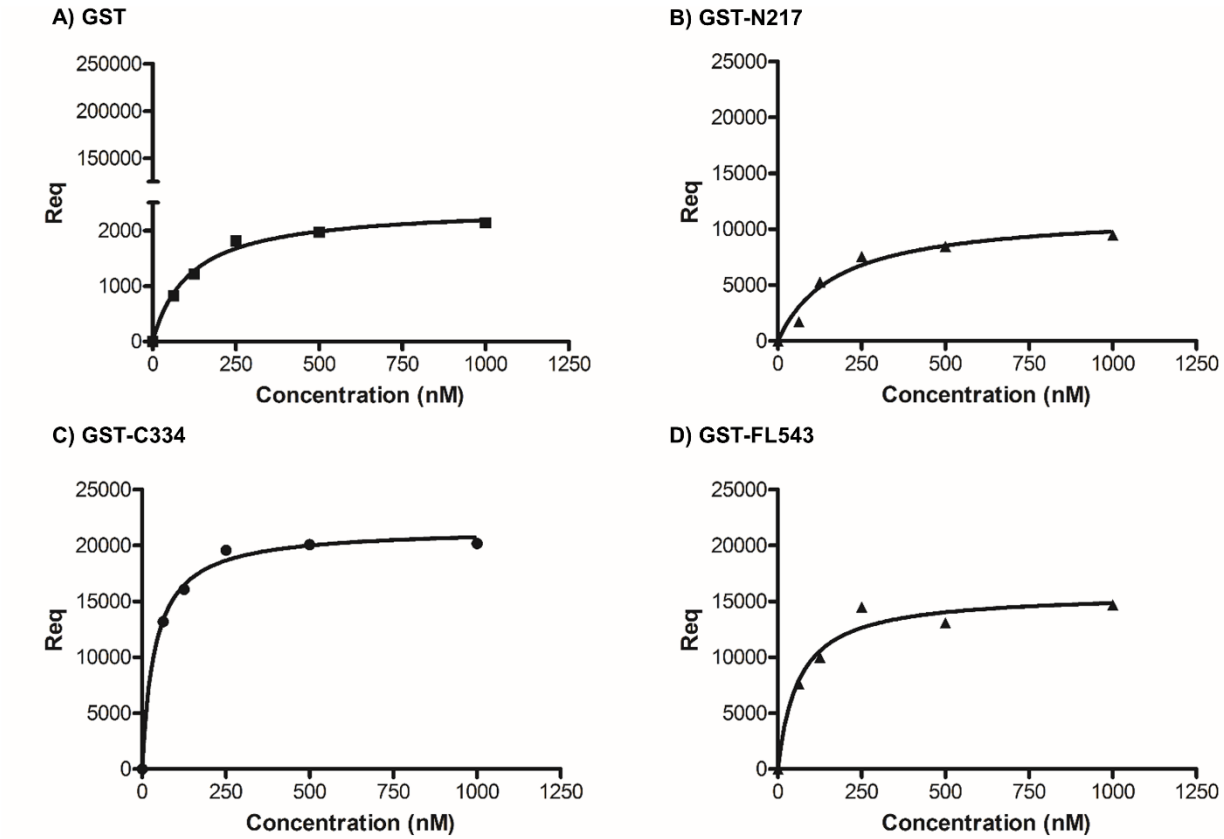

Figure 6.2 – Saturation plots of GST-tagged mSTI1 protein and truncations bound to actin at increasing concentrations for surface plasmon resonance analysis

Req values from SPR analysis showing saturation and specific binding of A) GST, B) GST-N217, C) GST-C334 and D) GST-FL543 at increasing concentration to immobilised actin (100 µg/ml). Data shown are representative of two independent experiments completed in triplicate.